COMPUTATIONAL FRAMEWORK FOR DURABILITY ASSESSMENT OF REINFORCED CONCRETE STRUCTURES UNDER COUPLED DETERIORATION PROCESSES

By

Dong Chen

Dissertation

Submitted to the Faculty of the

Graduate School of Vanderbilt University

in partial fulfillment of the requirements

for the degree of

DOCTOR OF PHILOSOPHY

in

Civil Engineering

August, 2006

Nashville, Tennessee

Approved:

Professor Sankaran Mahadevan

Professor Prodyot K. Basu

Professor David S. Kosson

Professor Florence Sanchez

To my beloved wife, Huihua, infinitely supportive

To my cute son, Eric Hanzhang, smart beyond his years

and

To my self-sacrificing parents: my father Congjun Chen and my mother Guihong Fu

ACKNOWLEDGEMENTS

I am grateful to all of those with whom I have had the pleasure to work during this research project. Especially, I am indebted to my academic advisor, Prof. Sankaran Mahadevan, who has been supportive of my career goals and has worked actively to provide me with the protected academic time to pursue those goals. As my teacher and mentor, he has taught me more than I could ever give him credit for here. He has shown me, by his example, what a good scientist and person should be.

I would like to give my sincerest appreciation to all members of my dissertation defense committee for their professional guidance and thoughtful review of my work from beginning to end. I would especially like to thank Prof. Prodyot K. Basu for his emotional support and academic advice during my whole graduate career. I would like to thank Prof. David S. Kosson for his valuable support, encouragement, and though-provoking guidance. A special thank you goes to Prof. Andrew C. Garrabrants and Prof. Florence Sanchez, for valuable support and unfailing patience in sharing their expertise in concrete with me. A general thanks is extended to Ms. Wenying Li, Dr. Kan Ni, Dr. Ramesh Rebba and all other IGERT students for their support, encouragement and friendship.

Nobody has been more important to me in the pursuit of this project than the members of my family. I would like to thank my parents, whose love and guidance are with me in whatever I pursue. They are the ultimate role models. Most importantly, I

wish to thank my beloved and supportive wife, Huihua, and my amazing son, Eric, who provide endless inspiration and funs.

This dissertation was prepared with the financial support of the U.S. Department of Energy, under Award No. DE-FG01-03EW15336 to the Institute for Responsible Management, Consortium for Risk Evaluation with Stakeholder Participation II. However, any opinions, findings, conclusions, or recommendations expressed herein are those of the author and do not necessarily reflect the views of the DOE or of IRM/CRESP II.

TABLE OF CONTENTS

Page

LIST OF FIGURES

Figure Page

LIST OF TABLES

Table Page

LIST OF NOMENCLATURES

a	MMF model parameter in the first level regression
b	MMF model parameter in the first level regression
c	MMF model parameter in the first level regression
d	MMF model parameter in the first level regression
A	Model parameter of relating moisture diffusivity to relative humidity
A	The atomic weight of iron (g/mol)
B	Kumaran's desorption isotherm model parameter
C	Kumaran's desorption isotherm model parameter
c	Specific heat capacity of concrete (J/kg $\cdot$ ^{0}C)
C_c	Concentration of free carbon dioxide (kg/m^3 of concrete)
$C_{c,\max}$	The maximum concentration of free CO_2 available in pore solution (kg/m^3 of solution)
C_{cl}	Chloride content (kg/m^3 of concrete)
$C_{cl,0}$	Surface chloride content (kg/m^3 of concrete)
$C_{cl,cr}$	Chloride threshold content value (kg/m^3 of concrete)
$C_{cl,b}$	Bound chloride content (kg/m^3 of concrete)
$C_{cl,f}$	Free chloride content (kg/m^3 of solution)
$C_{cl,t}$	Total chloride content (kg/m^3 of concrete)
$C1$	Concrete cover depth in the second level regression (mm)
$C2$	Reference chloride diffusivity in the second level regression (m^2/year)
$C3$	Surface chloride content in the second level regression (kg/m^3 of solution)
$C4$	Chloride threshold value in reliability analysis (kg/m^3 of solution)

$[Cl]$	Chloride content (ppm)
$\frac{\partial C_{cl,b}}{\partial C_{cl,f}}$	Chloride binding capacity of concrete (m^3 of solution/m^3 of concrete)
D_c	Diffusivity of carbon dioxide (m^2/s)
$D_{c,0}$	Reference diffusivity of carbon dioxide (m^2/s)
D_{cl}^*	Effective (or apparent) chloride diffusivity (m^2/s)
D_{cl}	Actual chloride diffusivity (m^2/s)
$D_{cl,0}$	Reference (or nominal) chloride diffusivity (m^2/s)
$D_{cl,crack}$	Chloride diffusivity of cracked concrete (m^2/s)
$D_{cl,\max}$	Chloride diffusivity of completely cracked concrete (m^2/s)
D_m	Moisture diffusivity of uncracked concrete (m^2/s)
$D_{m,0}$	Reference moisture diffusivity (m^2/s)
$D_{m,crack}$	Moisture diffusivity of cracked concrete (m^2/s)
$D_{m,\max}$	Moisture diffusivity of completely cracked concrete (m^2/s)
D_b	Original diameter of steel bar (m)
D_{eb}	Diameter of rust expansion front (m)
D_{rb}	Reduced diameter of steel bar after corrosion (m)
$[D]$	General stiffness matrix of reinforced concrete element
$[D_c]$	Stiffness matrix of uncracked plain concrete element
$[D_r]$	Stiffness matrix of reinforcement element
$[D_r]_i$	Stiffness matrix of reinforcement element in *i* direction

$\left[D_c^{ck}\right]$	Modified stiffness matrix of concrete element cracked in *x* direction only
E	Activation energy (J/mol)
E_0	Activation energy (J/mol)
E_c	Elastic modulus of concrete (MPa)
E_i^r	Elastic modulus of reinforcement (MPa)
F	Function of the principal stresses to define failure criteria
F	Faraday's constant (Coulomb/mol)
$F_1(h)$	Influencing factor of pore relative humidity on moisture diffusivity
$F_1^*(h)$	Influencing factor of pore relative humidity on CO_2 diffusivity
$F_2(T)$	Influencing factor of temperature
$F_1(C_{cl,b})$	Influencing factor of chloride binding capacity of concrete
$F_2(t)$	Influencing factor of age of concrete
$F_3(C_{cl,f})$	Influencing factor of free chloride content
$F_3(\xi)$	Influencing factor of carbonation-induced reduction of porosity
$F_4(T)$	Influencing factor of temperature
$F_4(\rho_{local})$	Influencing factor of elemental LRCD ρ_{local}
$F_5(\rho_{local})$	Influencing factor of elemental LRCD ρ_{local}
f_c	Influencing factor of free CO_2 concentration on carbonation reaction rate
f_h	Influencing factor of relative humidity on carbonation reaction rate
f_R	Influencing factor of degree of carbonation on carbonation reaction rate

f_T	Influencing factor of temperature on carbonation reaction rate
$f_c^{'}$	Compressive strength of concrete (MPa)
f_t	Tensile strength of concrete (MPa)
h	Pore relative humidity in concrete
$h_{ambient}$	Ambient relative humidity
I_{corr}	Amount of current (A)
i_{corr}	Corrosion current density (A/m^2)
K	Hydraulic conductivity (m/s)
MF	Multiplication factor
M_s	Mass of iron consumed (g)
m	Model parameter to determine influencing factor of concrete age $F_2(t)$
n	Model parameter to determine influencing factor of local chloride content $F_3(C_{cl,f})$
n	valence of reinforcement corrosion reaction
R_c	Ohmic resistance of cover concrete (ohms)
$\dot{Q}$	Heat source/sink term (J/m^3 concrete · s)
$\dot{Q}_c$	Sink/source term of CO_2 content (kg/m^3 of concrete · s)
$Q_{c,\max}$	The maximum amount of CO_2 that may combine with reactive alkali (kg/m^3 of concrete)
$\dot{Q}_m$	Sink/source term of moisture content (m^3 of moisture/m^3 of concrete · s)
R	Gas constant (J/mol · K)
r	The ratio of density of iron to density of corrosion product

r_m	The ratio of mass of iron corroded to mass of corrosion product generated
S	Spatial failure surface defined by failure criterion
T	Temperature of concrete (^{0}C or K)
$T_{ambient}$	Ambient temperature (^{0}C)
ΔT	Temperature gradient (^{0}C)
ΔT_{equiv}	Equivalent temperature variation (^{0}C)
T_c	Tensile stress relaxation factor
T_{ref}	Reference temperature (K)
t	Time elapsed (second or year)
t_c	Thickness of concrete cover (inch)
$t_{initiation}$	Corrosion initiation time (year)
t_{stress}	Expansive stress initiation time (year)
$t_{spalling}$	Spalling initiation time (year)
$u_{r,i}$	Radial displacement on rust expansion front surface at the i^{th} time step (m)
V_i^R	Volume ratio of reinforcement in concrete element
W	Free moisture content in concrete (m^3 of moisture/m^3 of concrete)
W_0	Kumaran's desorption isotherm model parameter (m^3 of moisture/m^3 of concrete)
WCR	Water to cement ratio by mass
α	Thermal expansion coefficient ($/^0$C)
α_{cl}	Model parameter of chloride binding isotherm model

β	Hydral contraction coefficient (m^3 of concrete/m^3 of moisture)
β_c	Shear transfer coefficient for closed crack
β_{cl}	Model parameter of chloride binding isotherm model
β_t	Shear transfer coefficient for open crack
δ_{por}	Equivalent thickness of ITZ (μm)
ε_0	Strain at the peak compressive stress
ε_1^{ck} , ε_2^{ck} , ε_3^{ck}	Three normal component strains with respect to crack orientation
ε_{ck}^{ck}	Crack strain
ε_{cu}	Ultimate strain
$\varepsilon_{shrinkage}$	Shrinkage strain
$\varepsilon_{thermal}$	Thermal strain
ϕ	General sink/source term
γ	Model parameter of relating moisture diffusivity to relative humidity
η_c	Carbonation and CO_2 transport interaction coefficient
η_m	Carbonation and freed moisture transport interaction coefficient
k	Thermal conductivity of concrete ($W/m \cdot {}^0C$)
κ	Model parameter to determine influencing factor of local chloride content $F_3(C_{cl,f})$
ϖ	Convergence criterion
θ	Model parameter of relating moisture diffusivity to relative humidity
ν	Poisson's ratio of concrete

υ_0	Ideal carbonation rate (/s · mol)
υ_r	Carbonation reaction rate (/s · mol)
ρ	Density of concrete (kg/m^3)
ρ_{local}	Local relative crack density (LRCD)
ρ_{global}	Global relative crack density (GRCD)
ρ_r	Density of corrosion products (g/cm^3)
ρ_s	Density of iron (g/cm^3)
$\sigma_1 = \max(\sigma_{xp}, \sigma_{yp}, \sigma_{zp})$	The first principal stress (Pa)
σ_2	The second principal stress (Pa)
$\sigma_3 = \min(\sigma_{xp}, \sigma_{yp}, \sigma_{zp})$	The third principal stress (Pa)
σ_{cu}	The maximal compressive strength (Pa)
σ_{tu}	The maximal tensile strength (Pa)
σ_{xp}	The principal stress in x direction (Pa)
σ_{yp}	The principal stress in *y* direction (Pa)
σ_{zp}	The principal stress in z direction (Pa)
ω_e	Constant saturated moisture content (m^3 of solution/m^3 of concrete)
ξ	Degree of carbonation
ψ	Model parameter of relating moisture diffusivity to relative humidity
ζ	Model parameter to determine influencing factor $F_3(\xi)$

CHAPTER I

INTRODUCTION

1.1. Overview

Although the durability of reinforced concrete structures has been a topic of research interest for several decades, the exact physical mechanisms of each deterioration process and the potential interactions among them are yet to be satisfactorily understood. To evaluate the durability of reinforced concrete structures exposed to various aggressive environments, substantive in-situ observations and laboratory experiments have been carried out world-wide, but development of the corresponding quantitative analysis and numerical simulation procedures are relatively lacking. Under such circumstances, conventional structural designs focus mainly on satisfying strength criteria with safety factors to guarantee serviceability and safety requirements. As for the durability requirements, only conceptual and empirical measures based on qualitative analysis of concrete durability, such as controlling the mixture compositions, the cover depth and the compressive strength of concrete etc., are proposed to prevent potential deterioration. With the increasing emphasis on minimizing the whole life-cycle cost of reinforced concrete structures, structural designers are making attempts to reform the conventional

structural design approaches and adopt durability-based structural design approaches, where the surrounding environments are taken into consideration and the durability of concrete structures is assessed quantitatively. The first durability design proposal may date back to the recommendation of the Japanese Society of Civil Engineers (JSCE 1989), wherein the overall durability performance is numerically scored using surrogate durability indices.

So far, a unanimous definition of durability has not been available. The ACI Committee 201 (ACI 2002) defines durability of concrete structure as the "*ability to resist weathering action, chemical attack and abrasion, or any other process of deterioration while maintaining its desired engineering properties."* Without exposure to any deterioration environment, an intact reinforced concrete structure is supposed to maintain durable eternally. However, two inevitable factors seriously impact the durability of reinforced concrete structures. First, numerous initial flaws existing in concrete, including a variety of multi-scale micropores and microcracks, make the concrete vulnerable to various deterioration processes, however perfectly the concrete is mixed, cast, placed and cured. Second, the resistance capability of a reinforced concrete structure against deterioration is impaired monotonically with time, and the structure will decay gradually while exposed to surrounding aggressive environments. Therefore, the durability of reinforced concrete can be thought of as controlled by both its intrinsic microstructure and its exposure to aggressive environments. The service life of a reinforced concrete structure is assumed to terminate when its resistance capability under

given working conditions has deteriorated to such an extent that design requirements cannot be fulfilled.

The deterioration processes can be classified briefly into three main groups, i.e. physical processes, chemical processes and mechanical processes (Mehta 1993, Mehta and Monteiro 2001). Physical deterioration processes may include temperature variation and the associated thermal expansion/contraction, relative humidity variation and the associated drying shrinkage/wetting expansion, freezing and thawing cycles (i.e. frost attack), wear and abrasion etc. Chemical deterioration processes usually consist of corrosion of reinforcement embedded in concrete, chloride penetration, carbonation, leaching of concrete constituents, acid attack, sulfate attack, and alkali-aggregate reaction etc. Mechanical deterioration processes generally comprise of externally applied overload or impact, cyclic fatigue loads, differential settlement of foundation, seismic activity and so on. All these deterioration processes are able to alter the porosity and permeability of concrete, cause or aggravate various material flaws (such as scaling and spalling, swelling and debonding, cracking and disintegration), impair the integrity and tightness of concrete structure, and lower the loading capacity of structural member.

The knowledge of concrete durability comes mainly from practical field observations, and it is difficult to experimentally simulate the joint impact of several coupled deterioration processes in the laboratory. The physical and chemical deterioration processes of reinforced concrete structures are so closely interconnected and mutually intensified that distinguishing any single deterioration process from the joint impact

becomes impossible. The aforementioned classification of deterioration processes makes sense only to clarify the deterioration mechanisms of concrete individually. Now that individual deterioration processes have been studied extensively in the past, a major current challenge is how to develop an integrated computational methodology to quantitatively assess the durability of reinforced concrete structures subjected to a variety of coupled deterioration processes simultaneously.

Maekawa (1999) observed that the microstructure of concrete governs its mechanical properties and resistance capability against various deterioration processes with respect to long-term durability. The intact microstructure of hardened concrete prior to deterioration depends mainly on the mix proportion of concrete components, the hydration maturity of cement, the initial and curing conditions etc. The physical characteristics of all concrete components including aggregate, the hydrated cement paste (hcp) matrix, and the interface transition zone (ITZ) differ greatly from each other. From the viewpoint of material science, the microstructure of concrete is highly heterogeneous and time-varying, which makes it extremely difficult to develop an exact microstructure model to predict the resistance capability of concrete against various deterioration processes. In spite of the difficulty, some attempts have been made to develop microstructure models. Among them, three microscopic models, including the NIST model (Benz and Garboczi 1997), the DUCOM model (Meakawa et al. 1999) and the HYMOSTRUC model (Van Breugel 1995, 1998), were proposed to simulate the formation of concrete microstructure and the development of concrete material properties.

However, the main interest of this study focuses mainly on the transport mechanism of various aggressive agents (including heat flow, fluid, gas and chemical ions) through the concrete microstructure, where concrete can be regarded as a network of interconnected and disconnected micropores and microcracks distributed randomly in a solid matrix. Therefore, it is possible to simulate the transport processes of aggressive agents through concrete using macroscopic models, where the spatially average transport properties of concrete are characterized over a specified local volume. In other words, the hardened concrete can be represented as a multi-phase isotropic and homogenous porous medium on macroscopic engineering scale without much deviation. Based on this assumption, the governing partial differential equations of mass and momentum conservation are presented in subsequent context to simulate the multiple coupled transport process occurring actually on a microscopic level. The governing equations can be solved numerically in temporal and spatial domains using finite element method. Meanwhile, this assumption conforms to the concept of smeared cracking, which will apply to simulating concrete cracking later.

During the recent years, some macroscopic models have been developed by Schmidt-Dohl and Rostasy (1999a,1999b), Martin-Perez et al. (2001), Bangert et al. (2003), Isgor and Razaqpur (2004), and Maltais et al. (2004) to evaluate the behavior of concrete structures exposed to fully coupled environmental loadings. A series of governing differential equations that characterize the mass/energy balance and

thermodynamic/chemical equilibrium of coupled heat conduction, ionic diffusion, moisture transport and chemical reaction were presented. Finite element/difference methods were utilized to solve the system of interactive and nonlinear governing equations with standard Galerkin procedure. All these macroscopic models were implemented in complex self-programmed computer codes, which still maintain confidential to most researchers. Meanwhile, the mechanical responses of concrete caused by various deterioration mechanisms (including stress, displacement and cracking state), as well as the accelerating effects of cracking on the transport processes of various aggressive agents, have not been considered.

Without any deterioration, the ordinary concrete usually possesses high porosity and low permeability. It should be emphasized that the overall connectivity of the micropore network, instead of the porosity of concrete, controls the transport properties of concrete. In other words, only those interconnected micropores and microcracks in concrete may make contribution to the permeability of concrete and its vulnerability to deterioration. With the decay of durability, more and more initially discontinuous micropores and microcracks grow, bridge and finally form a huge interconnected network of multi-scale pores and cracks. As a result, the permeability of concrete is increased accordingly. In return, the deterioration processes of concrete structure are accelerated further. Fig. 1.1 illustrates this cyclic deterioration mechanism.

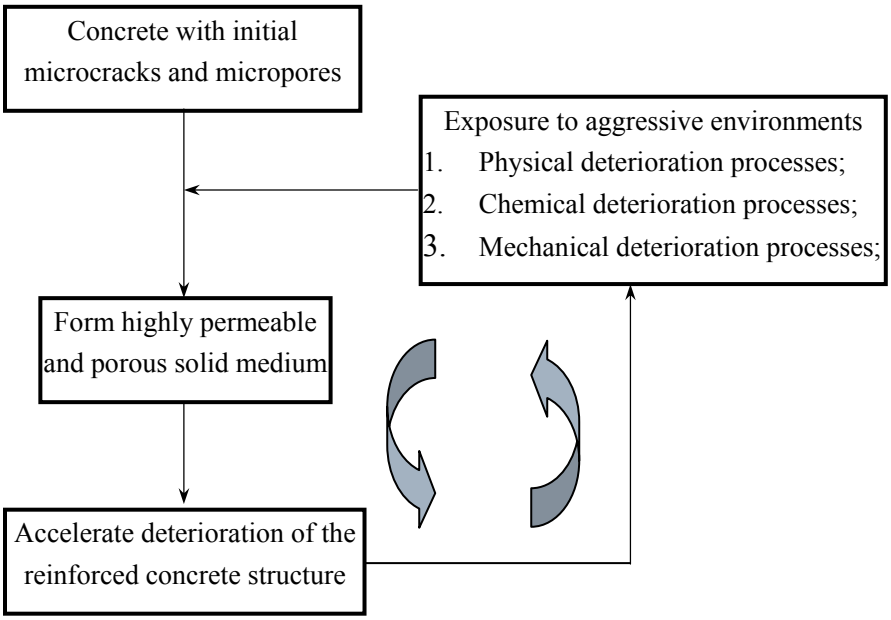

Figure 1.1. Schematic description of cyclic deterioration process

Among various aggressive agents, Mehta and Monteiro (2001) especially emphasize the principal role of water/moisture in affecting the durability of hardened concrete. The tremendous impact of water/moisture may result from three facts. First, water molecules are small enough to penetrate extremely fine pores in concrete microstructure. Second, apart from being a central cause of most physical and chemical deterioration processes, water/moisture also acts as a solvent to dissolve many concrete constituents and as a vehicle to transport most detrimental chemical ions through concrete. Third, the deterioration processes associated with water/moisture movement are controlled by the porosity and permeability of concrete. The Euro-International Committee for Concrete (CEB 1992) thus proposes a design guide for durable concrete structures and summarizes that "*the combined transportation of heat, moisture and chemicals, both within the*

concrete mass and in exchange with the surroundings, and the parameters controlling these transport mechanisms, constitute the principal elements of durability. The presence of water or moisture is the single most important factor controlling the various deterioration processes, apart from mechanical deterioration". The concrete microstructure and the transport mechanisms of various aggressive agents have thus occupied a central position in the assessment of durability of reinforced concrete structures.

In this study, the mechanical response of concrete under various deterioration processes is evaluated as an indicator of durability. In particular, the concept of relative crack density is proposed as a resistance-based index to quantitatively assess the durability of the concrete structure, as explained in Chapter 3. A threshold value of the relative crack density is computed, and the overall service life of the concrete structure is assumed to be terminated once the threshold value is reached.

1.2. Research motivation and objectives

To adequately isolate the radioactive contaminants from contact with the outside ecosphere, several engineered barriers must be designed and built especially between them. For example, at the Savannah River Site (SRS) of U.S. Department of Energy, the basic process of radioactive waste treatment and disposal can be summarized as: First, the high-level radioactive waste stream is solidified as a low-level radioactive solid waste

through the process of saltstone treatment. According to specific mixing proportions, the waste solution is mixed with cementitious materials (including blast furnace slag, fly ash and cement etc.) to form a grout, which solidifies into a dense, microporous and monolithic solid called saltstone. Second, saltstone is deposited in specially designed reinforced concrete engineered facility — Saltstone Disposal Facility (SDF) to prevent the potentially environmental hazards. While the saltstone wasteform provides itself with the primary containment barrier, the underground concrete containment vault in SDF can be considered to serve not only as formwork to cure saltstone mixture but also as secondary containment barrier to prevent the release of matrix constituents. Although specific SDF may be different from site to site, most of them can be represented schematically as shown in Fig. 1.2 (Martin Marietta Energy Systems, Inc. et al. 1992), where an engineered barrier below the ground surface is designed especially to intercept and deflect the surface water from the concrete containment vault.

The integrity and durability of the underground SDF concrete containment vault is extremely important to isolate saltstone from contact with the outside environment. As mentioned before, the reinforced concrete structure may degrade through a combination of coupled physical, chemical, and mechanical deterioration processes. These processes may result in formation and expansion of an interconnected network comprised of multi-scale pores and cracks in concrete, thus increasing the permeability of concrete containment vaults and facilitating the transport of various aggressive agents in concrete. To assess the durability of the underground SDF concrete containment vault and predict

its service life under multiple coupled deterioration processes, it is highly desired to develop an appropriate numerical simulation approach.

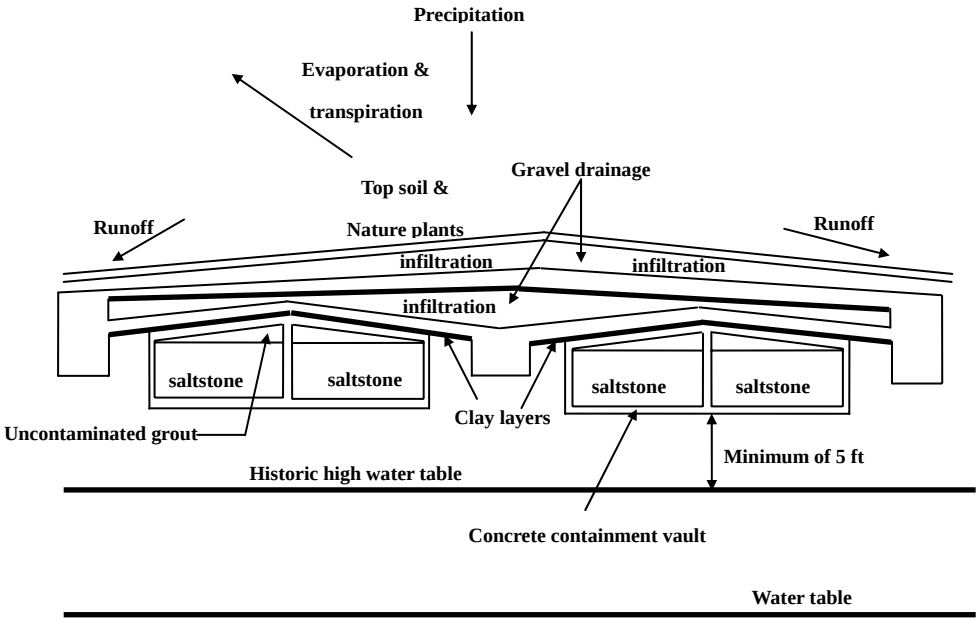

Figure 1.2. Schematic of underground SDF

Thoft-Christensen (2003) classified various deterioration models of concrete structures into three levels. Level 1 model is the empirical model, which is established on the basis of direct observations on existing structural elements instead of investigating deterioration mechanism. Level 1 model has been adopted extensively in current design codes as a rough estimate of the durability level of existing concrete structures. Level 2 model is medium level model from a sophistication viewpoint, which is based on semi-physical or average "material parameters" like concrete permeability and average "loading parameters" like the average chloride content applied on the surface of concrete.

Deterioration mechanisms are assumed to follow some formulated physical principles like Fisk's law. Level 2 model usually limits the deterioration to a single deterioration mechanism. Level 3 model is the most advanced level, where the modeling of the deterioration profile is based on a scientific basis from fundamental physical, chemical and mechanical viewpoint. Detailed information on concrete microstructure and applied environmental loading is required, and multiple coupled deterioration processes can be taken into account simultaneously. Although developing a level 3 model is very time-consuming and computationally expansive, more and more researchers are making contributions in this direction.

The overall goal of this study is to develop a finite element-based computational framework for integrating concrete durability and risk analysis methods, considering multiple coupled physical, chemical and mechanical deterioration mechanisms. Developing such a durability assessment system emphasizes particularly the transport processes of various aggressive agents through the concrete microstructure, the surrounding environments that concrete structures are exposed to, and the complex coupling mechanisms existing among various deterioration processes. To consider practical reinforced concrete structures with arbitrary geometries and dimensions subjected to randomly varying environmental loadings, finite element analysis is the most appropriate method currently available to perform the quantitative durability assessment. The spatial and temporal distribution of various aggressive agents and the subsequent mechanical responses of concrete structure caused by various detrimental environmental

loadings can be determined and tracked conveniently. Due to a large amount of variability and uncertainty existing in various deterioration processes and the proposed computational framework, the proper approach of assessing structural durability is a unique combination of coupled deterioration modeling with advanced stochastic modeling based on the concepts of structural reliability. Time-dependent reliability analysis will be performed to predict the service life of reinforced concrete structures under predefined environmental loadings. Sensitivity analysis may be performed to quantify the influence of important variables.

To realize the proposed overall goal, a series of objectives are supposed to be attained as follows:

1) A finite element-based computational framework is developed to simulate multiple coupled deterioration processes using the coupled multi-physics analysis solver in commercial finite element software ANSYS, where various coupling effects are considered by adjusting the transport properties of concrete through multifactor law. Typical deterioration processes including heat transfer, moisture transport and carbonation are simulated for illustration.
2) Mechanical stress response caused by multiple coupled deterioration processes is evaluated using the concept of equivalent temperature variation, where quasi-brittle material properties of concrete is considered through proper constitutive relationship model.

3) Smeared cracking approach is incorporated into finite element analysis to simulate the concrete cracking caused by multiple coupled deterioration processes. Based on stress state, relative crack density concept is proposed to characterize the cracking state of entire concrete structure and that of each concrete element. Numerical relationship between relative crack density and transport property of cracked concrete is proposed to accommodate the accelerating influence of concrete cracking on various deterioration processes.

4) The developed computational framework is utilized for illustration to simulate the chloride-induced reinforcement corrosion process, where the chloride penetration process is modeled by following an analogous transient thermal analysis, while the reinforcement rust expansion process is transformed into an equivalent time-dependent radial displacement boundary condition applied on the concrete-steel interface. Concrete cracking simulation is implemented using smeared cracking method. The service life of reinforced concrete structures exposed to chloride contaminant can thus be determined.

5) A risk assessment framework is developed to perform the time-dependent reliability analysis through combining response surface with Monte Carlo Simulation. Response surface is developed by combining full-factorial experimental design with multi-level regression. Sensitivity analysis is implemented to quantify the influence of important variables on durability of concrete structures.

1.3. Assumptions and limitations

In this study, a first attempt is made to integrate various highly nonlinear deterioration processes by utilizing existing FEA solver in commercial software. The potential limitations of the proposed computational framework, due to various model assumptions and approximate capturing of micro-scale and chemical phenomena, are summarized as follows.

1) Each deterioration mechanism is characterized using a transport process of a typical aggressive agent. The transport process is assumed to follow a governing differential equation, and the finite element method is used to numerically solve the differential equation. As an approximate approach, the finite element method may lead to errors in the simulation results, and convergence analysis is required.

2) It should be emphasized that only the mechanical responses due to chemical deterioration processes, instead of the micro-scale chemical deterioration phenomena, are modeled in this study.

3) Due to the limitation of commercial finite element software, the ability is currently lacking to model multiphase transport mechanisms that exist even in a single deterioration process. Therefore, only one dominant transport mechanism is identified under some assumptions to characterize that particular deterioration process, while other transport mechanisms are ignored for the sake of simplicity.

4) Mechanical stress response of concrete is highly dependent on the assumed

constitutive relationship model.

5) Mechanical cracking response of concrete is highly dependent on the assumed failure criterion. A smeared cracking approach is used to model concrete cracking, which has some intrinsic limitations (e.g., the sensitivity to mesh size etc.).

6) The effect of relative crack density on transport properties of the cracked concrete is only conceptually formulated here, and needs to be verified and quantified with experimental work in a future study.

7) Various potential coupling effects are considered by adjusting the transport properties of concrete through a multifactor law. As a simplistic assumption, the multifactor law may become inapplicable to highly nonlinear and correlated couplings existing among multiple deterioration processes.

8) Multiple coupled deterioration processes, including heat transfer process, moisture transport process, carbonation process, chloride penetration process, reinforcement corrosion and rust expansion process, and the subsequent concrete cracking process, are considered in this study. In the process of developing and illustrating the proposed computational framework, different combinations of coupled deterioration processes are taken into account. Different assumptions are adopted for the sake of illustration only, when modeling the same transport process for different types of deterioration in different chapters. Realistic application of the proposed framework needs to make these assumptions consistent.

9) As a preliminary attempt to quantitatively assess the concrete durability, the proposed computational framework needs to be verified/validate further through either experimental results or available literature.

In view of these limitations, the proposed computational framework only provides a first-level approximate estimate of concrete durability. More refined computational modeling may be necessary for detailed and accurate estimation. The main contribution of this study is to develop a finite element-based computational framework to quantitatively assess the durability of concrete, by integrating multiple deterioration processes.

1.4. Layout of the dissertation

In Chapter 1, the research significance of durability assessment of reinforced concrete structures under coupled physical, chemical, and mechanical deterioration processes is elaborated first, where the transport processes of various aggressive agents through the concrete microstructure, the surrounding environments concrete structures are exposed to, and the complex coupling mechanisms existing among various deterioration processes are emphasized especially. Then, the research motivation is presented as to isolate typical low level radioactive waste (LLW) — saltstone from contact with the outside environment and to guarantee the integrity and durability of the underground SDF concrete containment vault. The potential limitations of the proposed

computational framework due to various model assumptions and approximate capturing of micro-scale and chemical phenomena are summarized. Finally, the research objective is clarified as to develop an integrated risk assessment framework and apply it to quantitatively evaluate the time-dependent physical durability of reinforced concrete structures subjected to multiple coupled deterioration mechanisms.

In addition to externally applied mechanical loading, various environmental loadings, such as variation of ambient temperature, fluctuation of relative humidity, and exposure to chemically detrimental substances, etc., may cause progressive deterioration of concrete structures. In Chapter 2, a preliminary finite element-based computational framework is developed to simulate the coupled thermo-hydro-chemical-mechanical deterioration processes occurring in concrete. Three main coupled deterioration processes — heat transfer and associated thermal expansion/contraction, moisture transport and associated wetting expansion/drying shrinkage, carbon dioxide transport and associated carbonation — are simulated simultaneously for illustration using FEA solver in commercial software, where the temporal and spatial distribution of resultant stress in plain concrete caused by the joint impact of the coupled deterioration processes can be evaluated.

In Chapter 3, a smeared cracking approach is proposed to simulate the concrete cracking caused by the coupled heat transfer and moisture transport processes. Meanwhile, the quasi-brittle mechanical properties of concrete material and a 3-D stress state-based failure criterion are introduced to determine the initiation and propagation of

concrete cracking. The cracking state of each concrete element in finite element model is described using an original concept — the local relative crack density (LRCD). Furthermore, a numerical relationship between LRCD and the moisture transport property of cracked concrete element is proposed to consider the accelerating influence of cracking propagation on moisture transport. Finally, a global relative crack density (GRCD) is suggested to denote the cracking state of the entire concrete structures, which may serve as an appropriate index to evaluate the overall deterioration level of the structure. Therefore, the developed finite element-based computational framework in Chapter 2 is expanded further to implement the simulation of cracking propagation. An analytical basis for quantitative durability assessment of concrete structures is thus established.

As one of the major deterioration mechanisms for reinforced concrete structures exposed to marine environment or deicing salts, the chloride-induced reinforcement corrosion process has been studied over the past decades. To illustrate the finite element-based computational framework developed in Chapters 2 and 3, Chapter 4 implements the simulation of chloride penetration process and predicts the evolution of chloride content profile in concrete. The influences of the chloride binding capacity of concrete, the age of concrete, the local chloride content, the temperature, and the crack density on the transport rate of chloride are taken into consideration simultaneously by adopting a multifactor law.

Following the chloride penetration phase as elaborated in Chapter 4, the

chloride-induced reinforcement corrosion process is continued by two subsequent phases — the reinforcement rust expansion and the concrete cracking. Chapter 5 focuses mainly on implementing the simulation of the subsequent two phases. A chloride-induced reinforcement rust expansion model is proposed on the basis of Faraday's law, and the rust expansion is represented as an equivalent time-varying radial displacement boundary condition in finite element analysis. Two established corrosion rate model — the constant model and the dynamic model — are included to simulate the rust expansion and the associated concrete cracking process using the smeared cracking approach. Simulation results are presented for a reinforced concrete slab exposed to a constant chloride environment.

In Chapter 6, on the basis of the previously established deterministic computational framework, a risk assessment system is developed to predict the probabilistic service life of reinforced concrete structures and assess its time-dependent structural reliability when exposed to chloride contaminants. To include the effect of various random uncertainties in concrete material, modeling parameters and external environmental loadings, several influential random variables in the deterministic computational framework are identified. Based on the statistics information of random variables available from literature, nonlinear response surface is constructed through combining full-factorial experimental design and multilevel regression models. Monte Carlo simulation is then performed to predict the probabilistic service life and time-dependent reliability of reinforced concrete structures. Sensitivity analysis is carried out to quantify the influencing extent of each

random variable and identify the most influential one.

In Chapter 7, general conclusions are summarized. Important issues concerning the application of the developed computational framework to assess the time-dependent durability of underground SDF concrete containment vault are discussed, and other future research needs are outlined.

CHAPTER II

MECHANICAL STRESS ANALYSIS UNDER COUPLED DETERIORATION PROCESSES

2.1. Introduction

Various environmental loadings, such as variation of ambient temperature, fluctuation of relative humidity, exposure to chemically detrimental substances etc., cause progressive deterioration of concrete structures. The long-term durability of concrete is to a large extent governed by the resistance of concrete against various physical and chemical deterioration processes. The interactions between these deterioration processes are becoming increasingly necessary to be considered in durability assessment.

The deterioration of concrete structures caused by various environmental loadings has been studied extensively for several decades. Considerable literature is focused mainly on experimental study of various deterioration phenomena. As the design concerns of concrete structures have extended gradually from conventional strength-oriented requirements to allow for durability-oriented demands, many empirical models have been proposed to quantify the degradation effects of various deterioration processes. However, each empirical model usually characterizes a single deterioration process, without considering the interactions with other deterioration processes.

Moreover, various empirical models are limited to individual observation or experimental environments, and thus difficult to apply to more practical conditions, where reinforced concrete structures with arbitrary geometries and dimensions are subjected to randomly varying environmental loadings.

Finite element-based numerical simulation may be efficient in accounting for the highly interactive and nonlinear nature of the coupled transport processes of various aggressive agents, which governs the deterioration of concrete structures. With the rapid development of computer technology, numerical simulation has found more and more extensive application in modeling various deterioration processes. During recent years, some attempts have been made to assess the durability performance of concrete structure under multiple coupled deterioration mechanisms. Basheer et al. (2001) reviewed various degradation mechanisms in concrete and assessed the concrete durability qualitatively from its permeation properties. Ishida and Maekawa (2000) developed a systematic numerical framework to predict the hydration evolution of cementitious material, the formation of concrete microstructure, and the transport of moisture and various chemical ions through concrete exposed to arbitrary environmental conditions. This framework concentrates more on characterizing early age concrete. Xi et al. (2000) presented a multiscale model to describe the diffusion-related deterioration processes of concrete using a set of differential equations. It remains relatively premature to realize the proposed multiscale model in 3-D space with finite element codes for practical engineering applications. Schmidt-Dohl and Rostasy (1999) proposed an incremental

model in time and space domains to simulate the combined chemical reactions and transport processes of aggressive agents in concrete, which can be updated to finite element model. In this sense, Martin-Perez et al. (2001) made significant progress in numerical modeling of the coupled migrations of chloride, moisture, heat, and oxygen in concrete using a finite element formulation in space and a finite difference marching scheme in time. However, the subsequent mechanical stress caused by coupled deterioration processes was not taken into account. So it is with Isgor and Razaqpur (2004), who developed a finite element model CONDUR to trace the spatial and temporal advancement of the carbonation front in concrete structures.

So far, most available numerical models utilize various governing differential equations to describe the coupled heat transfer, ionic diffusion, moisture transport and chemical reaction processes, which are based on energy/mass/momentum conservation and thermodynamic/chemical equilibrium. Finite difference or finite element approaches are implemented to numerically solve the complex system of interactive and nonlinear differential equations with standard Galerkin procedure. However, all these numerical models are in self-programmed computer codes specific to the processes considered, which restricts their application to a broad variety of applications. In addition, the analysis of deterioration-induced mechanical stress has not become available, which makes it impossible to evaluate the accelerating influence of cracking on concrete deterioration and predict the service life of concrete structure after cracking.

This study overcomes the above limitations by developing a finite element-based

computational framework using existing FEA solver in commercial software, where the transport processes of various aggressive agents are modeled, while potential coupling effects are considered by adjusting the transport properties of concrete with a multifactor law. All numerical models of various influencing factors are referred to available reference literature. Three typical deterioration processes — heat transfer and associated thermal expansion/contraction, moisture transport and associated wetting expansion/drying shrinkage, and carbon dioxide transport and associated carbonation are considered herein to illustrate the proposed computational framework. The temporal and spatial distribution of the temperature, moisture content and carbon dioxide content can be determined. Under the coupled physical and chemical deterioration processes, local stress may be generated and accumulated in concrete when bulk expansion/shrinkage is restrained. Since concrete is weak in tension, the deterioration-induced mechanical stress may lead to initiation, growth and propagation of cracks. Thus, it is necessary to perform the transient analysis of the deterioration-induced mechanical stress, which forms the basis of service life prediction for concrete structures. Implemented with existing FEA solver, the proposed methodology can be utilized for a wide variety of practical applications, and can be expanded further to include additional deterioration processes.

2.2. Individual deterioration processes and related coupling effects

Before performing the simulation of the multiple coupled deterioration processes in

concrete structures, it is necessary to discuss the numerical modeling of each deterioration process. Based on the simulation of each deterioration process and the consideration of various couplings between them, the computational framework of simulating coupled deterioration processes is then developed.

2.2.1. Heat transfer and associated thermal expansion/contraction

As early as in 1973, Emerson (1973) made an attempt to calculate the temperature distribution in concrete bridges. Based on the principle of energy conservation, the heat transfer process is governed by Fourier's law as follows:

$$div\left[k \cdot grad(T)\right] + \dot{Q}(t) = \rho c \frac{\partial T}{\partial t} \tag{2.1}$$

where k is the thermal conductivity of concrete (W/m · ^{0}C), T is the temperature of concrete (^{0}C), ρ is the density of concrete (kg/m^3), c is the specific heat capacity of concrete (J/kg · ^{0}C), and $\dot{Q}$ is the heat source/sink term (J/m^3 concrete · s).

Considering that no heat source/sink exists in hardened concrete, the heat source/sink term $\dot{Q}$ can be ignored in this study. The thermal conductivity, density and specific heat capacity of concrete may vary with the relative humidity and temperature distribution in concrete. However, the influence is too small to be considered especially, which has been assumed by Martin-Perez et al. (2001) and Isgor and Razaqpur (2004). In this sense, the

governing differential equation of heat transfer may be solved as a linear problem without considering any potential influence caused by moisture transport and carbonation.

The relationship between temperature variation and the associated mechanical strain (i.e., thermal strain) can be expressed as follows:

$$\varepsilon_{thermal} = \alpha \cdot \Delta T \tag{2.2}$$

where $\varepsilon_{thermal}$ is the thermal strain, α is the thermal expansion coefficient (/^{0}C), and ΔT is the temperature gradient (^{0}C). The corresponding thermal stress can be obtained from the assumed constitutive model, which characterizes a nonlinear stress-strain relationship. It should be emphasized herein that creep/relaxation may exert considerable influences on the mechanical stress responses of concrete. To simplify the entire analysis and focus on mechanical stress responses caused by coupled heat transfer and moisture transport processes only, the influences caused by creep/relaxation are ignored in this study. The simulation of heat transfer and the associated thermal stress may be performed using the transient thermal-stress analysis, which is available in most existing commercial finite element codes, including ANSYS.

2.2.2. Moisture transport and associated wetting expansion/drying shrinkage

Various aggressive agents may transport through the interconnected network

comprised of multiscale micropores, microcracks and voids in concrete. Moisture is continuously transported through concrete in the combined form of liquid and vapor. As a primary agent for generation and decomposition of concrete constituents, moisture plays a central role in impacting the durability of concrete. In a porous solid like concrete, water may facilitate numerous physical deterioration processes. Besides being a vehicle for the transport of aggressive chemicals, water can also act as a source for chemical reactions and subsequent deterioration.

Mills (1985) regarded moisture transport through concrete either as coherent flow or water vapor, which depends on the characteristics of concrete microstructure and the relative humidity in concrete pores. Bentz et al. (1999) reviewed the state-of-the-art literature on the measurement of different transport properties of moisture, and proposed some empirical models to determine the moisture permeability. Perre and Turner (1999) developed a macroscopic drying model to simulate coupled heat and mass transfer processes in porous media.

Based on the pore relative humidity and the microstructure of concrete (including porosity, pore size scale, pore connectivity and pore saturation etc.), different transport mechanisms of moisture, such as convection, diffusion, desorption and adsorption, and capillary suction etc., may apply individually or simultaneously. Walton et al. (1990) simplified the complex mechanisms of moisture transport and summarized that the diffusion mechanism usually dominates the transport of moisture in concrete. To simplify the problem, this study follows this idea and describes the moisture transport process

using Fick's second law based on the principle of mass conservation as follows:

$$div\left[D_m \cdot grad(W)\right] + \dot{Q}_m(t) = \frac{\partial W}{\partial t} \tag{2.3}$$

where D_m is the moisture diffusivity (m^2/s), W is the free moisture content in concrete (m^3/m^3 of concrete), $\dot{Q}_m$ is the source term of moisture content, which may represent the generation rate of moisture content due to the coupled carbonation reaction (m^3/m^3 of concrete · s). The amount of water content consumed by hydration reaction is assumed to be very small and therefore ignored. The numerical modeling of moisture transport is essentially a nonlinear problem, with the moisture diffusivity dependent on various factors such as pore humidity, temperature, and carbonation-induced reduction of porosity etc.

The hydrostatic gradient of pore moisture in concrete serves as a driving force not only for the moisture transport but also for the associated bulk shrinkage/expansion (Granger et al. 1997). In view of practical environment where the pore relative humidity of concrete usually remains above 50%, the drying shrinkage is assumed to be proportional to the loss of moisture content (Granger et al. 1997, McDonald and Roper 1993, Torrenti et al. 1999), and a coefficient of proportionality β — the hydral contraction coefficient, an equivalent concept to the thermal expansion coefficient α — is introduced especially to calculate the coupled strain induced by the fluctuation of moisture content in concrete. Thus, the relationship between moisture content variation

and the associated mechanical strain (i.e., wetting expansion/drying shrinkage strain) can be expressed as:

$$\varepsilon_{shrinkage} = \beta \cdot (W - W_0) \tag{2.4}$$

where $\varepsilon_{shrinkage}$ is the shrinkage strain, β is the hydral contraction coefficient (m^3 of concrete/m^3), W_0 is the initial free moisture content (m^3/m^3 of concrete). The corresponding wetting expansion/drying shrinkage stress can be obtained from the assumed constitutive model.

Considering the analogy between the governing differential equation of the heat transfer process and that of the moisture transport process, it is possible to simulate the moisture transport process and the associated drying stress in concrete by following the transient thermal analysis procedure, which is available in commercial multi-purpose finite element codes. The physical parameters in the heat transfer process correspond to those in the moisture transport process as: for the main field variable, the temperature T maps to the free moisture content W; for the transport property, the thermal conductivity k maps to the moisture diffusivity D_m; for the associated mechanical response, the thermal expansion coefficient α maps to the hydral contraction coefficient β; for the source/sink term, the generation rate of water due to carbonation reaction $\dot{Q}_m$ maps to the heat source/sink term $\dot{Q}$.

Since the moisture diffusivity depends to a large extent on the free moisture content,

a numerical model suggested by Xi et al. (1994) is adopted herein:

$$D_m(h) = A\left\{\theta + \psi\left[1 - 2^{-10^{\gamma(h-1)}}\right]\right\} \tag{2.5}$$

where h is the pore relative humidity in concrete, which is expressed as a fraction; and A, θ, ψ and γ are undetermined model parameters. Following Torrenti et al. (1999), these parameters assume values of A = 7.0E-10 m^2/s, θ = 0.05, ψ = 0.4 and γ = 4. The numerical model is illustrated in Fig. 2.1, where the moisture diffusivity of concrete increases with the pore relative humidity.

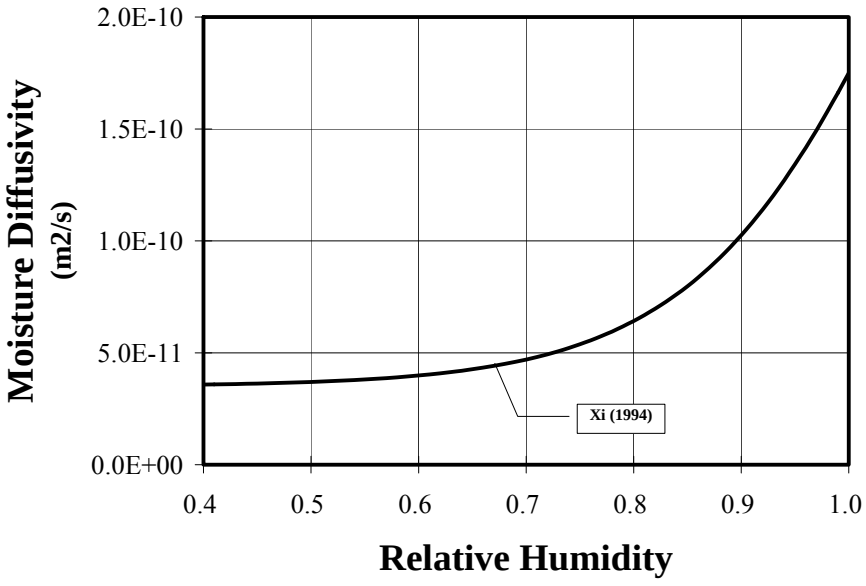

Figure 2.1. Relationship between moisture diffusivity and pore relative humidity

Eq. (2.5) can be reduced further to

$$D_m(h) = A\theta\left\{1+\frac{\psi}{\theta}\left[1-2^{-10^{\gamma(h-1)}}\right]\right\} = D_{m,0}\cdot F_1(h) \tag{2.6}$$

where $D_{m,0} = A\theta = 3.5\times10^{-11}$ m^2/s may be regarded as the reference moisture diffusivity under an imaginary situation with zero pore relative humidity. $F_1(h)$ represents the influencing factor of pore relative humidity on the moisture diffusivity as:

$$F_1(h) = 1+\frac{\psi}{\theta}\left[1-2^{-10^{\gamma(h-1)}}\right] \tag{2.7}$$

The influencing factor of the pore relative humidity $F_1(h)$ is illustrated in Fig. 2.2, where $F_1(h)$ increases with the pore relative humidity of concrete.

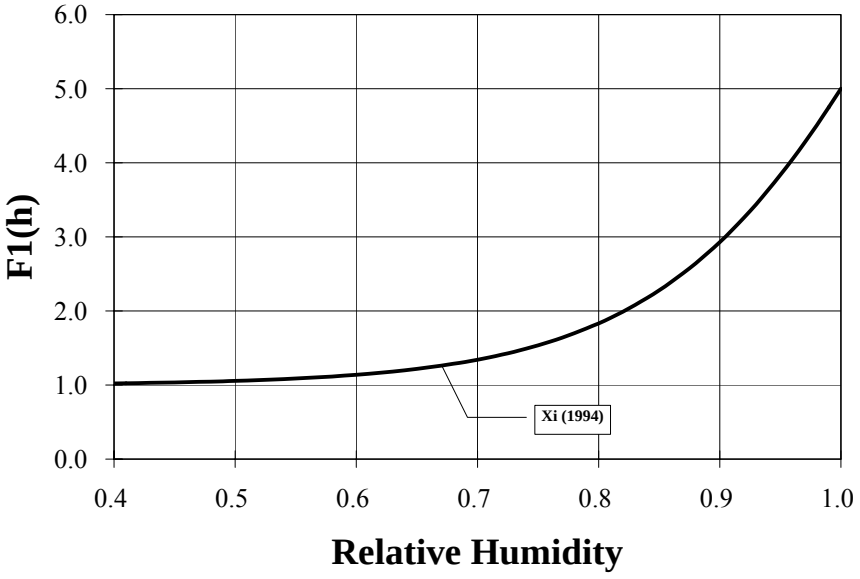

Figure 2.2. Influence of pore relative humidity on moisture diffusivity

To relate the free moisture content to the pore relative humidity, various desorption isotherm curves (Pihlajavaara 1982, Baroghel-Bouny 1994) were proposed in the past. Kumaran (1996) proposed a numerical relationship as follows:

$$\frac{W}{W_0} = \left(1 - \frac{\ln h}{B}\right)^{-\frac{1}{C}} \tag{2.8}$$

where the free moisture content at saturation $W_0 = 128.8 \times 10^{-3}$ (m^3/m^3 of concrete), model parameters B = 0.57, C = 0.64. The numerical relationship between the relative free moisture content W / W_0 and the pore relative humidity h is thus illustrated in Fig. 2.3, where the relative moisture content increases with the pore relative humidity.

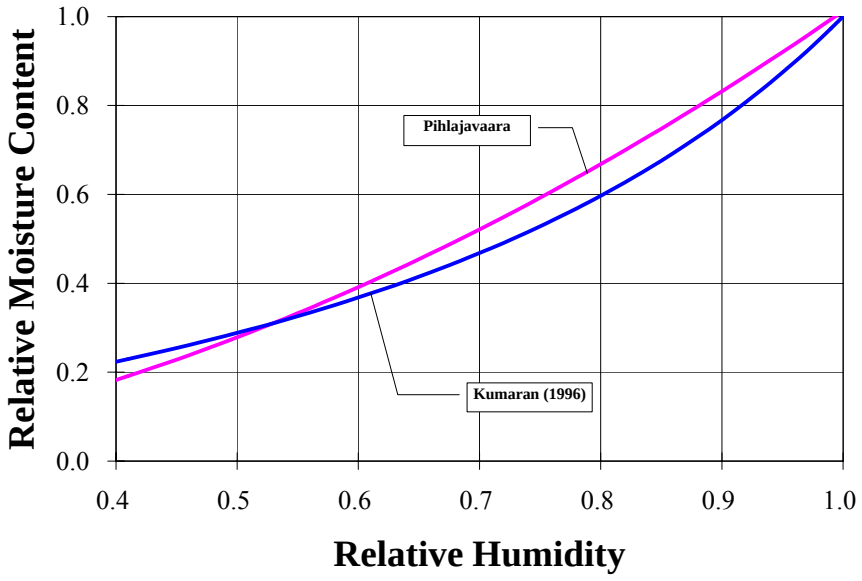

Figure 2.3. Relationship between moisture content and pore relative humidity

Combining Eqs. (2.6) and (2.8), the diffusivity of moisture D_m can be expressed implicitly as a function of free moisture content W in concrete.

Next, we consider the influence of temperature and carbonation on moisture diffusivity. Fig. 2.4 indicates the coupling effects induced by the fluctuation of relative humidity, variation of temperature and degree of carbonation reaction.

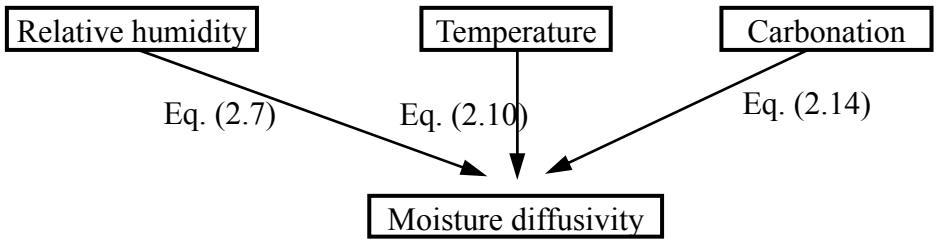

Figure 2.4. Influencing factors on moisture diffusivity

Adopting the multifactor law proposed by Bazant and Najjar (1972), the above coupling factors can be reflected by extending Eq. (2.6) as follows

$$D_m(h) = D_{m,0} \cdot F_1(h) \cdot F_2(T) \cdot F_3(\xi) \tag{2.9}$$

where $F_1(h)$ has been defined earlier in Eq. (2.7) and illustrated in Fig. 2.2.

Based on Saetta et al. (1995), the influencing factor of temperature takes the form

$$F_2(T) = \exp\left[\frac{E}{R}\left(\frac{1}{T_{ref}} - \frac{1}{T}\right)\right] \tag{2.10}$$

where E is the activation energy of the moisture diffusion process (= 2700 J/mol), R = 8.314 (J/mol · K) is the gas constant, T_{ref} is the reference temperature at which the reference diffusivity of moisture $D_{m,0}$ is determined (296.8 K), and T is the actual absolute temperature in concrete (K). The influencing factor of temperature $F_2(T)$ is illustrated in Fig. 2.5, where moisture diffusivity increases with temperature.

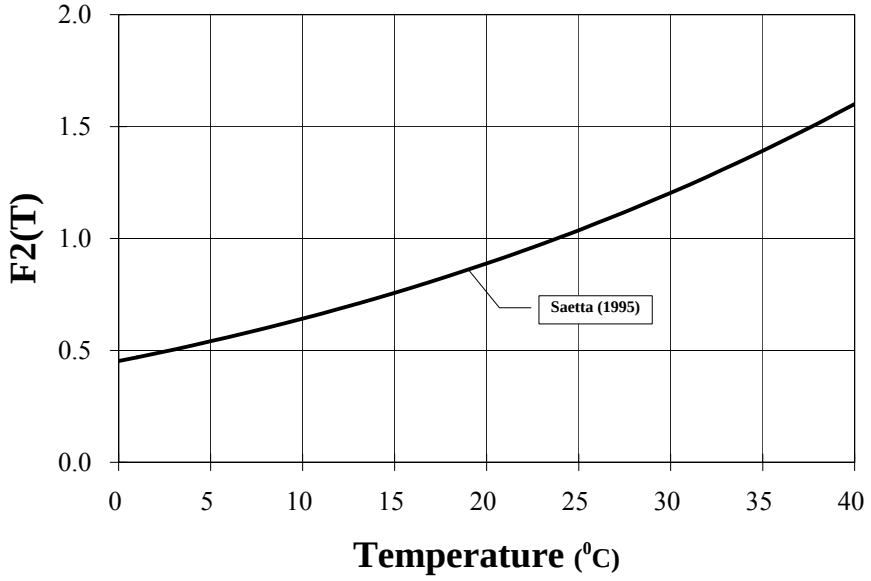

Figure 2.5. Influence of temperature on diffusivity

The influencing factor of carbonation-induced reduction of porosity $F_3(\xi)$ will be elaborated in Section 2.2.3 below.

2.2.3. Carbon dioxide transport and associated carbonation

Papadakis et al. (1991) presented a comprehensive review of the carbonation process. Steffens et al. (2002) predicted the reinforcement corrosion of concrete structures using a numerical carbonation model. Isgor and Razaqpur (2004) developed a nonlinear finite element program to trace the spatial and temporal advancement of carbonation front in concrete structures. In this study, the governing differential equation for the diffusion of carbon dioxide in concrete, which is based on the principle of mass conservation, is expressed as:

$$div\left[D_c \cdot grad\left(C_c\right)\right] + \dot{Q}_c = \frac{\partial C_c}{\partial t} \tag{2.11}$$

where D_c is the diffusivity of carbon dioxide (m^2/s), C_c is the concentration of free carbon dioxide (kg/m^3 of concrete), $\dot{Q}_c$ is the sink term of CO_2 content that represents the consumption rate of CO_2 due to the carbonation reaction (kg/m^3 of concrete $\cdot$ s).

Unlike physical deterioration processes such as the heat transfer and moisture transport processes discussed previously, carbonation of concrete is essentially a chemical deterioration process. As the hydration product of Portland cement, calcium hydroxide in concrete may react with carbon dioxide dissolved in pore solution, neutralize its high alkalinity environment, and finally result in depassivation of the passive layer and initiation of reinforcement corrosion — one of the major deterioration mechanisms for

reinforced concrete structure. Meanwhile, as the main product of the carbonation reaction, calcium carbonate will not dissolve in water but precipitates in the pores of concrete, thus decrease the porosity of concrete and alter its microstructure. In this case, carbonation reaction may be favorable to maintain the durability of plain concrete.

Based on an assumption that the carbonation front advances after the alkaline material (i.e., calcium hydroxide) has been neutralized completely, the carbonation process is dominated by the diffusion of carbon dioxide through the porous microstructure of concrete, where the concentration gradient of carbon dioxide acts as a driving force. As a neutralization reaction, the carbonation process generates a specific amount of moisture, which may affect the temporal and spatial distribution of moisture content in concrete and should be considered in the simulation of previous moisture transport process. To develop a numerical model for carbonation, several coupled processes, namely the diffusion of carbon dioxide, moisture transport, heat transfer, formation of calcium carbonate, availability of calcium hydroxide in the pore solution etc., should be considered simultaneously.

Following the multifactor law, the diffusivity of CO_2 is assumed to be dependent on the pore relative humidity, temperature and the carbonation-induced reduction of porosity as follows (Saetta et al. 1995):

$$D_c = D_{c,0} \cdot F_1^*(h) \cdot F_2(T) \cdot F_3(\xi) \tag{2.12}$$

where $D_{c,0} = 3 \times 10^{-8}$ m^2/s may be regarded as the diffusivity of uncarbonated concrete under reference relative humidity and temperature. Fig. 2.6 indicates the coupling effects induced by the fluctuation of relative humidity, variation of temperature and degree of carbonation reaction.

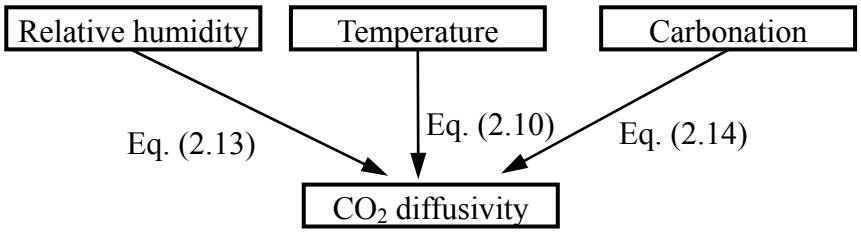

Figure 2.6. Influencing factors on CO2 diffusivity

According to Saetta et al. (1995), the influencing factor of pore relative humidity $F_1^*(h)$ takes the following form

$$F_1^*(h) = (1-h)^{2.5} \tag{2.13}$$

which is illustrated in Fig. 2.7, where the diffusivity of CO_2 decreases with the relative humidity. Considering that high pore relative humidity restricts the diffusion of CO_2 through concrete microstructure, the numerical model is reasonable.

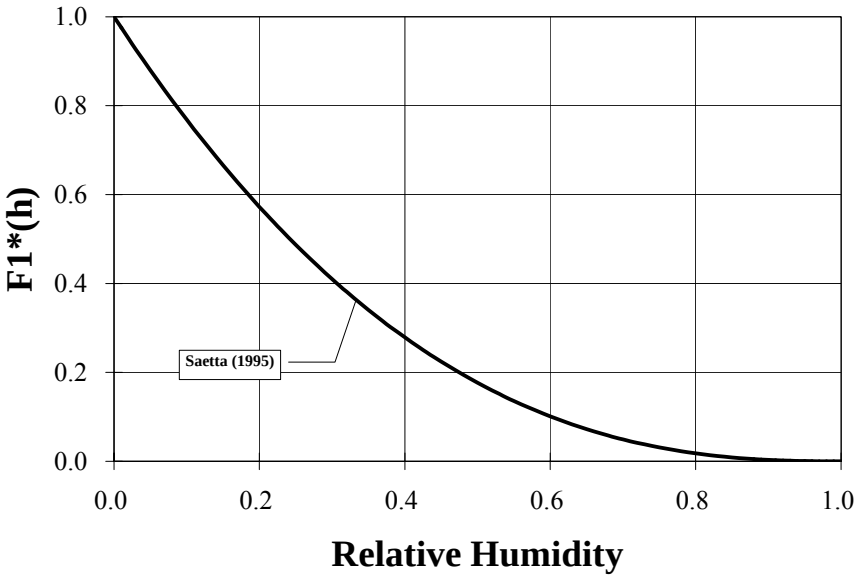

Figure 2.7. Influence of relative humidity on diffusivity of CO_2

As to $F_2(T)$ and $F_3(\xi)$, Saetta et al. (1995) proposed the identical influencing factors of temperature and carbonation for both moisture diffusivity and CO_2 diffusivity, which are adopted in this study. $F_2(T)$ has been described earlier in Eq. (2.10), where CO_2 diffusivity increases with temperature.

The influencing factor of the carbonation-induced reduction of porosity $F_3(\xi)$ proposed by Saetta et al. (1995) is very similar to a decay function proposed by Isgor and Razaqpur (2004), when an undetermined coefficient ζ is assumed a value of 0.5. In this case, the decay function $F_3(\xi)$ is adopted herein:

$$F_3(\xi) = \begin{cases} 1-\xi/1.8 & 0 \le \xi \le 0.90 \\ 0.50 & 0.90 \le \xi \le 1.0 \end{cases} \tag{2.14}$$

where ξ is the degree of carbonation, its definition will be discussed later. The numerical model is illustrated in Fig. 2.8, where CO_2 diffusivity decreases with the degree of carbonation due to the generation of calcium carbonate and the subsequent reduction of porosity.

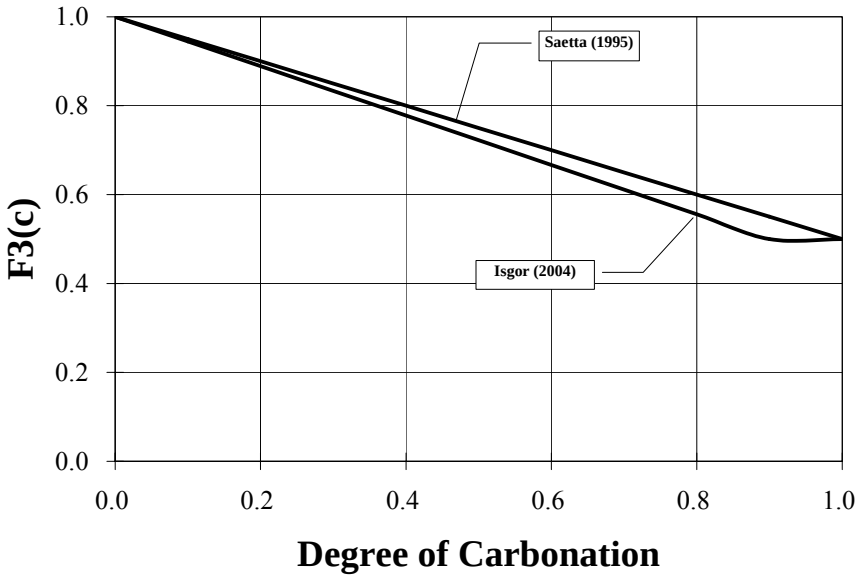

Figure 2.8. Influence of carbonation on diffusivity

Meanwhile, the sink term $\dot{Q}_c$ due to carbonation-induced consumption of CO_2 may be derived from the chemical and thermo-dynamical balance in pore solution, where all carbonation-related coupled processes should be considered simultaneously. Saetta et al. (1993, 1995, 2004) proposed such a numerical model of carbonation reaction rate as follows:

$$\upsilon_r = \upsilon_0 \cdot f_T \cdot f_h \cdot f_c \cdot f_R \tag{2.15}$$

where $\upsilon_0 = 2.80 \times 10^{-7}$ /s · mol indicates an ideal carbonation rate at which the carbonation reaction takes place in specified ideal conditions, f_T, f_h, f_c, and f_R represent the influences of temperature, relative humidity, concentration of free CO_2, and degree of carbonation on the reaction rate, respectively.

f_T describes the influence of temperature using the Arrhenius equation

$$f_T = \exp(-\frac{E_0}{RT}) \tag{2.16}$$

where E_0 is the activation energy of the carbonation process (= 91.52 kJ/mol), R is the gas constant (= 8.314 J/mol · K), and T is the actual absolute temperature (K).

f_h is introduced to consider the influence of the relative humidity

$$f_h = \begin{cases} 0 & 0 \le h < 0.5 \\ 2.5(h-0.5) & 0.5 \le h \le 0.9 \\ 1 & 0.9 \le h \le 1 \end{cases} \tag{2.17}$$

Carbonation reaction may occur only in presence of moisture. For almost dry concrete ($h \le 0.5$), carbonation is assumed to be terminated.

f_c represents the influence of the concentration of free CO_2 as

$$f_c = \frac{C_c}{C_{c,\max}} \tag{2.18}$$

where $C_{c,\max}$ is the maximum concentration of free CO_2 available in pore solution (kg/m^3 of concrete).

f_R reflects the influence of the degree of carbonation ξ as

$$f_R = 1 - \xi \tag{2.19}$$

With the progress of carbonation, the porous microstructure of concrete can be filled with deposited calcium carbonate, which decelerates the carbonation reaction.

In view of an atmospheric CO_2 concentration of 0.0012 kg/m^3 (corresponding to 0.06% vol.), Saetta and Vitaliani (2004) expressed the sink term $\dot{Q}_c$, or the consumption rate of CO_2 due to carbonation reaction, as follows:

$$\dot{Q}_c = \eta_c \cdot \upsilon_r \tag{2.20}$$

where $\eta_c = 0.733$ is the carbonation and CO_2 transport interaction coefficient.

The degree of carbonation ξ can be defined as the fraction of CO_2 that has been consumed by carbonation reaction as

$$\xi = \frac{\int_0^t \dot{Q}_c d\tau}{Q_{c,\max}} = \frac{\sum \dot{Q}_c \cdot \Delta t}{Q_{c,\max}} \tag{2.21}$$

According to Steffens et al. (2002), the maximum amount of CO_2 that may combine with reactive alkali is derived as

$$Q_{c,\max} = 0.0052 \cdot C \cdot \left([CaO] - 3.2 \right) \tag{2.22}$$

The CaO composition for ordinary Portland cement is about $[CaO] \approx 64\,\%$, and the cement concrete of concrete is assumed to be C = 350 kg/m^3. As a result, $Q_{c,\max}$ assumes a value of 110 kg/m^3.

As a measurable response species in solid phase, carbonate is steadily generated and precipitated in pores of concrete during the carbonation reaction. As the reactive alkali in concrete is exhausted completely, the concentration of carbonate reaches its maximum and the concrete is assumed fully carbonated. Therefore, the concentration of carbonate may serve as an indicator of the degree of carbonation.

Saetta and Vitaliani (2004) also suggested the varying rate of the pore relative humidity due to the carbonation-induced moisture generation as follows:

$$\dot{h} = \eta_m \cdot \upsilon_r \tag{2.23}$$

where $\eta_m = 0.002$ is the carbonation and freed moisture transport interaction coefficient.

Based on the proposed desorption isotherm model shown in Eq. (2.8), the corresponding source term in the governing differential equation for moisture transport $\dot{Q}_m$, i.e., the generation rate of carbonation-induced moisture content, can be obtained as follows:

$$\dot{Q}_m = \dot{W} = \frac{\left(1 - \frac{\ln h}{B}\right)^{-\frac{C+1}{C}}}{BCh} \cdot \dot{h} \tag{2.24}$$

Considering the analogy between the governing transport equation of the heat transfer process and that of the CO_2 diffusion process, it is also possible to simulate the CO_2 diffusion process in concrete by following the transient thermal analysis procedure. The physical parameters in the heat transfer process correspond to those in the CO_2 diffusion process as: for the main field variable, the temperature T maps to the CO_2 concentration C_c; for the transport property, the thermal conductivity k maps to the CO_2 diffusivity D_c; for the source/sink term, the consumption rate of CO_2 due to carbonation reaction $\dot{Q}_c$ maps to the heat source/sink term $\dot{Q}$.

Now that the simulation procedures for individual deterioration processes have been discussed, the next task is to combine all three deterioration processes and include the potential couplings between them.

2.3. Multiple coupled deterioration analysis procedure

In this section, a finite element-based computational framework is developed to simulate the aforementioned three coupled deterioration processes using existing FEA solver in commercial software (ANSYS, used for illustration), where each deterioration process is defined as an individual physics environment. The physics environment functions like an independent module, where all related finite element types, geometric model, constant material properties, fixed boundary conditions and loads, as well as meshing of solid model for one specific physics field (such as temperature field, moisture content field, and CO_2 concentration field etc.) are defined accordingly. Next, a coupled multi-physics analysis method is utilized to call each physical environment in turn, apply the time-dependent loads and material properties, and then perform the transient analysis of heat transfer, moisture transport and CO_2 diffusion processes iteratively within each time step. Each time step is divided into a number of substeps, which may vary with each physics environment and each time step. An automatic time stepping scheme (i.e. adaptive loading) is adopted to ensure the substep size is appropriate to achieve desired convergence. To account for the potential couplings between various deterioration processes, the output of one transport process at the i^{th} time step may be applied as input variable to modify the transport properties of another transport process at the next $(i+1)^{th}$ time step through the multifactor law. The flowchart of the simulation procedure of

multiple coupled degradation processes is shown in Fig. 2.9. A self-programmed code in ANSYS Parametric Design Language (APDL) is required to implement the proposed computational framework.

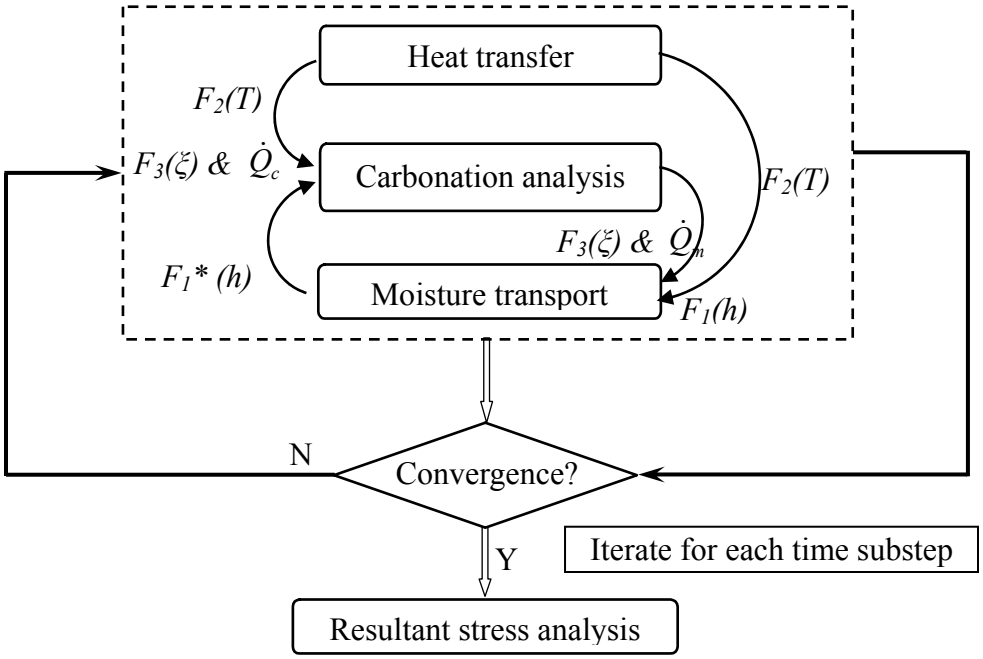

Figure 2.9. Multiple coupled-field analysis procedure

As indicated previously in Eqs. (2.9), (2.12) and (2.15), moisture transport and carbonation processes are coupled with each other, and both processes are affected by the heat transfer process. Due to the insensitivity of thermal properties of concrete, the heat transfer process is solved independently without considering the influences of other two deterioration processes. As a result, the multiple coupled-field analysis is performed in the following manner. For each time step, perform the transient thermal analysis first to obtain the spatial temperature distribution, where the nodal temperature is stored in an

array A. After considering the couplings in Eq. (2.12) caused by temperature, relative humidity, and carbonation degree, the carbonation analysis is performed to determine the spatial distribution of CO_2 concentration, where the nodal CO_2 concentration is stored in an array B. Meanwhile, according to the numerical model of carbonation reaction rate in Eq. (2.15), the carbonation-induced CO_2 consumption rate $\dot{Q}_c$ and the moisture generation rate $\dot{Q}_m$ can be computed and stored in two arrays B_SINK and C_SOURCE, respectively. They will be applied as source/sink terms to carbonation and moisture analysis for next time step, respectively. With the consideration of couplings in Eq. (2.9) caused by temperature, relative humidity and carbonation degree, the moisture transport analysis is performed to obtain the spatial distribution of moisture content, where the nodal moisture content is stored in an array C.

To ensure the computational convergence after considering couplings, within each time step the carbonation analysis and moisture transport analysis may need to be performed iteratively until the variation of the source/sink term is small enough to satisfy a desired convergence criterion. In this study, the convergence criterion ϖ can be expressed as

$$\left| \frac{\phi^{i+1} - \phi^{i}}{\phi^{i}} \right| \leq \varpi \tag{2.25}$$

where ϕ^{i+1} is the sink/source term at the $(i+1)^{th}$ time step, ϕ^{i} is that at the i^{th} time

step.

Finally, perform resultant mechanical stress analysis caused by the three coupled deterioration processes to obtain the spatial distribution of stress at each time step. Since the carbonation process will not induce stress directly, only thermal stress and shrinkage stress are considered. To assess the resultant stress, the variation of moisture content obtained in moisture analysis can be transformed into an equivalent temperature variation in thermal analysis. The transformation relationship can be expressed as

$$\Delta T_{equiv} = \frac{\beta}{\alpha} \cdot \Delta W \tag{2.26}$$

where ΔT_{equiv} is the equivalent temperature variation, and ΔW is the variation of moisture content.

It is known that the deterioration-induced stress may cause concrete cracking, and cracking will accelerate the concrete deterioration. The influence of cracking on various deterioration processes will be addressed in the next chapter.

2.4. Numerical simulation example

A plain concrete block 0.1m long, 0.1m wide, and 0.05m thick is selected herein to illustrate the proposed finite element-based computational framework. The total time length is assumed to be one year, which is divided uniformly into 365 time steps with up

to 30 substeps for each time step. The averaged duration of each time step is small enough to guarantee a balance between computation convergence and efficiency. The proposed finite element model is shown in Fig. 2.10.

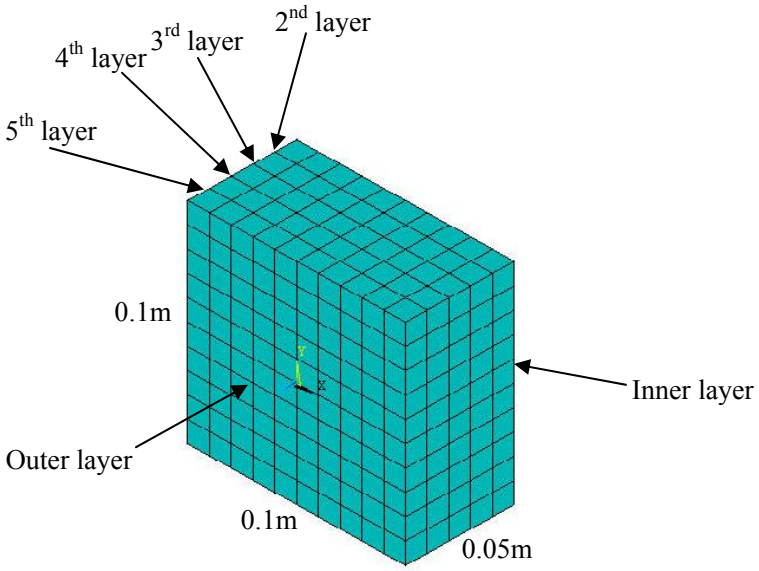

Figure 2.10. Finite element model

To consider the seasonal variation of ambient temperature, the annual variation of ambient temperature can be assumed as a sinusoidal function by following Saetta et al. (1995)

$$T_{ambient} = 15 + 10 \cdot \sin(2\pi \cdot t) \tag{2.27}$$

where $T_{ambient}$ is the ambient temperature (^{0}C), and t is time elapsed (year).

Similarly, to consider the seasonal variation of ambient relative humidity, the annual variation of ambient relative humidity can be expressed as a sinusoidal function

$$h_{ambient} = 0.65 + 0.25 \cdot \sin(2\pi \cdot t) \tag{2.28}$$

where $h_{ambient}$ is the ambient relative humidity, and t is time elapsed (year).

The time-dependent temperature and relative humidity boundary conditions formulated in Eqs. (2.27) and (2.28), as well as a constant atmospheric CO_2 concentration of 0.0012 kg/m^3 of concrete, are enforced on the outer layer of the plain concrete block. On the inner layer, a constant temperature of 15 ^{0}C, a constant relative humidity of 65% and zero CO_2 concentration are applied. For the whole concrete block, the initial temperature is assumed to be constant 15 ^{0}C, while the initial relative humidity is assumed 100% (i.e., saturation), and the initial degree of carbonation is zero. Meanwhile, the four side surfaces of the concrete block are assumed to be isolated from any heat/moisture/CO_2 flux. In addition, structural displacements in all three orthogonal directions are restrained on the four side surfaces as structural boundary conditions.

Concrete is a quasi-brittle material and behaves differently in tension and compression states. The tensile strength of concrete is typically 10% of its corresponding compression strength. Fig. 2.11 shows a typical constitutive relationship curve for normal weight concrete (Bangash 1989).

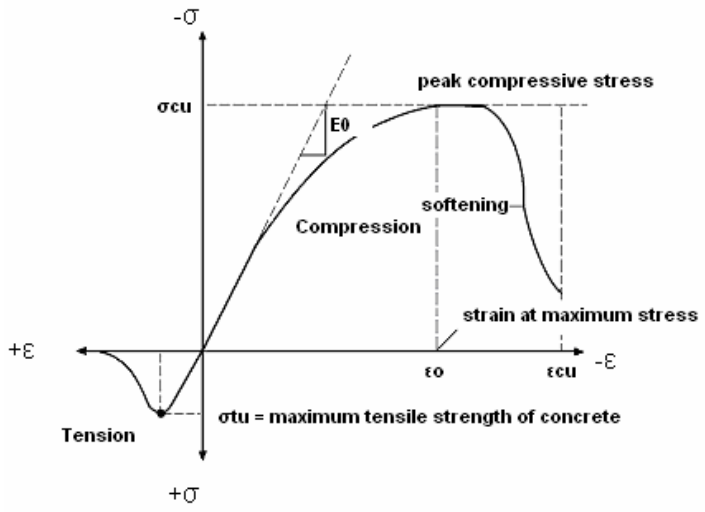

Figure 2.11. Typical constitutive relationship for concrete

In compression, the constitutive relationship curve for concrete is linearly elastic up to about 30% of the maximal compressive strength σ_{cu}. Above this point, the curve enters a strain hardening region while stress increases nonlinearly up to the maximal compressive strength. After it reaches the maximal compressive strength, the curve descends into a strain softening region, and eventually crushing failure occurs at the ultimate strain ε_{cu}. The post-peak response reflects the ductility of concrete, which depends strongly on the level of lateral confinement enforced on concrete. In tension, the constitutive relationship curve for concrete is approximately linearly elastic up to the maximal tensile strength σ_{tu}. After this point, the concrete cracks and the tensile strength decreases rapidly to zero (Bangash 1989).

To determine the mechanical response of concrete, ANSYS requires the uniaxial stress-strain relationship for concrete. Developing an appropriate constitutive relationship

model for concrete is challenging, and substantive efforts have been made to propose various numerical models in the past (Hognestad 1951, Desayi and Krishnan 1964). A perfectly plastic model — Druker-Prager model — is chosen in this study, where the ascending part of the constitutive relationship curve follows the Desayi and Krishnan model (Bangash 1989) as

$$\sigma = \frac{E_c \varepsilon}{1 + (\varepsilon / \varepsilon_0)^2} \tag{2.29}$$

where $\varepsilon_0 = \frac{2 f_c^{'}}{E_c}$ and E_c is the elastic modulus, $f_c^{'}$ the maximal compressive strength.

After the ultimate compressive strength $f_c^{'}$ is reached, a perfectly plastic behavior is assumed till the crushing failure occurs at the ultimate strain ε_{cu}. According to European Concrete Committee (Bangash 1989), the ultimate strain ε_{cu} may be assumed as 0.003. As to the uniaxial tensile constitutive relationship, a linear elastic model can satisfy the simulation requirement, and the strain softening phase after the maximal tensile strength f_t can be neglected without much error. Therefore, the proposed uniaxial constitutive model in this study is shown in Fig. 2.12 below.

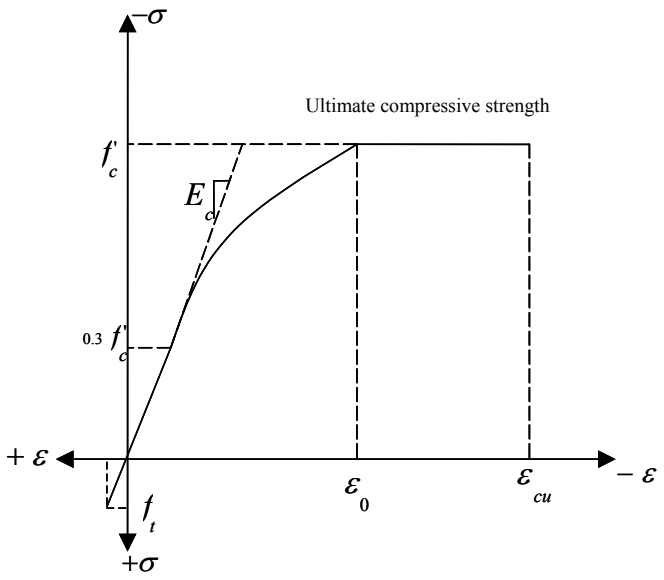

Figure 2.12. Uniaxial constitutive model

An 8-node 3-D thermal element SOLID70 with one temperature DOF at each node is selected for the simulation of heat transfer, moisture transport, and carbon dioxide diffusion processes. For subsequent mechanical stress analysis, a corresponding 8-node 3-D concrete element SOLID65 with three translation DOFs at each node is selected. The concrete element SOLID65 will be discussed in details in Chapter 3. The assumed material properties for the concrete in this example are summarized in Table 2.1.

Unless stated otherwise, the concrete considered in this study is normal structural concrete built with a continuous cement paste matrix and normal weight aggregates, and it achieves a compressive strength in an intermediate range of commonly observed values in practice. As a macroscopic model, the computational framework does not require concrete composition information. Rather, it only uses macroscopic material properties listed in Table 2.1. In contrast, a microscopic model would be more focused on material

composition effects. Internal factors, i.e., material parameters (including w/c ratio, cement content etc.) may exert considerable influence on mechanical responses of concrete. However, this study focuses only on analyzing the mechanical responses of concrete induced by external factors — various environmental loadings instead of internal factors.

Table 2.1. Material properties of concrete

Material properties	Value adopted
Compressive strength†	$f_c^{'} = 30$ MPa
Tensile strength†	$f_t = 3$ MPa
Strain at peak stress†	$\varepsilon_0 = 0.002$
Ultimate strain†	$\varepsilon_{cu} = 0.003$
Elastic modulus†	$E_c = 30$ GPa
Poisson's ratio†	$\nu = 0.2$
Density†	$\rho = 2400\,\text{kg/m}^3$
Thermal conductivity†	$k = 2.0$ W/m·K
Specific heat capacity†	$c = 1000$ J/kg·K
Thermal expansion coefficient†	$\alpha = 1.0 \times 10^{-5}$ /K
Hydral contraction coefficient††	$\beta = 9.96 \times 10^{-3}$ m^3 of concrete/m^3 of moisture

† Courtesy of Mehta (1993)

†† Courtesy of Torrenti et al. (1999)

The simulation results of the multiple coupled deterioration processes are

summarized in the following Figs. 2.13~2.21. The time-varying temperature, free moisture content, CO_2 concentration, and the first principal stress at the central nodes of six layers, are demonstrated in Figs. 2.13~2.16, respectively (Note that the 1st layer denotes the inner layer, while the 6th layer denotes the outer layer). Then, the time-varying CO_2 sink term (i.e., the CO_2 consumption rate), the degree of carbonation, and the carbonate concentration of the five central elements, which are located from the inner layer to the outer layer in sequence, are shown in Figs. 2.17~2.19, respectively. Finally, the structural displacement contour and the 1st principal stress contour at the final time step are illustrated in Figs. 2.20~2.21, respectively.

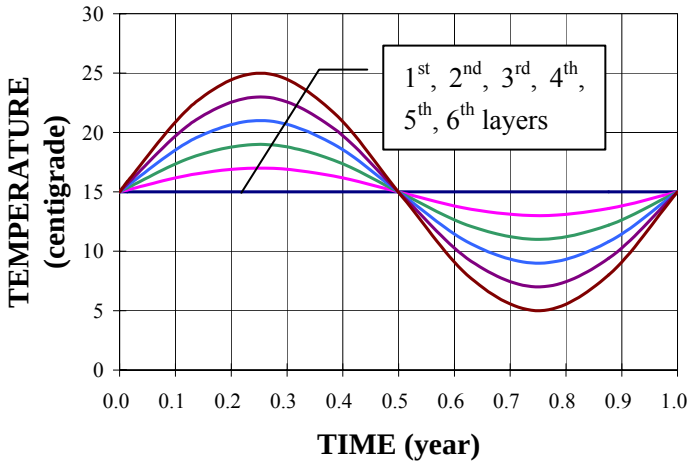

Figure 2.13. Temperature history on six layers

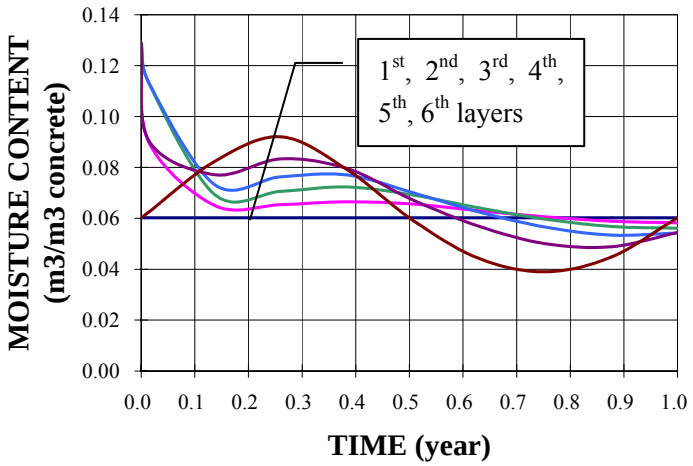

Figure 2.14. Moisture content history on six layers

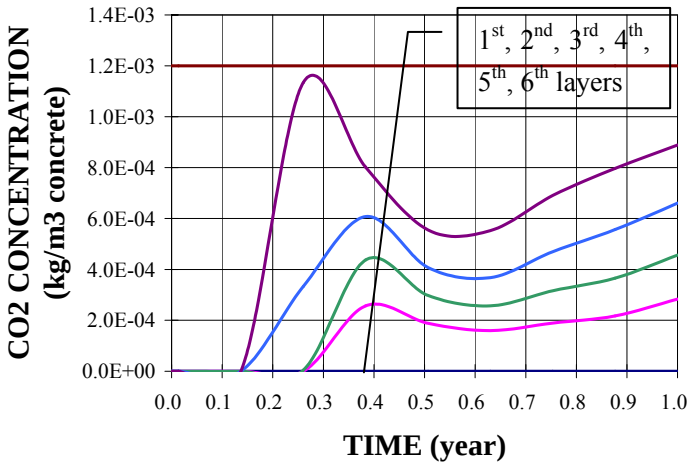

Figure 2.15. CO_2 concentration history on six layers

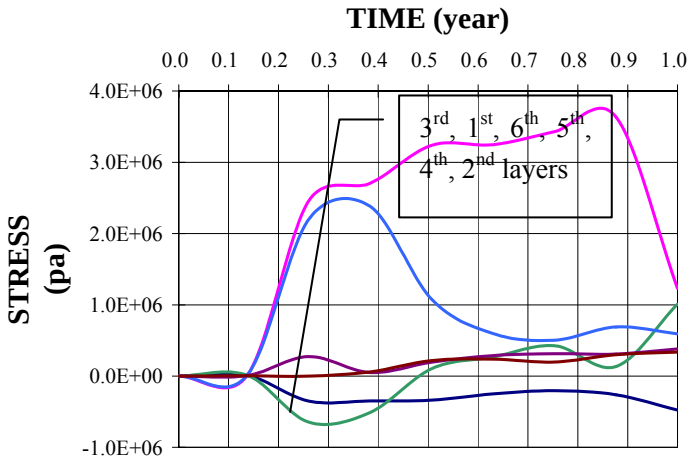

Figure 2.16. 1st principal stress history on six layers

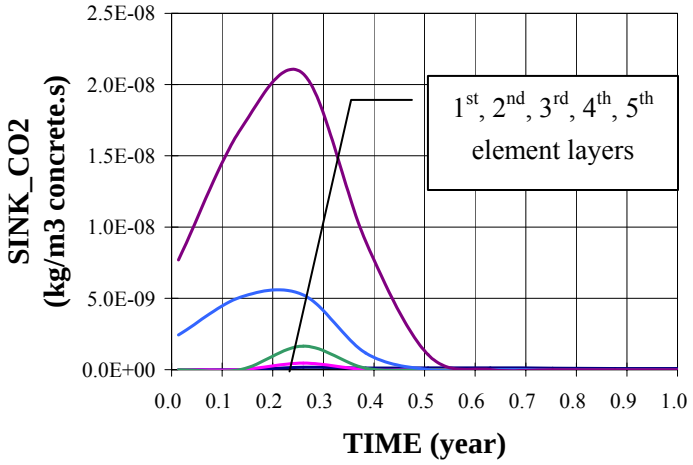

Figure 2.17. CO_2 sink term history on five elemental layers

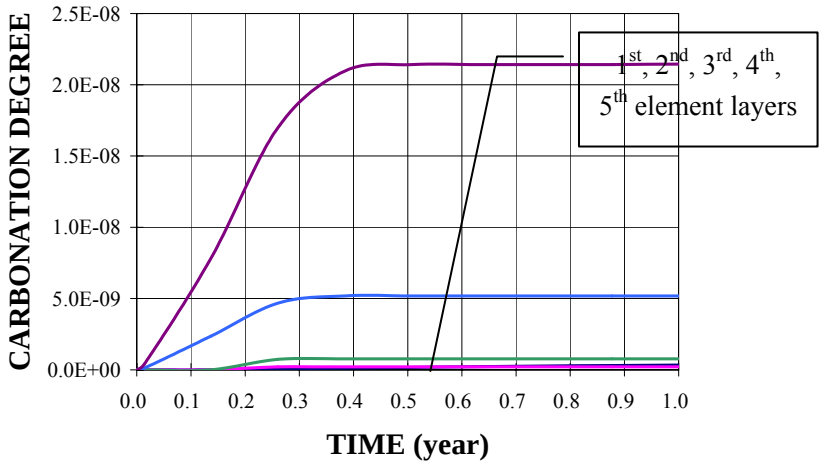

Figure 2.18. Carbonation degree history on five elemental layers

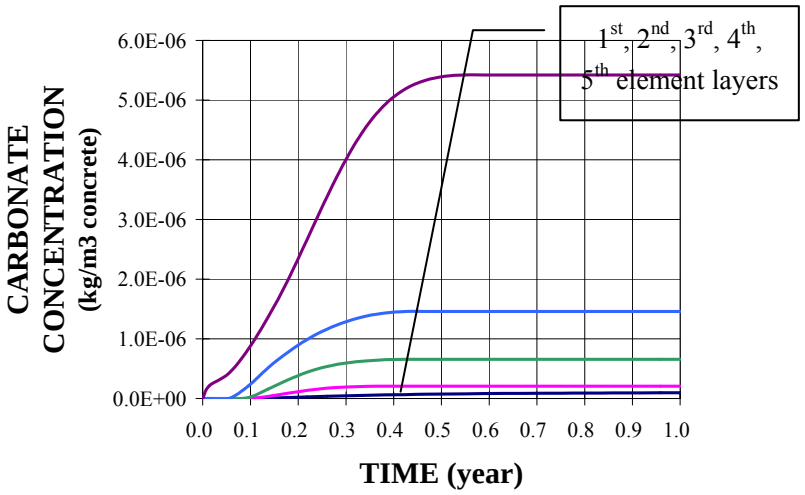

Figure 2.19. Carbonate concentration history on five elemental layers

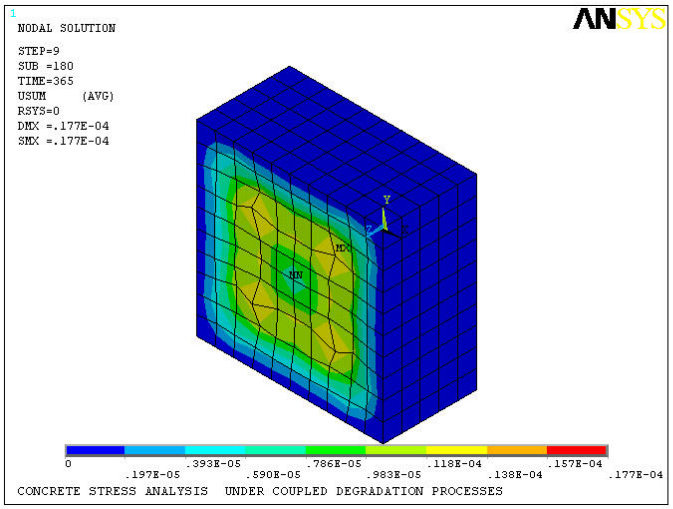

Figure 2.20. Nodal displacement contour at final time step

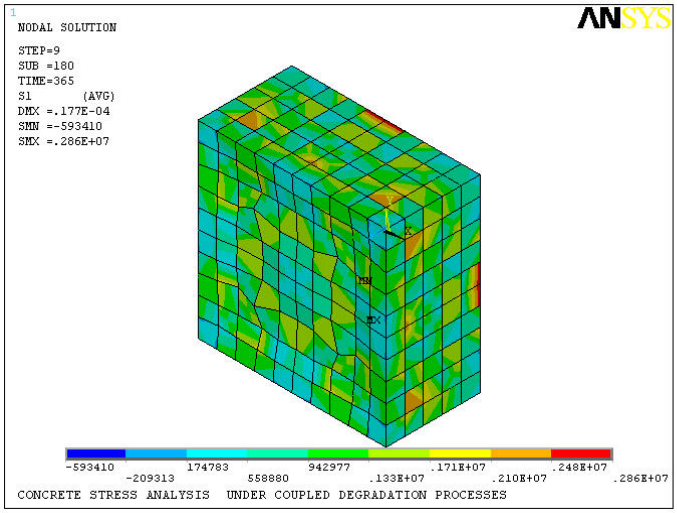

Figure 2.21. 1st principal stress contour at final time step

Since the presented example addresses an approximate one-dimensional problem, and the ambient temperature fluctuates very slowly within one year, the internal temperature can always achieve thermal equilibrium with the ambient temperature. Therefore, a regularly distributed temperature pattern is observed in Fig. 2.13. The nodal temperature history can even be obtained by directly prescribing the temperature fluctuation at the nodes, although this may not necessarily apply to practical concrete structures with arbitrary geometries exposed to randomly ambient temperature.

Due to the low value of moisture diffusivity and the highly coupling and nonlinear natures of moisture transport, the moisture content history curves on different layers in Fig. 2.14 show inconsistent paces with each other. However, it still agrees well with the expectation that moisture content on the layer closer to the outer layer fluctuates more intensively, while all moisture content history curves approximately follow the sinusoidal function of moisture transport boundary condition.

Unlike the moisture transport process, a constant CO_2 concentration boundary condition is applied on the outer layer of the plain concrete block. Without considering various influencing factors, the CO_2 concentration history curves on different layers are supposed to be straight lines with different slopes. The simulation results in Fig. 2.15 reflect the significant influences of heat transfer and moisture transport processes as well as carbonation reaction itself. It can be observed that CO_2 concentration on the layer closer to the outer layer increases faster and fluctuates more intensively, which meets the experience. As indicated in Eqs. (2.13) and (2.17), carbonation can occur only within an

appropriate range of pore relative humidity. This can explain why it will take about 0.14~0.26 year to initiate the carbonation reaction on different layers. In addition, carbonation process usually advances very slowly, and it may even takes hundreds of years to completely carbonate a concrete structural member. The regularly distributed history curves for CO_2 consumption rate, the degree of carbonation and the carbonate concentration in Figs. 2.17~2.19 can confirm the practical observation to a large extent.

So far, the mechanical responses due to coupled deterioration processes, as shown in Figs. 2.16, 2.20 and 2.21, are used only for illustrating the feasibility of the proposed finite element-based computational framework. It should be emphasized here that the stress-induced cracks, the subsequent crack-induced mechanical degradation and stress redistribution have not been considered herein. In this sense, the obtained mechanical stress responses makes theoretical sense only.

Further work may be required to verify the computational framework using available experimental results or reference literature. Compared with the existing numerical models, the prominent advantages of the proposed computational framework can be summarized as follows. Making use of existing FEA solver in commercial software, the methodology is rather straightforward and efficient in simulating multiple coupled transport process of various aggressive agents. This facilitates 3-D simulation for practical concrete structures with arbitrary geometries exposed to randomly varying environmental loadings. Second, the various coupling effects can be taken into account conveniently by adjusting the transport properties of concrete with a multifactor law. Third, plentiful simulation results

— including the spatial distribution of temperature, relative humidity, moisture content, CO_2 concentration, as well as various source/sink terms — can be extracted easily at each time step and be postprocessed further. The obtained information deepens the insight on the deterioration mechanism of concrete structures. Finally, the methodology is flexible and can be expanded to incorporate other deterioration processes as physics environments, thus facilitating the overall assessment of durability and service life of concrete structures under multiple coupled deterioration processes.

2.5. Conclusion

A finite element-based computational framework has been developed in this chapter to simulate the multiple coupled deterioration processes of concrete subjected to various environmental loadings, while potential coupling effects are considered by adjusting the transport properties of concrete with a multifactor law. The temporal and spatial distribution of various aggressive agents as well as the resultant stress caused by the coupled deterioration processes can be determined. Implementation of the entire simulation procedure with existing FEA solver in commercial software allows its application to practical problems, and inclusion of more deterioration processes. The proposed computational framework also forms a basis for simulating the formation and growth of cracks and evaluating their accelerating influence on various deterioration processes.

CHAPTER III

CRACKING ANALYSIS OF CONCRETE UNDER COUPLED DETERIORATION PROCESSES

3.1. Introduction

Most deterioration processes are able to alter the porosity and permeability of concrete, trigger the initiation and growth of cracks, and thus impair the integrity of the concrete structure. With respect to long-term durability, both the microstructure of concrete and the transport mechanisms of various aggressive agents through concrete govern the resistance of concrete against various deterioration processes. Substantial efforts have been dedicated to developing appropriate microstructural models to describe the behavior of concrete under various environment loadings, e.g., the NIST model (Bentz and Garboczi 1997), the DUCOM model (Meakawa et al. 1999) and the HYMOSTRUC model (Van Breugel 1995, 1998). From the viewpoint of material science, the microstructure of concrete is highly heterogeneous and time-varying, which makes it extremely difficult to develop an exact microstructure model to predict the material properties of concrete accurately. However, concrete can be regarded as a network of interconnected and disconnected micropores and microcracks distributed randomly in a solid matrix on a macroscopic engineering scale. Therefore, it is possible to simulate the

transport processes of aggressive agents through concrete using macroscopic models, where the spatially averaged transport behaviors of concrete can be characterized over a specified local volume. In this sense, concrete can be assumed to be a multi-phase homogenous porous medium. Based on this assumption, multiple coupled deterioration processes are characterized using the governing partial differential equations on the basis of energy and mass conservation, which can be solved numerically in temporal and spatial domains using finite element method.

When exposed to various physical, chemical and mechanical deterioration processes, the durability of a concrete structure will decays gradually. With the progressive deterioration of concrete, more and more local stresses may be initiated and accumulated when internal or external deformation constraints exist. Since concrete is weak in tension, the deterioration-induced local stress may eventually cause the initiation, growth and linking of microcracks, and finally form a network of interconnected multi-scale cracks. The permeability of concrete is thus increased, and the transport rates of various aggressive agents are accelerated accordingly. In turn, the durability of concrete structure decays further due to the accelerated deterioration processes. This cyclic deterioration mechanism of concrete structures has been illustrated earlier in Fig. 1.1.

A preliminary finite element-based computational framework has been developed in Chapter 2 to simulate coupled thermo-hydro-chemo-mechanical deterioration processes in concrete, where the temporal and spatial distribution of temperature, moisture content and other aggressive agents in concrete can be tracked, and the resultant stress

distribution induced by the multiple coupled deterioration processes can be evaluated. In this chapter, the computational framework is expanded further to perform the simulation of crack initiation and propagation caused by coupled heat transfer and moisture transport processes, i.e., the thermal cracking and drying shrinkage cracking. An original concept based on the 3-D stress state of integration points in each finite element — the local relative crack density (LRCD) — is introduced to denote the cracking state of the concrete element. Furthermore, a numerical relationship between LRCD and the transport property is proposed to take into account the accelerating influence of crack propagation on the moisture transport process. Finally, another analogous concept — the global relative crack density (GRCD) — is suggested to indicate the cracking state of the entire concrete structure, which may serve as an appropriate index to evaluate the overall deterioration level of the concrete structure.

3.2. Smeared cracking analysis of concrete

Ngo and Scordelis (1967) first introduced the effect of cracking into the finite element analysis of reinforced concrete structures. Since then, numerous researchers (Alfaiate et al. 1997; DeBorst 1997; Loo and Guan 1997) have made substantive contributions in this field. There usually exist two finite element-based approaches to simulate the concrete cracking — discrete cracking approach and smeared cracking approach.

Based mainly on fracture mechanics (Shah et al. 1995; Bazant and Planas 1998), the

discrete cracking approach regards the crack propagation as the result of stress singularity or strain energy release at the tip of crack. Cracks are treated directly as geometric discontinuities, where the intact portion of concrete is generally assumed to behave elastically, while the crack propagation is modeled by changing the topology of the finite element model. The separation of two crack faces may be accomplished by introducing additional duplicate nodes and remeshing the local domain around the crack. Therefore, adaptive remeshing is required to implement the simulation. Considering that numerous initial microcracks and structural flaws have existed in concrete even before various structural and environmental loadings apply, while deterioration processes usually cause densely and evenly distributed microcracks, it is extremely difficult to implement the simulation of concrete cracking caused by the multiple coupled deterioration processes using the discrete cracking approach.

In the smeared cracking approach, the cracked concrete is described as a fictitious continuum, and the crack propagation is modeled within the continuum framework. Cracks are assumed to be spatially distributed over the entire volume represented by a local finite element, or only by the volume attached to one integration point within the finite element. The stiffness matrix of each concrete element is modified accordingly to accommodate the mechanical deterioration due to cracking. The smeared cracking approach is consistent with the previous assumption that regards concrete as a multi-phase homogenous porous medium. Without changing the topology of finite element model, this approach proves efficient when incorporated in finite element

analysis (Darwin 1993; Kachlakev et al. 2001). When concrete is exposed to the coupled heat transfer and moisture transport processes, the restrained volume change usually result in relatively dense microcracks distributed over the entire concrete volume. Therefore, the smeared cracking approach is a reasonable choice in this study to implement the simulation of crack propagation.

Commercial finite element software ANSYS is adopted herein to simulate the mechanical responses of concrete subjected to multiple coupled deterioration processes, where the uniaxial constitutive model of concrete shown in Fig. 2.12 is adopted.

An 8-node 3-D solid element Solid65 is designed especially for modeling concrete. This concrete element has eight nodes with three DOFs at each node — translations in the nodal x, y and z directions, and eight integration points inside. Based on specified constitutive model and failure criterion, the concrete element allows smeared reinforcement, plastic deformation, cracking in tension in three orthogonal directions, shear transfer capacity, and crushing in compression. The geometry and node locations for the concrete element are shown in Fig. 3.1.

The William and Warnke failure criterion (William and Warnke 1975) under multi-axial stress state is adopted to assess the initiation of failure and identify the corresponding failure modes (including cracking and crushing) at the centroid of a concrete element or one of its integration points. The criterion is expressed uniformly as

$$\frac{F}{f_c^{'}} - S \geq 0 \tag{3.1}$$

where F is a function of the principal stresses, S is the spatial failure surface expressed in terms of the principal stresses and the material properties of concrete, and $f_c^{'}$ is the maximal compressive strength of concrete. Only if Eq. (3.1) is satisfied, will the failure of concrete element or that of its integration points be assumed to occur (ANSYS 2002).

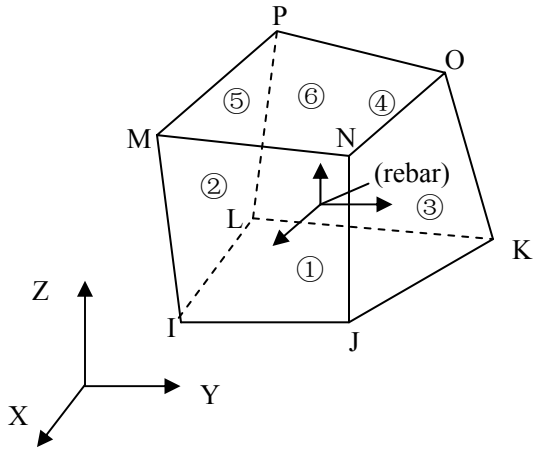

Figure 3.1. SOLID65 concrete element

Fig. 3.2 represents the projection of 3-D failure surface S in biaxial or nearly biaxial stress states. Suppose the most significant nonzero principal stresses are in the x and y directions, represented by σ_{xp} and σ_{yp}, and the three failure surface projections presented are for the third principal stress σ_{zp} slightly greater than zero, σ_{zp} equal to zero, and σ_{zp} slightly less than zero, respectively. The corresponding failure mode is a function of the sign of σ_{zp} (principal stress in the z direction). For example, if σ_{xp} and σ_{yp} are both

negative (compressive) and σ_{zp} is slightly positive (tensile), cracking would be predicted in a direction perpendicular to σ_{zp}. However, if σ_{zp} is zero or slightly negative, the material is assumed to crush.

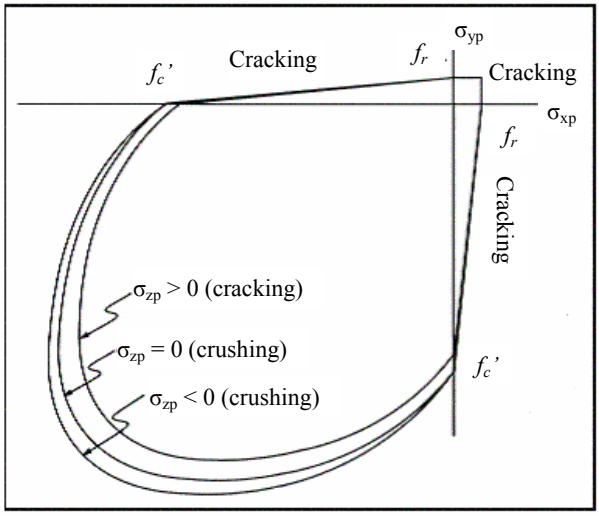

Figure 3.2. Failure surface projection for concrete (ANSYS, 2002)

The above failure surface in Fig. 3.2 can be divided into four domains according to different failure modes as:

1. $0 \geq \sigma_1 \geq \sigma_2 \geq \sigma_3$ (compression – compression – compression)

   Concrete is assumed to be crushed provided Eq. (3.1) is satisfied.

2. $\sigma_1 \geq 0 \geq \sigma_2 \geq \sigma_3$ (tension – compression – compression)

   If Eq. (3.1) is satisfied, cracking will occur in a direction perpendicular to σ_1.

3. $\sigma_1 \geq \sigma_2 \geq 0 \geq \sigma_3$ (tension – tension – compression)

   If Eq. (3.1) is satisfied, the ultimate tensile strength linearly decreases with the drop

of σ_3. Meanwhile, cracking occurs in the planes perpendicular to principal stresses σ_1 or σ_2 separately.

4. $\sigma_1 \geq \sigma_2 \geq \sigma_3 \geq 0$ (tension – tension – tension)

If Eq. (3.1) is satisfied, the ultimate tensile strength assumes f_t. Meanwhile, cracking occurs in the planes perpendicular to principal stresses σ_1, σ_2 or σ_3.

In all above four cases, $\sigma_1 = \max(\sigma_{xp}, \sigma_{yp}, \sigma_{zp})$ is the first principal stress, and $\sigma_3 = \min(\sigma_{xp}, \sigma_{yp}, \sigma_{zp})$ is the third principal stress. Both the function F and the failure surface S take different forms to accommodate corresponding failure modes. As any failure mode occurs, the stiffness matrix of the concrete element is modified accordingly to consider the crack-induced mechanical degradation.

The general stiffness matrix for reinforced concrete element is defined as

$$[D] = \left(1 - \sum_{i=1}^{N_r} V_i^R\right)[D_c] + \sum_{i=1}^{N_r} V_i^R [D_r]_i \tag{3.2}$$

It is noticed in the above Eq. (3.2) that the contributions to the general elemental stiffness $[D]$ made by plain concrete $[D_c]$ and reinforcement $[D_r]$ can be distinguished easily from each other. The smeared reinforcement concept has been adopted implicitly. The reinforcement has stiffness only in its uniaxial direction and is assumed to be smeared over the entire finite element. The stiffness of steel rebars in the uniaxial direction is weighted by its ratio of volume V_i^R.

The stiffness matrix for intact plain concrete element is expressed as:

$$[D_c]=\frac{E_c}{(1+\nu)(1-2\nu)}\begin{bmatrix}(1-\nu) & \nu & \nu & 0 & 0 & 0\\ \nu & (1-\nu) & \nu & 0 & 0 & 0\\ \nu & \nu & (1-\nu) & 0 & 0 & 0\\ 0 & 0 & 0 & \frac{(1-2\nu)}{2} & 0 & 0\\ 0 & 0 & 0 & 0 & \frac{(1-2\nu)}{2} & 0\\ 0 & 0 & 0 & 0 & 0 & \frac{(1-2\nu)}{2}\end{bmatrix} \tag{3.3}$$

where ν is the Possion's ration, and E_c is the elastic modulus of concrete.

If the smeared reinforcement function of concrete element SOLID65 is utilized, for reinforcement *i* in *x* direction within the concrete element, its reinforcing effect to the concrete element can be reflected as

$$\begin{Bmatrix}\sigma^r_{xx}\\ \sigma^r_{yy}\\ \sigma^r_{zz}\\ \sigma^r_{xy}\\ \sigma^r_{yz}\\ \sigma^r_{xz}\end{Bmatrix}=\begin{bmatrix}E^r_i & 0 & 0 & 0 & 0 & 0\\ 0 & 0 & 0 & 0 & 0 & 0\\ 0 & 0 & 0 & 0 & 0 & 0\\ 0 & 0 & 0 & 0 & 0 & 0\\ 0 & 0 & 0 & 0 & 0 & 0\\ 0 & 0 & 0 & 0 & 0 & 0\end{bmatrix}\begin{Bmatrix}\varepsilon^r_{xx}\\ \varepsilon^r_{yy}\\ \varepsilon^r_{zz}\\ \varepsilon^r_{xy}\\ \varepsilon^r_{yz}\\ \varepsilon^r_{xz}\end{Bmatrix}=[D_r]_i\begin{Bmatrix}\varepsilon^r_{xx}\\ \varepsilon^r_{yy}\\ \varepsilon^r_{zz}\\ \varepsilon^r_{xy}\\ \varepsilon^r_{yz}\\ \varepsilon^r_{xz}\end{Bmatrix} \tag{3.4}$$

where E^r_i is the elastic modulus of the reinforcement.

In a concrete element, cracking occurs when the principal tensile stress in any direction exceeds the ultimate tensile strength f_t. After cracking, the elastic modulus of

the concrete element is reduced to zero only in the direction parallel to the principal tensile stress direction. Crushing occurs when all three principal stresses are compressive and the stress state lies outside the failure surface *S*. Subsequently, the elastic modulus is reduced to zero in all directions and the structural integrity is completely degraded (ANSYS, 2002).

Cracking is permitted in three orthogonal directions at the centroid of each concrete element or one of its integration points. As cracking occurs, the stiffness matrix of an initially intact plain concrete element is modified accordingly to accommodate the mechanical degradation, where the cracking is effectively treated as a "virtual smeared band" rather than discrete cracks. The presence of a crack at an integration point of a concrete element is represented by introducing a weakness plane in a direction normal to the crack face. The shear transfer coefficient β_t is introduced particularly to represent a shear strength reduction factor for those subsequent loads that induce slippage across the open crack face. The value of β_t ranges from 0 to 1, where 0 represents a smooth crack and complete loss of shear transfer, and 1 represents a rough crack and no loss of shear transfer. The modified stiffness matrix for concrete element cracked in *x* direction only can be expressed as:

$$\left[D_c^{ck}\right]=\frac{E_c}{(1+\nu)}\begin{bmatrix} R^t(1+\nu)/E_c & 0 & 0 & 0 & 0 & 0 \\ 0 & 1/(1-\nu) & \nu/(1-\nu) & 0 & 0 & 0 \\ 0 & \nu/(1-\nu) & 1/(1-\nu) & 0 & 0 & 0 \\ 0 & 0 & 0 & \beta_t/2 & 0 & 0 \\ 0 & 0 & 0 & 0 & 1/2 & 0 \\ 0 & 0 & 0 & 0 & 0 & \beta_t/2 \end{bmatrix} \tag{3.5}$$

where the superscript *ck* signifies that the constitutive relationships refer to a coordinate system parallel to principal stress directions with the x^{ck} axis perpendicular to the crack face. R^t is the secant modulus as defined in Fig. 3.3, where T_c is the multiplier for the amount of tensile stress relaxation, which can be derived from the fracture energy of concrete G_f as:

$$T_c = \frac{G_f - f_t\varepsilon^{ck}}{5f_t\varepsilon^{ck}} \tag{3.6}$$

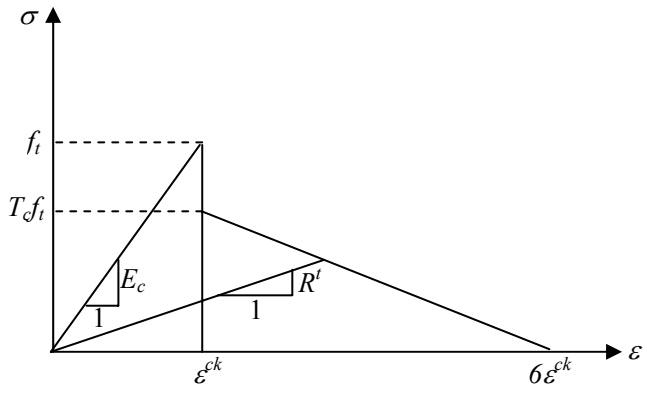

Figure 3.3. Strength of cracked concrete (ANSYS, 2002)

If the crack closes, unlike the tensile stresses, the compressive stresses normal to the

crack plane still can be transmitted across the crack. The shear transfer coefficient β_c applies to a closed crack only, which is usually greater than β_t. The corresponding stiffness matrix for concrete element with closed crack in x direction only can be expressed as

$$\left[D_c^{ck}\right]=\frac{E_c}{(1+\nu)(1-2\nu)}\begin{bmatrix} (1-\nu) & \nu & \nu & 0 & 0 & 0 \\ \nu & (1-\nu) & \nu & 0 & 0 & 0 \\ \nu & \nu & (1-\nu) & 0 & 0 & 0 \\ 0 & 0 & 0 & \beta_c\dfrac{(1-2\nu)}{2} & 0 & 0 \\ 0 & 0 & 0 & 0 & \dfrac{(1-2\nu)}{2} & 0 \\ 0 & 0 & 0 & 0 & 0 & \beta_c\dfrac{(1-2\nu)}{2} \end{bmatrix} \tag{3.7}$$

Cracking is permitted in three orthogonal directions on the centroid of a concrete element or one of its integration points. The open or closed state of a crack in any one direction is determined by the sign of the "crack strain". For the case of a possible crack in direction "1", the crack strain ε_{ck}^{ck} is evaluated as follows:

$$\varepsilon_{ck}^{ck}=\begin{cases} \varepsilon_1^{ck}+\dfrac{\nu}{1-\nu}\varepsilon_2^{ck}+\varepsilon_3^{ck} & \text{If no cracking occurs} \\ \varepsilon_1^{ck}+\nu\varepsilon_3^{ck} & \text{If cracking occurs in direction 2} \\ \varepsilon_1^{ck} & \text{If cracking occurs in directions 2 \& 3} \end{cases} \tag{3.8}$$

where ε_1^{ck}, ε_2^{ck} and ε_3^{ck} are three normal component strains with respect to the crack

orientation (ANSYS 2002). If the crack strain is negative, then the associated crack is assumed to be closed, otherwise the associated crack is assumed to be open. There exist four cracking states — crushed crack, open crack, closed crack, intact — for crack in any one direction. Consequently, there are totally sixteen possible combinations of cracking states (see Table 3.1) and corresponding modifications in constitutive relationships for a concrete element or one of its integration points.

Table 3.1. Cracking state combinations

Combination Number	Cracking state in direction 1†	Cracking state in direction 2	Cracking state in direction 3
1	Crushed	Crushed	Crushed
2	Open	Intact	Intact
3	Closed	Intact	Intact
4	Open	Open	Intact
5	Open	Open	Open
6	Closed	Open	Open
7	Closed	Open	Intact
8	Open	Closed	Open
9	Closed	Closed	Open
10	Open	Closed	Intact
11	Open	Open	Closed
12	Closed	Open	Closed
13	Closed	Closed	Intact
14	Open	Closed	Closed
15	Closed	Closed	Closed
16	Intact	Intact	Intact

(† — direction 1 denotes the direction of first principal stress, and $\sigma_1 \geq \sigma_2 \geq \sigma_3$)

Therefore, both the number, location and state of cracked integration points in each

concrete element and those of cracked elements in entire concrete structure can be obtained, which forms the basis of original concept — relative crack density.

3.3. Relationship between crack density and transport properties

Cracking may result in increase of the concrete permeability and acceleration of the transport processes of various aggressive agents, thus impair the structural durability. To reflect the influence of cracks on the concrete permeability more accurately, it is necessary to quantify the relationship between the cracking state of concrete and the associated transport properties of various aggressive agents in concrete. Based on this relationship, it is then possible to develop an integrated computational framework with consideration of cracking on affecting durability of concrete structures.

Substantial contributions have been made to evaluate the permeability of cracked concrete. As early as in 1987, Bazant and Oh (1987) investigated the effect of cracking on drying permeability and diffusivity of concrete. Wang et al. (1997) studied the permeability of cracked concrete on the basis of water permeation test and concluded that crack opening displacement (COD) accelerates water permeation in concrete at different rates. Rapoport et al. (2002) explored the relationship between permeability and crack width and approximated the logarithm of permeability coefficient as a linear function of crack width. Snyder (2001) proposed a composite permeability model to assess the permeability of cracked concrete on the basis of given crack width and crack spacing.

Bangert et al. (2003) introduced a crack width-dependent anisotropic permeability tensor to evaluate the influence of crack on the moisture transport. Gerard and Marchand (2000) predicted the effect of cracking on the concrete diffusivity on the basis of crack density and crack width. Breysse and Gerard (1997) presented a state-of-the-art survey on the permeability of cracked concrete. Most researchers related crack width directly to the transport property of cracked concrete. However, the exact crack width cannot be obtained using the smeared cracking approach, which makes it difficult to directly adopt those existing numerical models that characterize the relationships between crack width and transport property.

The number of cracks per unit volume of concrete is usually defined as the crack density. This concept may be modified to take advantage of the results of smeared cracking analysis — the number, location and state of cracked integration points in one concrete element or those of cracked elements in the entire concrete structure. In this study, two relative crack density concepts — the global relative crack density (GRCD) and the local relative crack density (LRCD) — are proposed to evaluate the cracking state of the entire concrete structure and that of a concrete element, respectively. GRCD is defined as

$$\rho_{global} = \frac{N_{crack}}{N_{total}} \tag{3.9}$$

where $0 \le \rho_{global} \le 1$, N_{total} is the total number of concrete elements, while N_{crack} is the number of cracked concrete elements. GRCD is able to quantify the overall cracking state of the concrete structure and serve as an appropriate failure index. Once GRCD exceeds a specified threshold value based on practical engineering requirements, the service life of the concrete structure can be assumed to end.

One possible shortcoming of GRCD is that the distribution state of cracks in concrete structures cannot be reflected accurately. In many cases, the cracks in concrete are not distributed evenly, thus a local relative crack density is preferred. There are eight integration points in each concrete finite element, and cracking is permitted in three orthogonal directions at each integration point. In this case, LRCD of a concrete element can be evaluated on the basis of the cracking state of all eight integration points. If n ($0 \le n \le 24$) open cracks are found at all eight integration points of a concrete element, then LRCD of the concrete element can be defined as

$$\rho_{local} = \frac{n}{24} \tag{3.10}$$

where $0 \le \rho_{local} \le 1$. Thus LRCD is able to quantify the cracking state of each concrete element.

It is appropriate to formulate the relationship directly between LRCD and the transport properties of cracked concrete element. Under some idealized assumptions, Aldea et al. (1999a) developed conceptual models and drew the conclusion that the

permeability of water flow through cracked concrete is a third-power function of the crack width, whereas the chloride diffusivity through cracked concrete is proportional to the crack width. Considering that both LRCD and crack width are analogous indices to measure the cracking state, it is reasonable to modify Aldea's conceptual models by replacing the crack width with LRCD. Thus, direct relationships between LRCD and transport properties of cracked concrete are developed without considering the crack width. The moisture diffusivity of concrete element is assumed a third-power function of its LRCD, while the chloride diffusivity of concrete is assumed linear function of its LRCD. The difference between moisture and chloride ion may be attributed to their transport mechanisms in concrete. Since LRCD is an original concept proposed in this study, the above assumptions need to be verified further using available literature or experimental results.

Assume the moisture diffusivity and the chloride diffusivity of an intact concrete element without deterioration-induced cracks are D_m and D_{cl}. Moreover, the maximal LRCD, $\rho_{local,\max}$, is supposed to correspond to the maximal moisture diffusivity $D_{m,\max}$ and the maximal chloride diffusivity $D_{cl,\max}$ of the completely cracked concrete element. Therefore, the moisture diffusivity $D_{m,crack}$ and chloride diffusivity $D_{cl,crack}$ of the cracked concrete element can be formulated as a function of its LRCD

$$D_{m,crack} = \left(D_{m,\max} - D_m\right)\left(\frac{\rho_{local}}{\rho_{local,\max}}\right)^3 + D_m \tag{3.11}$$

$$D_{cl,crack} = \left(D_{cl,\max} - D_{cl}\right)\left(\frac{\rho_{local}}{\rho_{local,\max}}\right) + D_{cl} \tag{3.12}$$

In terms of its definition in Eq. (3.10), the elemental LRCD may reach its maximum $\rho_{local,\max} = 1$, which means n=24, i.e., open cracks are found in three orthogonal directions at all eight integration points of the concrete element. Thus, the above numerical relationship can be reduced further as

$$D_{m,crack} = \left(D_{m,\max} - D_m\right)\rho_{local}^3 + D_m \tag{3.13}$$

$$D_{cl,crack} = \left(D_{cl,\max} - D_{cl}\right)\rho_{local} + D_{cl} \tag{3.14}$$

Several researchers, such as Bazant and Oh (1987), Wang et al. (1997), Aldea et al. (1999a, 1999b) and Cerny et al. (2000, 2001, 2003), have suggested a series of recommended values of multiplication factors (*MF*) to accommodate the increased transport properties of cracked concrete with respect to uncracked concrete. Based on different concrete materials and experimental results, these recommended values fluctuate significantly. In this study, a multiplication factor ($MF = 20$) of moisture diffusivity, which was proposed by Cerny et al. (2001) for high performance concrete made of calcareous aggregates exposed to 300 frost cycles, is adopted tentatively to

express the maximal moisture diffusivity of the completely cracked concrete element $D_{\max}$ as

$$D_{m,\max} = MF \cdot D_m \tag{3.15}$$

Thus, the numerical relationship between the moisture diffusivity of cracked concrete element and its LRCD can be reduced further as

$$D_{m,crack} = \left[\left(MF - 1\right) \cdot \rho_{local}^3 + 1\right] \cdot D_m \tag{3.16}$$

3.4. Simulation procedure of coupled heat transfer and moisture transport processes

A preliminary finite element-based computational framework has been developed in Chapter 2, which can track the temporal and spatial distribution of temperature and moisture content in concrete and evaluate the distribution of resultant stress induced by the multiple coupled deterioration processes. This computational framework is expanded further to perform the simulation of crack propagation due to the coupled heat transfer and moisture transport processes.

Based on Eq. (3.16), the influencing factor of LRCD, $F_4\left(\rho_{local}\right)$, on the moisture diffusivity can be obtained as

$$F_4\left(\rho_{local}\right)=\left(MF-1\right)\cdot\rho_{local}^3+1 \tag{3.17}$$

which is illustrated in Fig. 3.4, where the moisture diffusivity increases with the LRCD. This influencing factor of LRCD $F_4\left(\rho_{local}\right)$ is introduced into Eq. (2.9). Since carbonation process will not taken into consideration herein, the influencing factor of carbonation reaction $F_3\left(\xi\right)$ is ignored. Based on the multifactor law, the moisture diffusivity can be expressed as

$$D_m\left(h\right)=D_{m0}\cdot F_1\left(h\right)\cdot F_2\left(T\right)\cdot F_4\left(\rho_{local}\right) \tag{3.18}$$

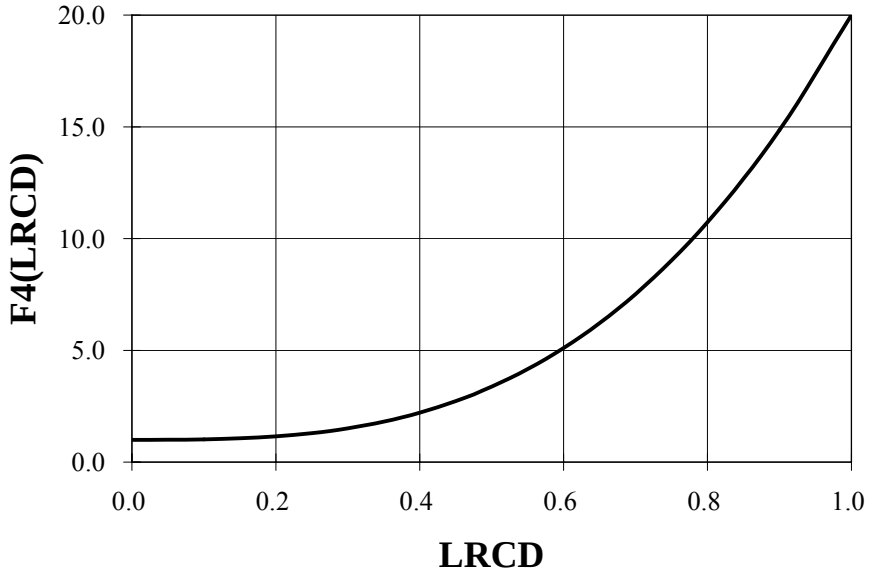

Figure 3.4. Influence of LRCD on moisture diffusivity

The proposed computational framework is implemented using existing FEA solver in

commercial software. The whole simulation procedure can be summarized as follows: the heat transfer, moisture transport and mechanical stress processes are defined as individual physics environments first. The physics environment functions like an independent module, where all related finite element types, geometric model, constant material properties, fixed boundary conditions and loads, as well as meshing of the solid model for the specific physics field (such as temperature field, moisture content field, and structural displacement field) are defined accordingly. Next, a coupled multi-physics analysis method is utilized to call each physical environment in turn, apply the time-dependent loads and material properties, and then perform the simulation of each deterioration process iteratively within each time step. Each time step is divided into a number of substeps, which may vary with each physics environment and each time step. An automatic time stepping scheme (i.e. adaptive loading) is adopted to ensure the substep size is appropriate to achieve desired convergence. To account for the potential couplings between various deterioration processes, the output result of one deterioration process at the i^{th} time step may be applied as input variable to modify the transport properties of another deterioration process at the next $(i+1)^{th}$ time step through the multifactor law. The flowchart of the simulation procedure for the multiple coupled heat transfer and moisture transport processes is summarized as in Fig. 3.5. A self-programmed code in ANSYS Parametric Design Language (APDL) is required to implement the proposed computational framework.

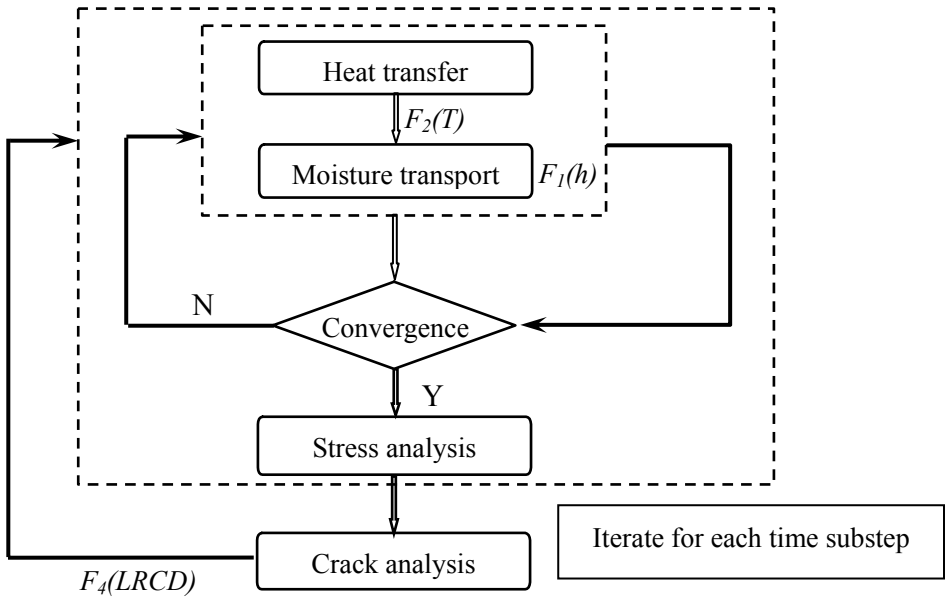

Figure 3.5. Coupled-field simulation procedure

The coupled-field analysis is performed in the following manner. At each time step, perform the transient heat transfer analysis first to obtain the spatial temperature distribution, where the nodal temperature is stored in an array A. After considering the influences caused by the temperature, relative humidity and LRCD as shown in Eq. (3.18), moisture transport analysis is performed to determine the spatial distribution of moisture content, where the nodal moisture content is stored in an array B. Finally, stress analysis and associated cracking analysis are performed to obtain the spatial distribution of the resultant stress, where the nodal stress are stored in an array C, and the corresponding LRCD of each concrete element is stored in an array D. To obatin the resultant stress, the variation of moisture content obtained in the moisture analysis is transformed into an equivalent temperature variation in the thermal analysis as shown in

Eq. (2.22). Following the evaluation of LRCD, the global index GRCD of the entire structure at each time step can be evaluated using Eq. (3.9), and may serve as an appropriate failure index for the overall concrete structure.

3.5. Numerical example

A plain concrete block 1.0 m long, 1.0 m wide, and 0.5 m thick is selected herein to illustrate the simulation procedure of crack propagation for concrete exposed to the coupled deterioration processes. The total time length is assumed to be one year, which is divided into 9 time steps with an average of 40 substeps for each time step. The average duration of each substep (i.e., about 1 day) is small enough to guarantee a stable solution. The finite element model is shown in Fig. 3.6.

The nodes and elements chosen to represent the time-dependent simulation results are shown in Figs. 3.6 and 3.7. Cross section A-A in Fig. 3.7 is exactly along the middle plane of the concrete block. The nodal results are evaluated at the inner, 3^{rd}, 5^{th}, 7^{th}, 9^{th} and outer nodal layers on cross section A-A, while the elemental results are evaluated at center, mid or corner elements of the block, and on the 1^{st}, 3^{rd}, 5^{th}, 7^{th}, 9^{th} and 10^{th} elemental layers of cross section A-A.

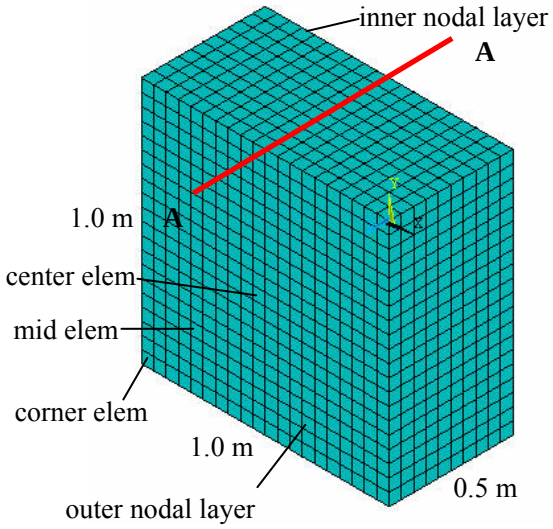

Figure 3.6. Finite element model

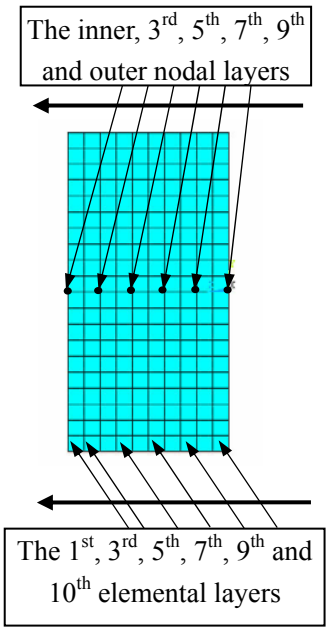

Figure 3.7. A-A cross section

To consider the seasonal variation of ambient temperature, the annual variation of ambient temperature takes the same form as Eq. (2.23). Similarly, to consider the

seasonal fluctuation of ambient relative humidity, the annual variation of ambient relative humidity takes the same form as Eq, (2.24).

The time-dependent temperature and relative humidity boundary conditions are enforced on the outer layer of the plain concrete block. On the inner layer, a constant temperature of 15 ^{0}C and a constant relative humidity of 65% are applied. The initial temperature of the entire concrete block is assumed to be 15 ^{0}C, and the initial relative humidity is assumed to be 100% (i.e. saturation). Meanwhile, the four side surfaces of the concrete block are assumed to be isolated from any heat/moisture flux. In addition, structural displacements in all three orthogonal directions are restrained on the four side surfaces as structural boundary conditions. The assumed material properties of concrete in Table 2.1 are remained.

An 8-node 3-D thermal element SOLID70 with one temperature DOF at each node is selected for simulating the heat transfer and moisture transport processes. For subsequent mechanical stress and crack analysis, the concrete element SOLID65 is selected.

The simulation results of the coupled heat transfer and moisture transport processes and the associated mechanical responses are summarized in Figs. 3.8~3.16. The time-varying temperature, equivalent temperature, free moisture content, and the first principal stress and strain at the central nodes of six nodal layers are demonstrated in Figs. 3.8~3.12, respectively.

It can be observed that the temperature distribution seems rather even and regular when compared with the distribution of moisture content, because heat transfer proceeds

much faster than moisture transport does. Actually, most nodes on mid nodal layers maintain near-saturation after one year, which coincides with the common sense that the drying proceeds very slowly (since the moisture diffusivity is very low). Meanwhile, the stress and strain increase with time, which might be the result of stress concentration due to crack propagation. The time-varying LRCDs at center and corner elements are shown in Figs. 3.13 and 3.14, respectively. It is observed that the values of LRCD can be divided roughly into three phases. During the first phase (0~0.3 year), almost no crack occurs, and LRCD approaches zero. During the second phase (0.3~0.6 year), a great number of cracks are generated, and LRCD increases quickly. During the third phase (0.6~1.0 year), LRCD gradually approaches its maximum value, which may be explained as follows. The cracking state of the concrete element has reached to such an extent that its degraded stiffness doesn't allow it to carry more loads (the other uncracked or less cracked concrete elements may take over the additional load). In addition, those concrete elements close to the outer layer usually have higher LRCD, which might be the result of more intense fluctuation of environmental loadings on the outer layer. Finally, the time-varying moisture diffusivities at the center and corner elements are shown in Figs. 3.15 and 3.16, respectively. It is observed that LRCD plays an important role on affecting the moisture diffusivity of cracked concrete elements, which demonstrates the accelerating influence of cracks on the moisture transport process.

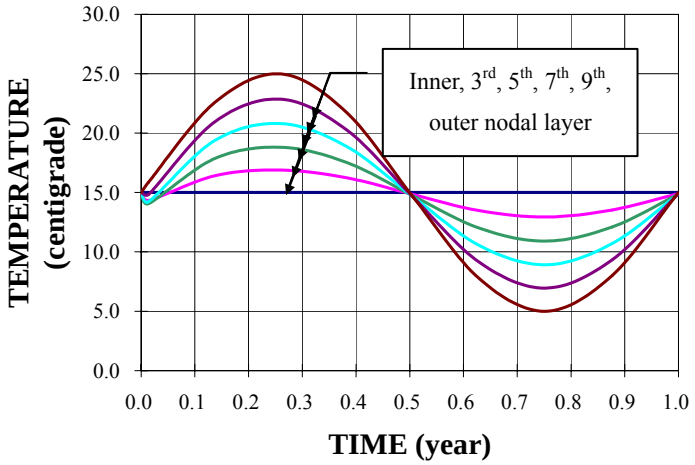

Figure 3.8. Temperature at selected nodes of cross section A-A

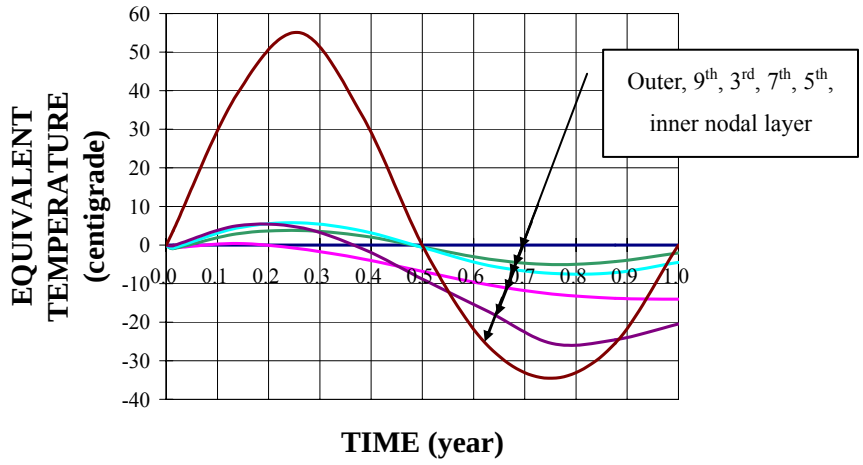

Figure 3.9. Equivalent temperature at selected nodes of cross section A-A

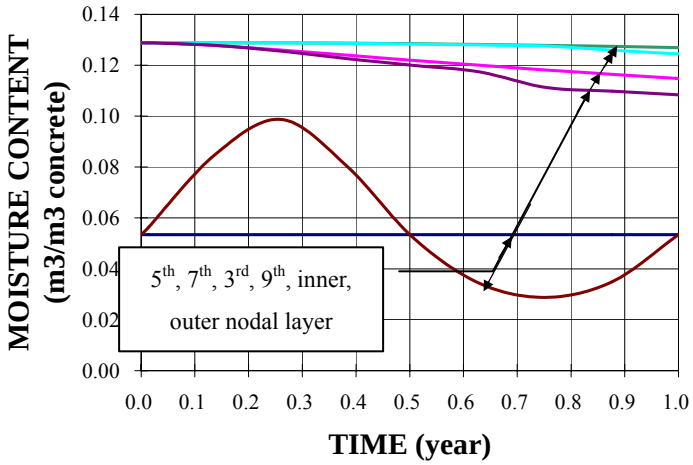

Figure 3.10. Moisture content at selected nodes of cross section A-A

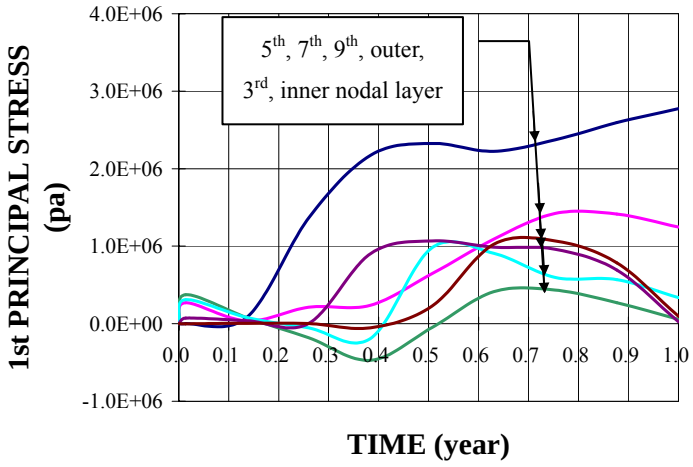

Figure 3.11. 1st principal stress at selected nodes of cross section A-A

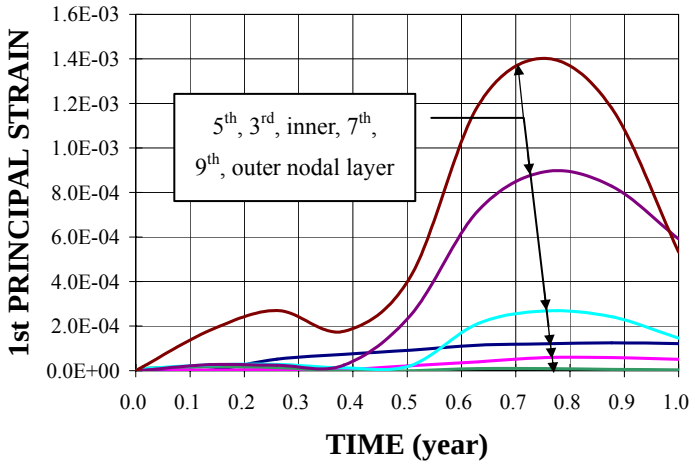

Figure 3.12. 1st principal strain at selected nodes of cross section A-A

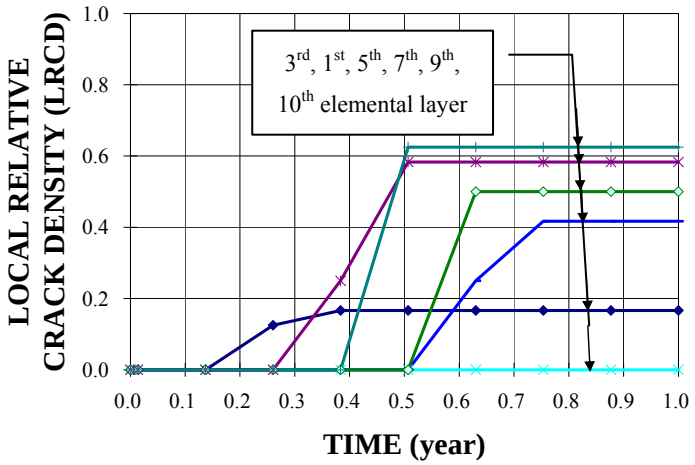

Figure 3.13. LRCD at selected center elements

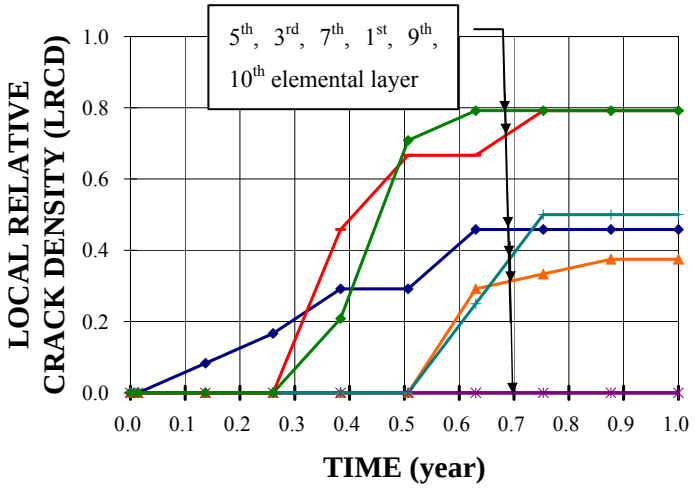

Figure 3.14. LRCD at selected corner elements

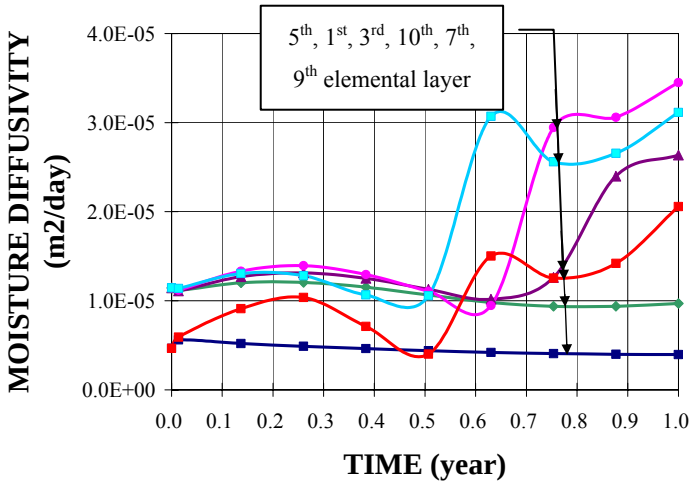

Figure 3.15. Moisture diffusivity at selected center elements

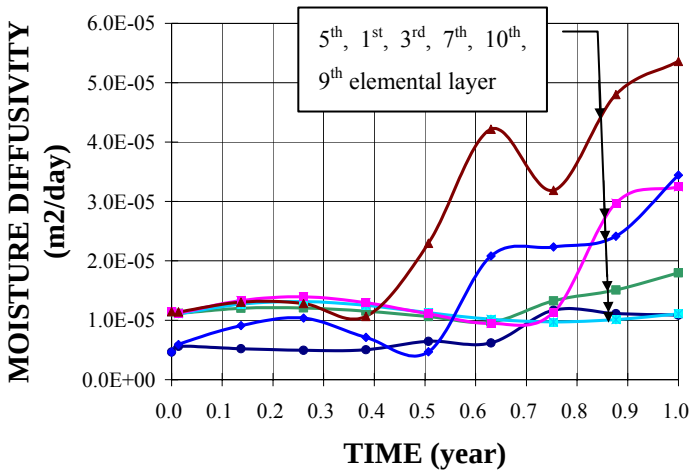

Figure 3.16. Moisture diffusivity at selected corner elements

Note: In Figs. 3.8~3.16, the sequence of the curves in the legend goes from the furthest to the nearest curve at the arrow.

The structural displacement contour and the 1st principal stress contour at the final time step are illustrated in Figs. 3.17 and 3.18, respectively.

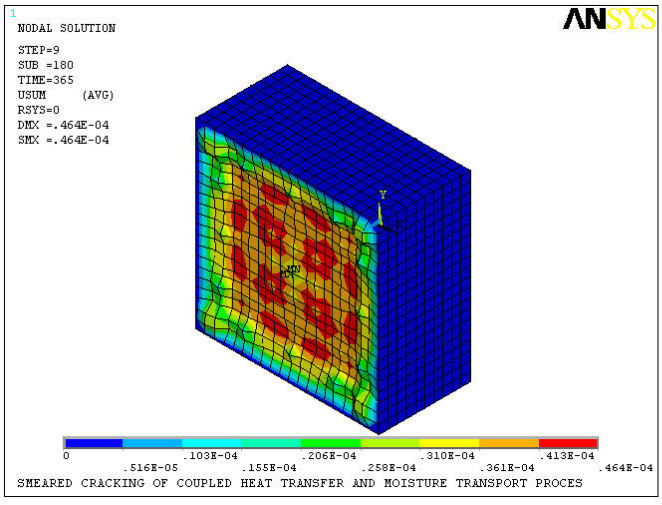

Figure 3.17. Nodal displacement contour at final time step

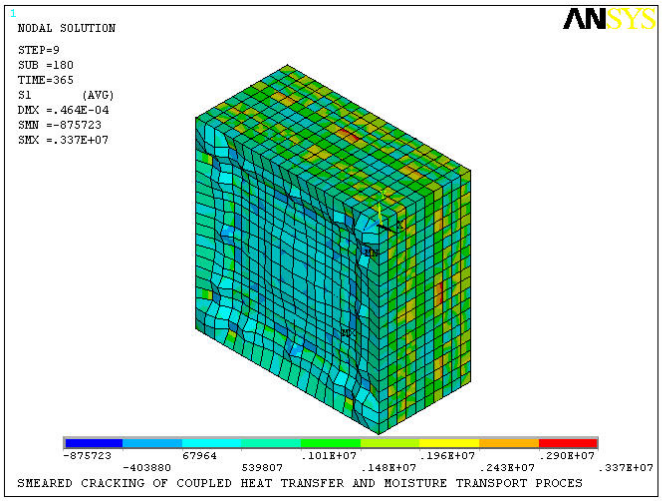

Figure 3.18. 1st principal stress contour at final time step

The cracking state of the entire concrete block at each time step is illustrated in Fig. 3.19, where the right side view of the plain concrete block in Fig. 3.6 is shown. It can be observed that more and more dense microcracks uniformly distributed over the entire concrete volume propagate with time. A series of Scanning Electron Microscopy (SEM) test results (Bisschop and van Mier 2002) verifies this simulation result to a large extent, where densely distributed drying shrinkage microcracks on surface and cross-section of specimen were observed. Walton (1990) also found that evenly spaced cracks resulting from temperature variation and drying shrinkage are likely to penetrate the entire slab thickness.

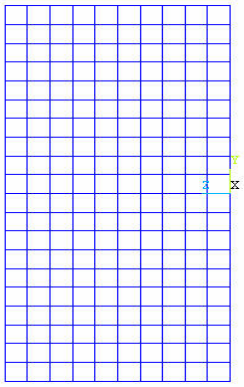

Fig. 3.19(a). Time=0.11 year

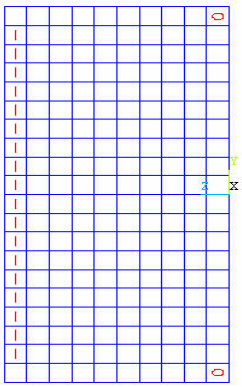

Fig. 3.19(b). Time=0.22 year

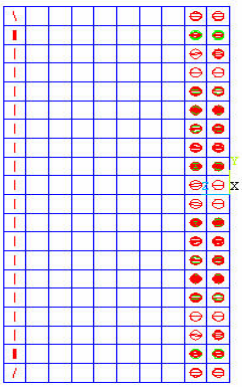

Fig. 3.19(c). Time=0.33 year

Fig. 3.19(d). Time=0.44 year

Fig. 3.19(e). Time=0.56 year

Fig. 3.19(f). Time=0.67 year

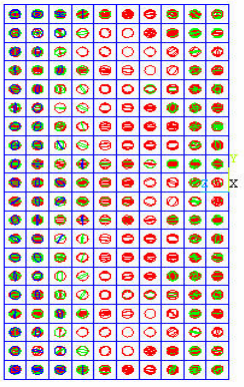

Fig. 3.19(g). Time=0.78 year

Fig. 3.19(h). Time=0.89 year

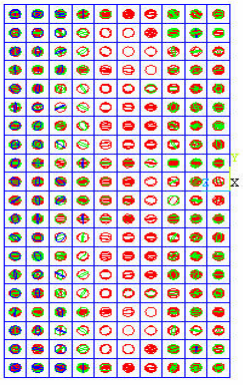

Fig. 3.19(i). Time=1.0 year

Note: The symbols | and ○ indicate different orientations of the cracks, and symbol ⊕ indicates that multiple cracks distinguished with different colors occur at the centroid of one finite element (ANSYS 2002).

Figure 3.19. Crack accumulation in the concrete structure

The corresponding GRCD is shown in Fig. 3.20, which increases with time and verifies the observation in Fig. 3.19. Meanwhile, the development of GRCD follows three phases similar to LRCD. It can be observed that about 70% concrete finite elements are cracked, though each element may attain different cracking degree.

For concrete structure under mechanical loading (such as concrete beam under bending, or reinforced concrete structure under reinforcement corrosion-induced rust expansion), cracks may localize at some points and then form in a single region while the other cracks do not continue to develop. The proposed smeared cracking approach is still able to simulate the cracking propagation process even when crack localization exists. We have observed this in some literature references (Mandke and Smalley 1994, Kachlakev et al. 2001, Saouma and Chang 2003).

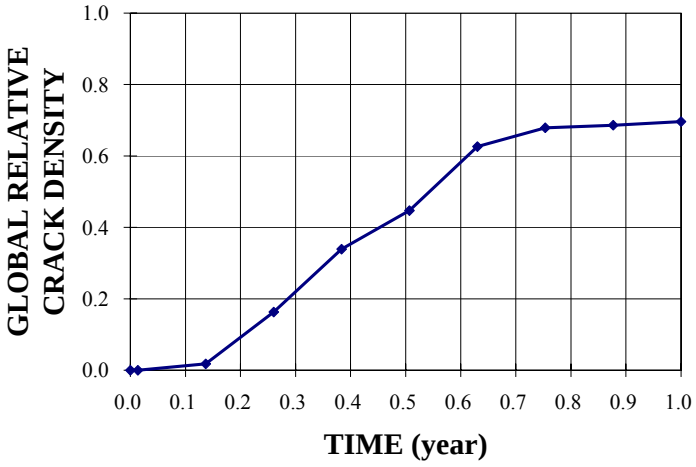

Figure 3.20. GRCD of the concrete structure

Since densely distributed cracked elements are presented in Fig. 3.19, it is difficult to

observe the actual crack propagation process of each concrete element clearly. Therefore, 9 representative concrete elements distributed evenly in the concrete structure (center, mid and corner elements on the 1st, 6th and 10th elemental layers, respectively) are chosen herein, and their crack propagation process is shown in Figs. 3.21. It can be observed that for each concrete element, the initiation time of crack and the cracking state are significantly different from each other. While some concrete elements (e.g. elem 3601 and elem 3790) experience extensive cracking, some others (e.g. elem 190 and elem 2085) don't crack at all.

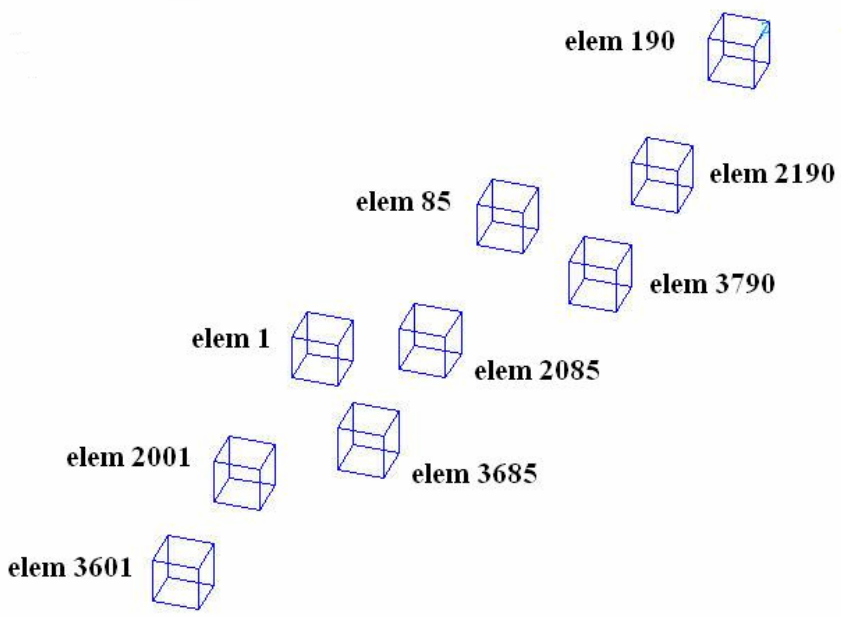

Fig. 3.21(a). Time=0.11 year

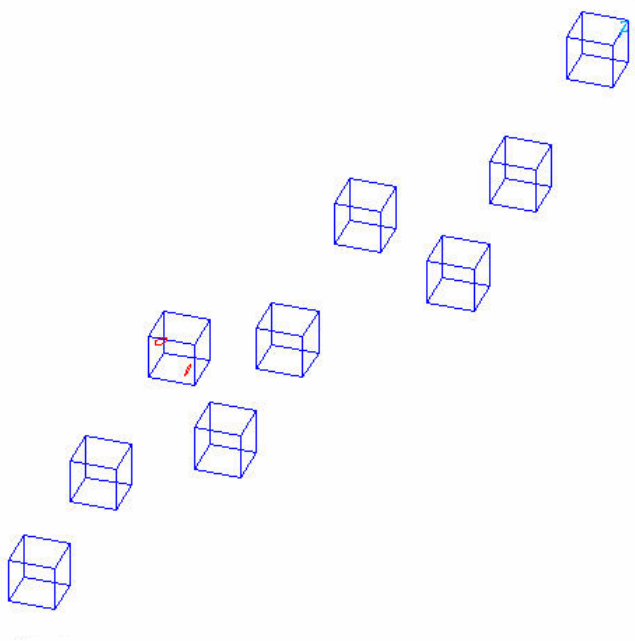

Fig. 3.21(b). Time=0.22 year

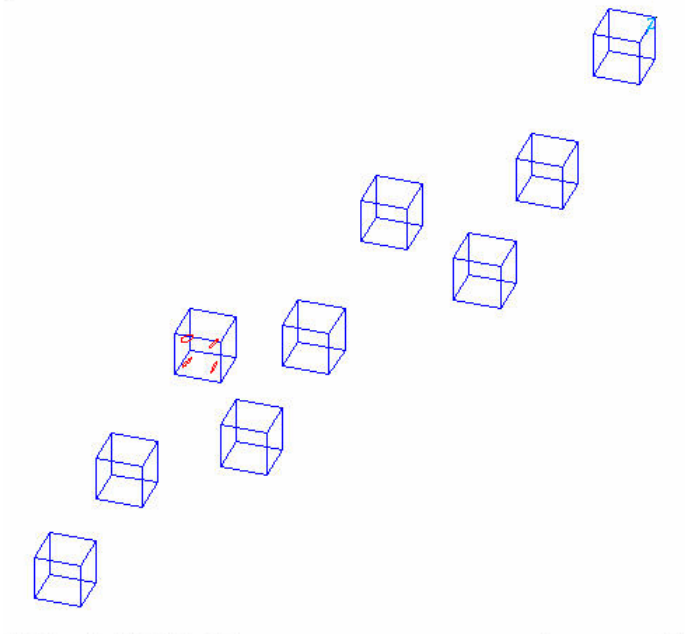

Fig. 3.21(c). Time=0.33 year

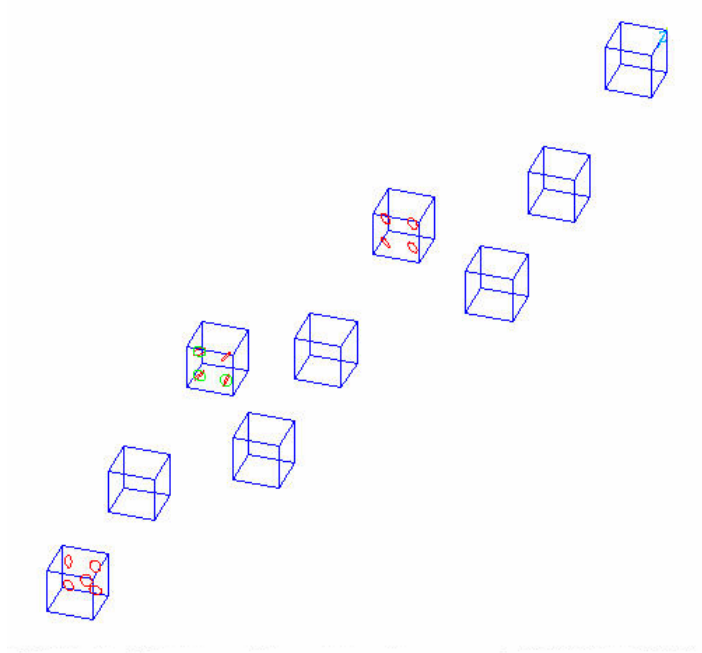

Fig. 3.21(d). Time=0.44 year

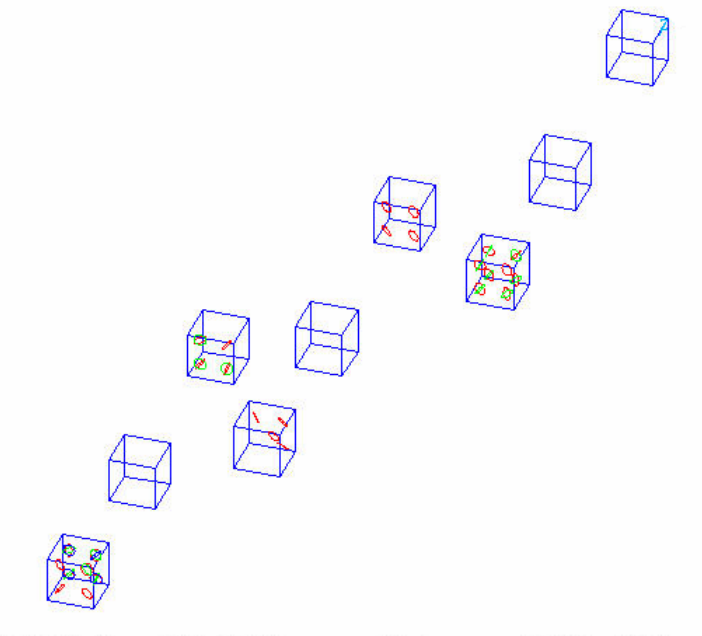

Fig. 3.21(e). Time=0.56 year

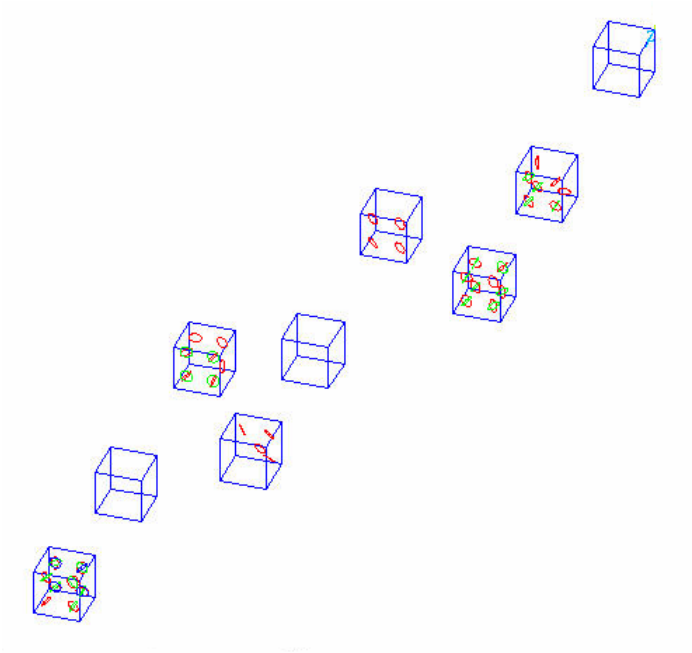

Fig. 3.21(f). Time=0.67 year

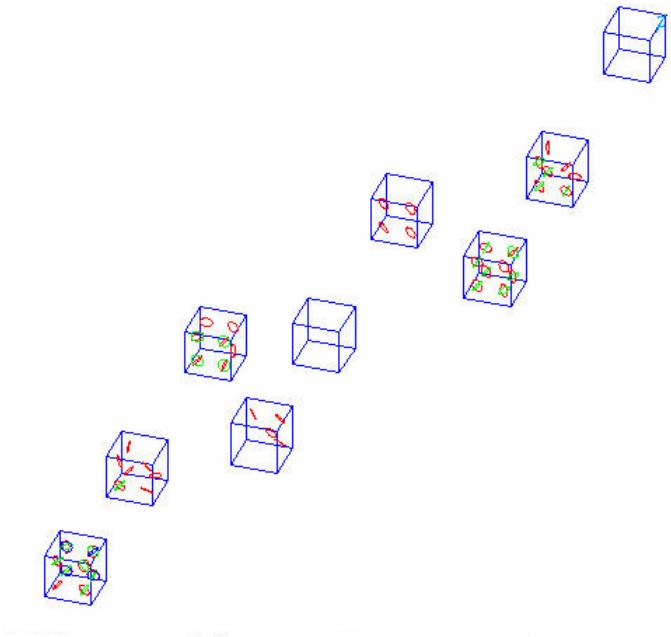

Fig. 3.21(g). Time=0.78 year

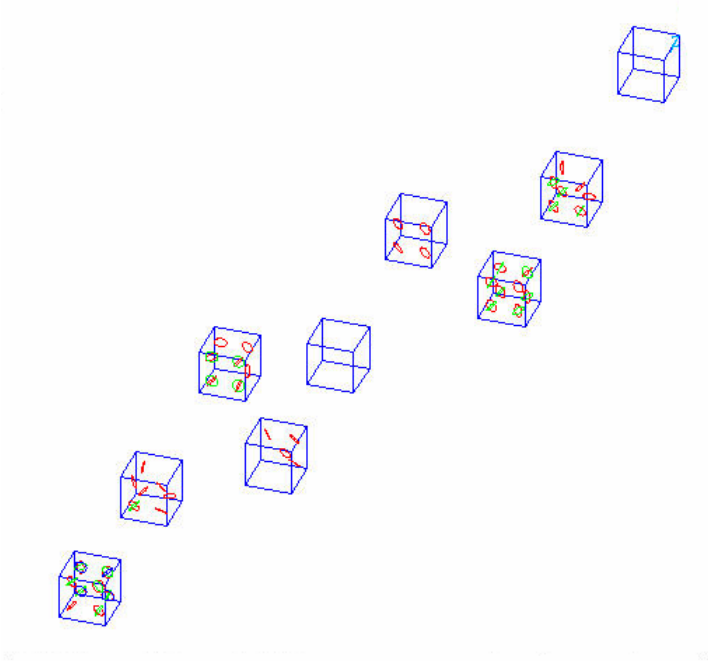

Fig. 3.21(h). Time=0.89 year

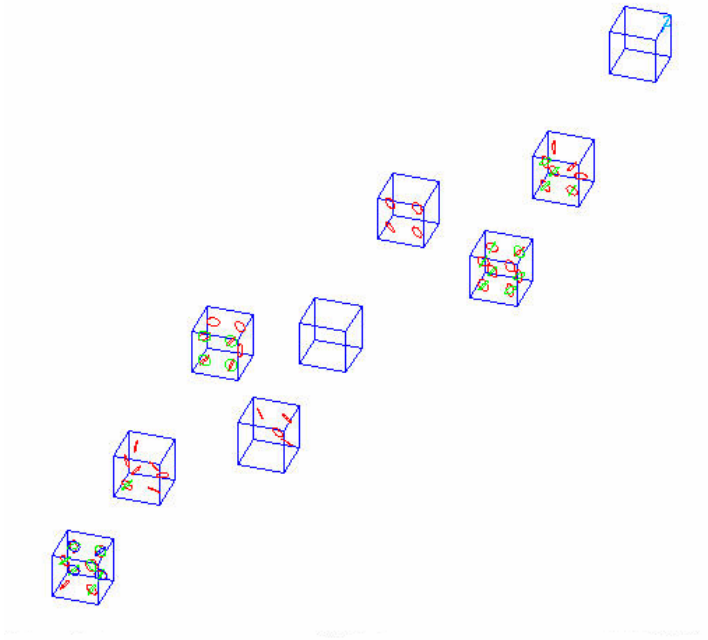

Fig. 3.21(i). Time=1.0 year

Figure 3.21. Crack propagation in representative concrete elements

The graphic results of cracking processes for representative concrete elements shown in Fig. 3.21 can be confirmed further by the values of LRCD obtained from the output files of the simulation as shown in Table 3.2.

Table 3.2. LRCD of representative concrete elements

Elem # / Time (yr)	1	2001	3601	85	2085	3685	190	2190	3790
0.000	0.00	0.00	0.00	0.00	0.00	0.00	0.00	0.00	0.00
0.014	0.00	0.00	0.00	0.00	0.00	0.00	0.00	0.00	0.00
0.137	0.08	0.00	0.00	0.00	0.00	0.00	0.00	0.00	0.00
0.260	0.17	0.00	0.00	0.00	0.00	0.00	0.00	0.00	0.00
0.384	0.29	0.00	0.21	0.17	0.00	0.00	0.00	0.00	0.00
0.507	0.29	0.00	0.71	0.17	0.00	0.17	0.00	0.00	0.63
0.630	0.46	0.00	0.79	0.17	0.00	0.17	0.00	0.46	0.63
0.753	0.46	0.33	0.79	0.17	0.00	0.17	0.00	0.46	0.63
0.877	0.46	0.33	0.79	0.17	0.00	0.17	0.00	0.46	0.63
1.000	0.46	0.33	0.79	0.17	0.00	0.17	0.00	0.46	0.63

3.6. Conclusion

An integrated finite element-based computational framework has been developed in this chapter to simulate the crack propagation in concrete structure exposed to multiple coupled deterioration processes (heat transfer and moisture transport). The accelerating influence of cracks on the transport process of moisture is taken into consideration. The smeared cracking approach is utilized to simulate the crack propagation. The cracking state of each finite element is characterized using LRCD. A numerical relationship between LRCD and the transport property of moisture is developed. Finally, GRCD is

suggested to denote the cracking state of the entire concrete structure and serve as an appropriate index to evaluate the overall deterioration level of the structure. This computational framework establishes a reasonable basis for quantitative durability assessment of concrete structures under multiple coupled deterioration processes.

CHAPTER IV

SIMULATION OF CHLORIDE PENETRATION IN CONCRETE

4.1. Introduction

The durability of a concrete structure against various deterioration processes depends to a large extent on the transport mechanisms of various aggressive agents through the porous microstructure of concrete. Chloride-induced reinforcement corrosion is one of the major deterioration mechanisms for reinforced concrete structures exposed to marine environment, deicing salts or underground environment. It leads to a series of structural degradations, such as loss of the concrete-steel interface bond, reduction of the cross-section area of reinforcement, and cracking and spalling of the concrete cover, thus severely reduces the load carrying capacity of the structure. Considering its unique significance, substantial studies have been carried out on the chloride-induced reinforcement corrosion process for several decades. The simulation of the chloride penetration process in concrete is the first step in assessing the durability of the reinforced concrete structures against chloride-induced deterioration.

The chloride-induced reinforcement corrosion process of reinforced concrete structures can be divided roughly into three phases as shown in Fig. 4.1 (Xi and Ababneh

2000). The first phase is characterized by the penetration process of chloride, during which the chloride diffuses gradually from the concrete surface through the concrete cover toward the embedded reinforcement. When the chloride content at the reinforcement reaches a threshold value to initiate the corrosion process at time $t_{initiation}$, the second phase is assumed to begin. The second phase is dominated by the reinforcement rust expansion process, during which the rust (i.e., the corrosion products) forms in the concrete-steel Interface Transition Zone (ITZ). Once all voids in ITZ are occupied completely by the rust at time t_{stress}, further rust accumulation will trigger expansive stress and cracking in the surrounding concrete, which indicates the start of the third phase. During the third phase, the reinforcement rust expansion-induced cracks propagate in concrete surrounding the reinforcing steels until some critical failure mode, such as the spalling or delamination of concrete cover, occurs at time $t_{spalling}$. This indicates the end of the third phase.

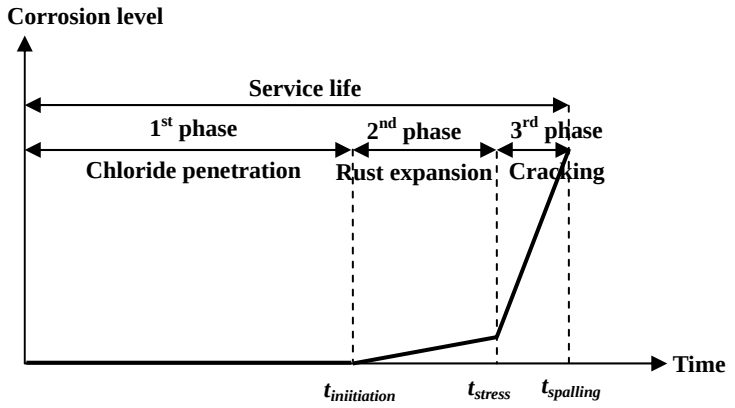

Figure 4.1. Chloride-induced reinforcement corrosion process

Among the three phases, the first phase usually lasts for a relatively long period, depending on many influencing factors such as the corrosion resistance of reinforcement, the thickness and quality of concrete cover, and the corrosion protection measures taken etc. The second phase is shorter than the first one, which is determined mainly by both the porosity of the ITZ and the corrosion rate of reinforcement. The third phase is the shortest since the reinforcement rust expansion-induced cracks propagate rapidly through the surrounding concrete. The whole service life of the reinforced concrete structure may be defined as the sum of all three phases. Considering the difficulty to accurately model concrete cracking and subsequent spalling/delamination, many studies simplify the analysis by ignoring the third or even second phase and approximate the service life of reinforced concrete structure as t_{stress} or $t_{initiation}$ only. In addition, some appropriate index that quantifies an unacceptable performance level of reinforced concrete structure before the occurrence of critical failure (e.g., spalling/delamination) may be proposed to determine the overall service life.

In the previous Chapters 2 and 3, an integrated finite element-based computational framework has been developed to simulate the multiple coupled deterioration processes, where the temporal and spatial distribution of various aggressive agents can be tracked. Meanwhile, a numerical relationship between the transport properties of cracked concrete and the LRCD of concrete element has been proposed to consider the accelerating influence of concrete cracking on the transport process of various aggressive agents in concrete. In this chapter, the developed computational framework is utilized for

illustration to implement the simulation of the chloride-induced reinforcement corrorion process.

Based on an analogous transient thermal analysis, a finite element methodology is developed to simulate the temporal and spatial distribution of chloride content and thus predict the evolution of chloride content profile in concrete. The influences of the chloride binding capacity of concrete, the age of concrete, the local chloride content, the temperature, and the LRCD on the transport rate of chloride are taken into account simultaneously by adopting a multifactor law. Based on three established chloride binding isotherm models, three sets of simulation results are presented for a reinforced concrete slab exposed to a constant chloride environment.

4.2. Previous work in chloride penetration modeling

Based on experimental results and site observations, Clear (1976) suggested an empirical model for determining the corrosion initiation time $t_{initiation}$ as follows:

$$t_{initiation} = \frac{129 \cdot t_c^{1.22}}{WCR \cdot [Cl]^{0.42}} \tag{4.1}$$

where t_c is the thickness of concrete cover (inch), WCR is the water to cement ratio by mass, $[Cl]$ is the chloride content in groundwater (ppm). Herein $t_{initiation}$ (year) is assumed to be affected only by the concrete cover depth t_c and the water to cement ratio

WCR, without considering many other possible influencing factors.

Although adopted extensively in various design codes of concrete structures, empirical models are generalized directly from a range of observations on existing structural elements instead of investigating the physical deterioration mechanism, and they may not be applicable to circumstances beyond the observation range. Furthermore, some important factors influencing the chloride penetration process may be ignored in these empirical models, such as in Eq. (4.1). Therefore, the application of empirical models is limited to some extent.

Some numerical models based on the physical mechanism of chloride transport through concrete have been proposed (Sergi et al. 1992, Mangat and Molloy 1994, Berke and Hicks 1994, Tang 1996, Wee et al. 1997, Onyejekwe and Reddy 2000), where some physical "material parameters" like the permeability of concrete and average "loading parameters" like the average chloride content on the concrete surface were adopted, while the chloride-induced deterioration mechanism was assumed to follow the Fick's second law of diffusion. Bazant (1979a, 1979b) first reduced the chloride penetration process to a one-dimensional diffusion process through a semi-infinite medium. Based on Fick's second law, the governing equation of chloride penetration in concrete can be expressed as:

$$\frac{\partial C_{cl}(x,t)}{\partial t} = D_{cl} \cdot \frac{\partial^2 C_{cl}(x,t)}{\partial x^2} \tag{4.2}$$

where $C_{cl}(x,t)$ is the chloride content at spatial coordinate x and time t, and D_{cl} is the chloride diffusivity.

Suppose that constant diffusivity and constant initial and boundary conditions apply as follows:

$$C_{cl} = 0 \qquad \text{For x > 0 when t = 0}$$

$$C_{cl} = C_{cl,0} \qquad \text{For x = 0 when t > 0} \tag{4.3}$$

Then Eq. (4.2) has a closed-form analytical solution as

$$C_{cl}(x,t) = C_{cl,0} \cdot \left[1 - erf\left(\frac{x}{2\sqrt{D_{cl}t}}\right)\right] \tag{4.4}$$

where the error function $erf(z)$ is defined as

$$erf(z) = \frac{2}{\sqrt{\pi}} \int_0^z e^{-\tau^2} d\tau \tag{4.5}$$

Let $C_{cl,cr}$ be the threshold value of chloride content to initiate the corrosion process, and t_c is the thickness of concrete cover, then the corrosion initiation time $t_{initiation}$ can be obtained analytically as

$$t_{initiation} = \frac{t_c^2}{4D_{cl}}\left[erf^{-1}\left(1-\frac{C_{cl,cr}}{C_{cl,0}}\right)\right]^{-2} \tag{4.6}$$

However, the above analytical solution is of limited use. Chatterji (1995) has questioned the applicability of Fick's second law to chloride migration through concrete for several reasons. First, constant initial and boundary conditions as well as the one-dimensional diffusion assumption are not applicable for most practical circumstances, where the reinforced concrete structures with arbitrary geometries and dimensions are subjected to randomly varying environmental loadings. Second, the chloride diffusivity D_{cl} may vary with many influencing factors, such as temperature, chloride content, age of concrete, and chloride binding capacity etc. Third, not all the chloride in concrete is involved in the diffusion process and the chloride binding effect of concrete needs to be considered. Therefore, the above numerical model has to be improved to overcome these limitations. This chapter develops such an advanced numerical model to fulfill this objective.

The modeling of the chloride-induced deterioration profile is based on a scientific basis from fundamental physical, chemical and mechanical viewpoint, where the characteristics of concrete microstructure and the time-varying environmental loading, as well as multiple coupled deterioration processes are taken into consideration. As a result, developing such a finite element-based methodology is computationally expansive.

During recent years, some fully coupled models on macroscopic level, including Schmidt-Dohl and Rostasy (1999), Martin-Perez et al. (2001), Bangert et al. (2003), Isgor and Razaqpur (2004), and Maltais et al. (2004), have been developed to evaluate the behavior of concrete structures exposed to various environmental loadings. A series of governing differential equations based on mass/energy balance and thermodynamic/chemical equilibrium on coupled heat conduction, ionic diffusion, moisture transport and chemical reaction were presented, and finite element/difference methods were utilized to solve the complex system of interactive and nonlinear equations with standard Galerkin procedure. All these numerical models were implemented in self-programmed computer codes. The focus of this study, however, is to utilize an existing FEA solver in commercial software for this implementation, and various potential coupling effects are considered by adjusting the transport property of concrete. The proposed approach is relatively simpler and efficient to implement with existing commercial software.

4.3. Proposed numerical methodology

Since the processes of chloride penetration and thermal conduction through concrete are governed by analogous differential equations, it is reasonable to propose a simplified approach and simulate the chloride penetration process by following an analogous transient thermal analysis. Although the chloride transport mechanism occurs essentially

at a micro scale, a macroscopic/engineering level model is developed in this study, where the spatially averaged transport property of concrete (i.e. the chloride diffusivity) is characterized over a representative volume — finite element, while potential coupling effects due to various influencing factors are considered by adjusting transport property using a multifactor law and existing numerical models. Moreover, existing FEA solver in commercial software is adopted to implement the approach, which facilitates its extensive application and further development.

There actually exist two types of chloride in concrete. One is the free chloride $C_{cl,f}$ (kg/m^3 of pore solution), which is dissolved in the pore solution and can diffuse through concrete; the other is the bound chloride $C_{cl,b}$ (kg/m^3 of concrete), which is chemically and physically bound to the cement hydrates and cannot move. The total chloride content $C_{cl,t}$ (kg/m^3 of concrete) can be expressed as the sum of the bound chloride $C_{cl,b}$ and the free chloride $C_{cl,f}$

$$C_{cl,t} = C_{cl,b} + W \cdot C_{cl,f} \tag{4.7}$$

where W is the free moisture content (m^3 of moisture/m^3 of concrete).

Chloride-induced reinforcement corrosion is related only to the free chloride (Tuutti 1982), since the bound chloride is immovable and does not initiate the reinforcement corrosion. However, the bound chloride exerts a tremendous influence on the transport of

free chloride through concrete, and the chloride binding effect of concrete must be considered in any sound numerical model.

Liang et al. (1999) proposed a complex mathematical model to solve the governing partial differential equation of chloride diffusion analytically through nondimensional parameters and Laplace's transform, with the chloride binding effect taken into consideration. However, the one-dimensional assumption and the time only-dependent diffusivity still limit its application.

Although the transport mechanism of chloride in concrete may occur in several forms (including diffusion, permeation, capillary sorption, and dispersion etc.), ionic diffusion may be identified as the main transport mechanism, where the chloride content gradient serves as the driving force. It is known that moisture transport may influence chloride penetration to some extent. However, the lack of established numerical models quantifying the coupling relationship makes it difficult to adopt the partial saturation assumption as in Chapter 2. Following Xi and Bazant (1999) and Martin-Perez et al. (2000), the concrete is assumed to be completely saturated, thus the free moisture content W assumes a saturated free moisture content ω_e = 0.08 m^3 of moisture/m^3 of concrete. The Darcy's law under hydraulic pressure dominates the moisture transport in concrete. Acting as vehicle, fluid flow may facilitate the transport of various aggressive agents through forced convection. To simplify the analysis further, the potential influence of hydraulic pressure on chloride penetration is ignored. As a result, it is assumed that no coupling exists between moisture transport and chloride penetration. These assumptions

may be reasonable for many underground concrete structures, and will not impair the illustration of the developed computational framework too much.

Based on mass conservation, the chloride penetration process can be formulated as

$$\frac{\partial C_{cl,f}}{\partial t} = div\left[D_{cl} \cdot grad\left(C_{cl,f}\right)\right] - \frac{1}{\omega_e} \cdot \frac{\partial C_{cl,b}}{\partial t} \tag{4.8}$$

The governing equation Eq. (4.8) can be reduced further to a modified form of Fick's second law as

$$\frac{\partial C_{cl,f}}{\partial t} = div\left[D_{cl}^{*} \cdot \left(C_{cl,f}\right)\right] \tag{4.9}$$

where D_{cl}^{*} is the effective (or apparent) chloride diffusivity, which can be measured experimentally. From a theoretical viewpoint, the effective chloride diffusivity D_{cl}^{*} is supposed to be less than the actual chloride diffusivity D_{cl}. Their relationship can be expressed as

$$D_{cl}^{*} = D_{cl} \cdot F_1\left(C_{cl,b}\right) \tag{4.10}$$

$$F_1\left(C_{cl,b}\right)=\frac{1}{1+\frac{1}{\omega_e}\cdot\frac{\partial C_{cl,b}}{\partial C_{cl,f}}} \tag{4.11}$$

where $\frac{\partial C_{cl,b}}{\partial C_{cl,f}}$ has been referred to as the chloride "binding capacity" of concrete (m^3 of moisture/m^3 of concrete) by Tang and Nilsson (1993). $F_1\left(C_{cl,b}\right)$ is the influencing factor due to the chloride binding capacity of concrete. It can be observed that the sink term $\frac{1}{W}\cdot\frac{\partial C_{cl,b}}{\partial t}$ in Eq. (4.8) caused by the chloride binding effect of concrete appears to be "eliminated" skillfully by substituting Eqs. (4.10) and (4.11) in Eq. (4.8), which leads to a reduced form Eq. (4.9), thus simplifying the simulation algorithm and enhancing the computation efficiency. This idea may also be useful in handling other physical and chemical sink/source terms in solving governing partial differential equations.

The chloride binding capacity of concrete $\frac{\partial C_{cl,b}}{\partial C_{cl,f}}$, i.e., the derivative of the bound chloride with respect to the free chloride, can be computed based on any appropriate chloride binding isotherm model. The chloride binding isotherm characterizes the relationship between bound and free chlorides in concrete. Following Martin-Perez et al. (2000), three established chloride binding isotherm models — linear, Langmuir, and Freundlich — are to be included in this study. The corresponding chloride binding capacity and the associated influencing factor $F_1\left(C_{cl,b}\right)$ are given as follows:

1) Linear isotherm model

$$C_{cl,b} = \alpha_{cl} \cdot C_{cl,f} \qquad \frac{\partial C_{cl,b}}{\partial C_{cl,f}} = \alpha_{cl} \qquad F_1\left(C_{cl,b}\right) = \frac{1}{1+\dfrac{\alpha_{cl}}{\omega_e}} \tag{4.12}$$

2) Langmuir isotherm model

$$C_{cl,b} = \frac{\alpha_{cl} \cdot C_{cl,f}}{1+\beta_{cl} \cdot C_{cl,f}} \qquad \frac{\partial C_{cl,b}}{\partial C_{cl,f}} = \frac{\alpha_{cl}}{\left(1+\beta_{cl} \cdot C_{cl,f}\right)^2} \qquad F_1\left(C_{cl,b}\right) = \frac{1}{1+\dfrac{\alpha_{cl}}{\omega_e \cdot \left(1+\beta_{cl} \cdot C_{cl,f}\right)^2}} \tag{4.13}$$

3) Freundlich isotherm model

$$C_{cl,b} = \alpha_{cl} \cdot C_{cl,f}^{\beta_{cl}} \qquad \frac{\partial C_{cl,b}}{\partial C_{cl,f}} = \alpha_{cl}\beta_{cl}C_{cl,f}^{\beta_{cl}-1} \qquad F_1\left(C_{cl,b}\right) = \frac{1}{1+\dfrac{\alpha_{cl}\beta_{cl}C_{cl,f}^{\beta_{cl}-1}}{\omega_e}} \tag{4.14}$$

where the values of model parameters α_{cl} and β_{cl} in Eqs. (4.12)~(4.14) are determined through interpolation from suggested values (Onyejekwe and Reddy 2000) for OPC concrete with $WCR = 0.5$.

The three chloride binding isotherm models in Eqs. (4.12)~(4.14) are illustrated in

Fig. 4.2. (Note: To maintain consistency, the unit of free chloride $C_{cl,f}$ needs to be transformed into kg/m^3 of concrete by multiplying with the free moisture content).

Based on the above three chloride binding isotherm models, the chloride binding capacity of concrete $\frac{\partial C_{cl,b}}{\partial C_{cl,f}}$ can be expressed as a function of the free chloride $C_{cl,f}$ for the three binding isotherm models, as shown in Fig. 4.3. The influencing factor due to the binding capacity $F_1(C_{cl,b})$ as a function of the free chloride $C_{cl,f}$ for the three binding isotherm models is shown in Fig. 4.4.

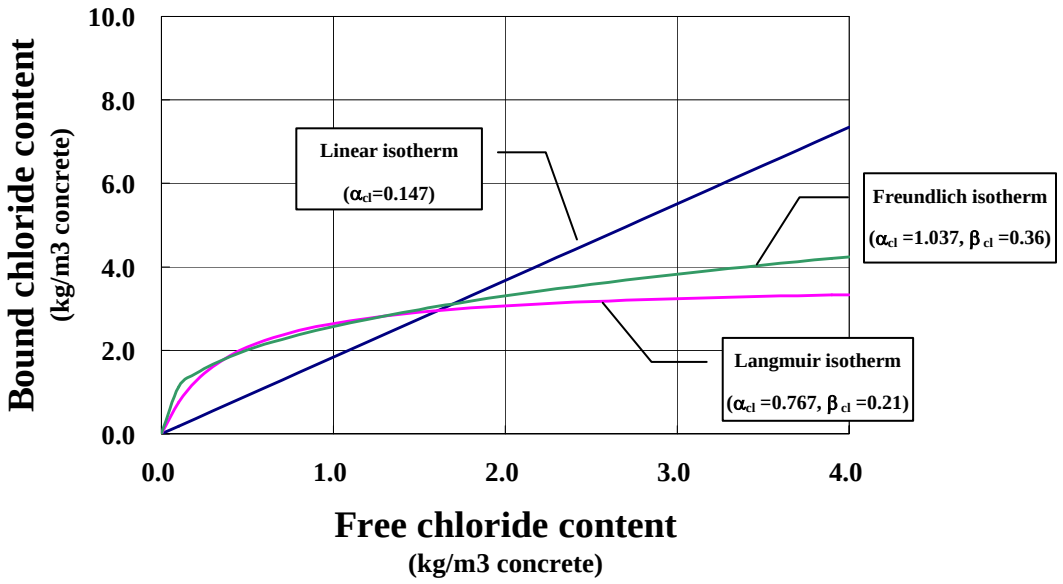

Figure 4.2. Chloride binding isotherm models

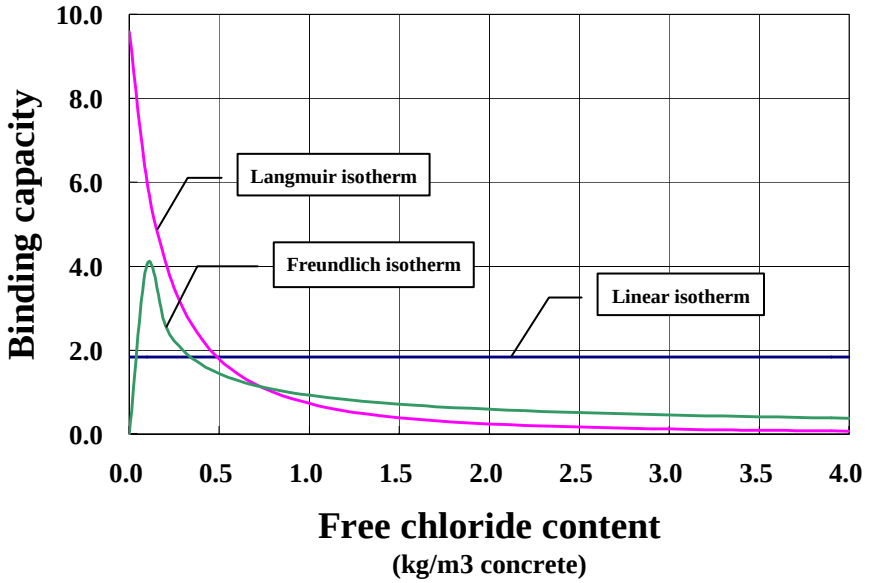

Figure 4.3. Binding capacity of concrete

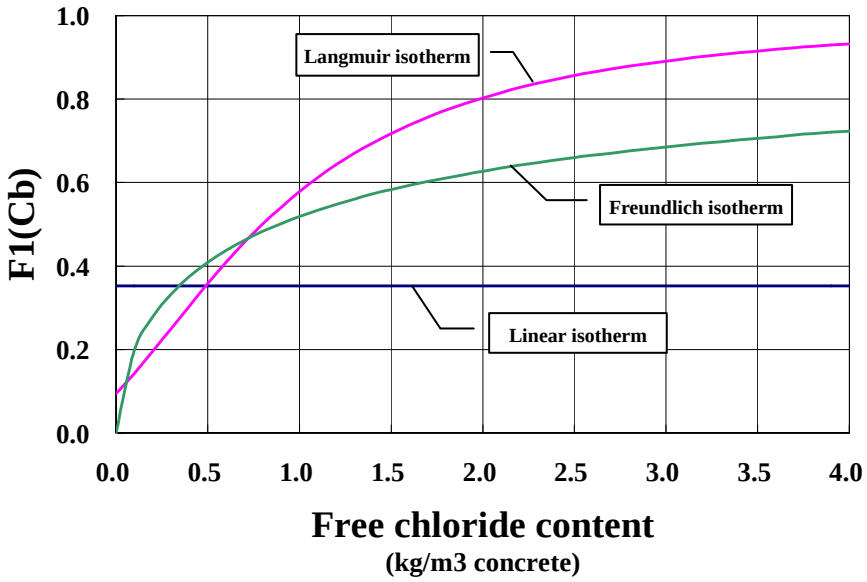

Figure 4.4. Influence of binding capacity on diffusivity

Various factors affecting the chloride-induced reinforcement corrosion in concrete

can be classified into two major groups (Ahmad 2003). One group consists of internal factors such as the mineral composition of cement, mixture proportion and quality of concrete ingredients, casting and curing condition, chemical composition of the reinforcing steel, corrosion protection measures etc. The other group consists of external factors such as availability of oxygen and moisture at reinforcement, relative humidity and temperature, and chloride content etc. In this study, the external influencing factors are the main concerns.

Environmental conditions may exert substantial influences on the chloride diffusivity of concrete. A computational framework for modeling multiple coupled transport processes has been developed before, where various influencing factors on the transport rate were considered using a multifactor law. In this study, the dependence of the actual chloride diffusivity D_{cl} on the age, the local chloride content, the temperature, and the LRCD of concrete are included in a multifactor law as

$$D_{cl} = D_{cl,0} \cdot F_2(t) \cdot F_3\left(C_{cl,f}\right) \cdot F_4(T) \cdot F_5\left(\rho_{local}\right) \tag{4.15}$$

where $D_{cl,0}$ may be regarded as the reference or nominal chloride diffusivity when all influencing factors assume values of unity. $F_2(t)$ denotes the influence of the age of concrete, which reflects the cement hydration-induced reduction in the concrete porosity with time. $F_3\left(C_{cl,f}\right)$ represents the influence of the free chloride content, which reflects the hindering effect of high chloride content on the chloride diffusion. $F_4(T)$ indicates

the influence of temperature, which reflects the thermodynamic effect of high temperature on the chloride diffusion. $F_5(\rho_{local})$ reflects the influence of elemental LRCD ρ_{local}.

Following Snyder (2001), the reference chloride diffusivity $D_{cl,0}$ can be estimated as a function of the water to cement ratio WCR as

$$\log_{10}(D_{cl,0}) = 6.0 \cdot WCR - 13.84 \tag{4.16}$$

With the water to cement ratio WCR = 0.5, the reference chloride diffusivity $D_{cl,0}$ assumes a value of 14.45×10^{-12} m^2/s herein.

According to Martin-Perez et al. (2001), the influencing factor due to the age of concrete $F_2(t)$ takes the form

$$F_2(t) = \left(\frac{t_{ref}}{t}\right)^m \tag{4.17}$$

where t_{ref} is the reference age from which $D_{cl,0}$ is derived (assumed to be 1 year herein), t is the actual age of concrete (year), and the empirical parameter m assumes a value of 0.04.

The influencing factor due to the local chloride content $F_3(C_{cl,f})$ follows Xi and Bazant (1999) and Kong et al. (2002) as

$$F_3\left(C_{cl,f}\right)=1-\kappa\cdot\left(C_{cl,f}\right)^n \tag{4.18}$$

where the empirical parameters κ = 8.333, and n = 0.5. Note that the unit of the free chloride content $C_{cl,f}$ herein assumes kg/kg of concrete herein.

Based on Arrhenius' law, both Martin-Perez et al. (2001) and Kong et al. (2002) suggested the influencing factor due to temperature as

$$F_4\left(T\right)=\exp\left[\frac{E}{R}\left(\frac{1}{T_{ref}}-\frac{1}{T}\right)\right] \tag{4.19}$$

where E is the activation energy of the chloride diffusion process (kJ/mol), assuming a value of 44.6 for WCR = 0.5; R is the gas constant (= 8.314 J/mol · K), T_{ref} is the reference temperature at which $D_{cl,0}$ is determined (= 296 K), and T is the actual absolute temperature in concrete (K).

As elaborated in Chapter 3, Aldea et al. (1999a) developed some conceptual models and drew the conclusion that the chloride diffusivity through cracked concrete is proportional to the crack width. Considering both LRCD and crack width are analogous indices of the cracking state, it is reasonable to assume that the chloride diffusivity of the concrete element is similarly a linear function of its LRCD. Assume the initial chloride diffusivity of the concrete element without deterioration-induced cracks is $D_{cl,0}$.

Moreover, the maximum LRCD = 1 is supposed to correspond to the chloride diffusivity $D_{cl,\max}$ of a completely cracked concrete element. Therefore, the chloride diffusivity of the cracked concrete element can be formulated as a function of its LRCD

$$D_{cl,crack} = \left(D_{cl,\max} - D_{cl,0}\right)\rho_{local} + D_{cl,0} \tag{4.20}$$

Gerard and Marchand (2000) suggested a recommended value of multiplication factors ($MF = 8$) to accommodate the increased chloride diffusivity of completely cracked concrete compared with uncracked concrete. Therefore,

$$D_{cl,\max} = MF \cdot D_{cl,0} \tag{4.21}$$

Thus, the relationship between the chloride diffusivity of cracked concrete element and its LRCD can be reduced further as

$$D_{cl,crack} = \left[\left(MF - 1\right)\cdot \rho_{local} + 1\right]\cdot D_{cl,0} \tag{4.22}$$

The influencing factor of elemental LRCD on the chloride diffusivity can be expressed as

$$F_5(\rho_{local}) = (MF - 1) \cdot \rho_{local} + 1 \tag{4.23}$$

The aforementioned influencing factors that affect the apparent chloride diffusivity of concrete D_{cl}^{*} are summarized in the Fig. 4.5.

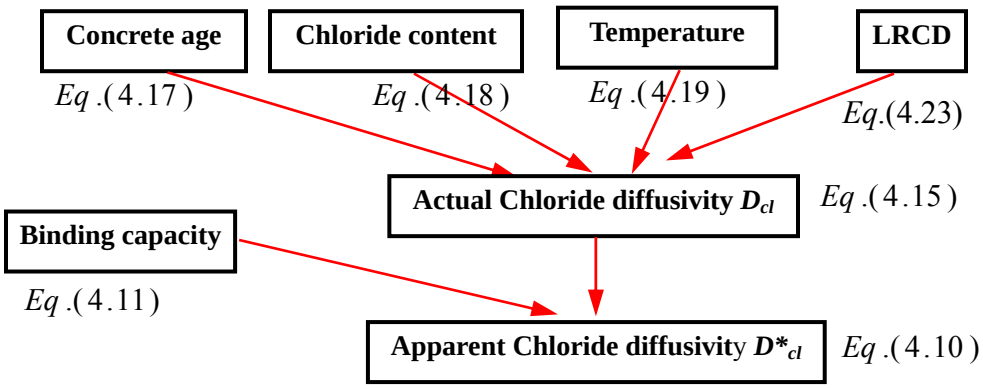

Figure 4.5. Influencing factors on apparent chloride diffusivity

4.4. Implementation of proposed methodology

Considering the dependence of the chloride diffusivity on several influencing variables as well as the time-varying boundary conditions, it is impossible to solve the nonlinear partial differential equation in Eq. (4.9) analytically. Different numerical methods have thus been developed in the literature (Martin-Perez 2001, Kong et al. 2002, Shin and Kim 2002, Masi et al. 1997, Wang et al. 2005) to simulate the chloride penetration process in concrete. These simulation algorithms are implemented using self-programmed computer codes. This study is making efforts to develop a computational framework to solve Eq. (9) numerically using existing FEA solver in

commercial 3-D software, where the chloride transport process is numerically solved in space as a boundary-value problem and in time as an initial-value problem. Potential coupling effects due to various influencing factors are conveniently considered by adjusting the transport property using a multifactor law and existing numerical models, as discussed in Section 4.3.

Considering the analogy between the governing differential equations of chloride penetration and heat transfer, it is possible to simulate the chloride diffusion process following the transient thermal analysis available in commercial finite element codes. The physical parameters in the heat transfer process need to be transformed to correspond to those in the chloride penetration process. For the main field variable, the temperature T maps to the free chloride content $C_{cl,f}$; for the transport property, the thermal conductivity k maps to the actual chloride diffusivity D_{cl}; and for the source/sink term, the heat source/sink term $\dot{Q}(t)$ maps to the sink term, i.e., the binding rate of free chloride content $\frac{1}{\omega_e} \cdot \frac{\partial C_{cl,b}}{\partial t}$.

In this study, the proposed computational framework is implemented using existing FEA solver in commercial software (ANSYS used for illustration). The heat transfer, chloride penetration and stress/cracking processes are defined as individual physics environments first, where the 8-node 3-D thermal element Solid70 with one DOF of temperature at each node is selected for heat transfer and chloride penetration processes, while the corresponding 8-node 3-D concrete element Solid65 with three translation

DOFs at each node is selected for stress/cracking process. Next, a coupled multi-physics method is utilized to call each physics environment in turn, apply the time-dependent environmental loads and material properties (i.e., the chloride diffusivity in this study), and then perform the transient simulation of three deterioration processes iteratively within each time step. To account for the influences of various possible factors on chloride penetration as shown in Fig. 4.5, the output results at the i^{th} time step — including the age of concrete, the spatial distributions of temperature, local chloride content and LRCD, as well as the associated chloride binding capacity — are extracted to modify the apparent chloride diffusivity D_{cl}^{*} of each finite element at the next $(i+1)^{th}$ time step using the multifactor law in Eq. (4.15). All output results are classified and stored in individual arrays at each time step. The numerical simulation procedure for the coupled heat transfer, chloride penetration and stress/cracking processes is summarized in Fig. 4.6. A self-programmed code in ANSYS Parametric Design Language (APDL) is required to implement the flow chart and the proposed methodology.

Although the sink term of the chloride diffusion process, i.e. the binding rate of free chloride content $\frac{\partial C_{cl,b}}{\partial t}$, has been "eliminated" skillfully using the influencing factor $F_1\left(C_{cl,b}\right)$ by adopting Eq. (4.9), the equivalent sink term at each time step can be evaluated explicitly as follows:

$$\dot{C}_{cl,b} = \frac{\partial C_{cl,b}}{\partial t} \cong \begin{cases} \dfrac{C_{cl,b,i}}{\Delta t_i} & i = 1 \\ \dfrac{C_{cl,b,i+1} - C_{cl,b,i}}{\Delta t_i} & i > 1 \end{cases} \tag{4.24}$$

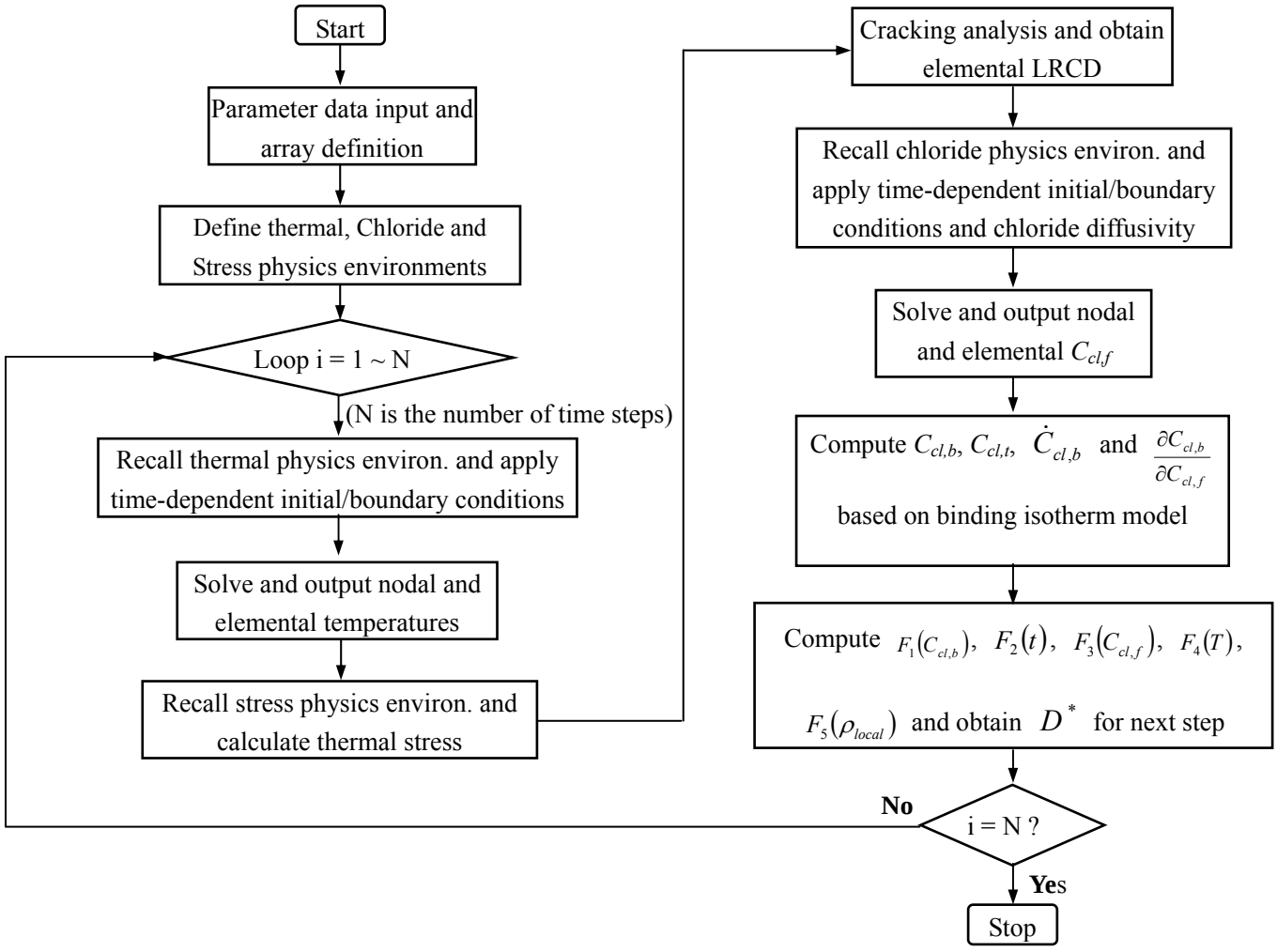

Figure 4.6. Simulation procedure of chloride penetration process

As shown in Fig. 4.5, it is observed that all influencing factors function in one-way direction. Such one-way coupling relationships help avoid time-consuming iterative

computation within each time step and simplify the convergence algorithm. The length of each time step can be controlled to achieve stable results, corresponding to the desired convergence criterion.

Compared with the existing numerical models, the prominent advantages of the proposed finite element-based computational methodology can be summarized as follows. Making use of an existing commercial FEA solver and transient thermal analysis capacity, the proposed methodology is rather straightforward and efficient in simulating the chloride penetration process and predicting the evolution of chloride content profile in concrete. This facilitates 3-D chloride diffusion simulation, and the inclusion of randomly varying boundary conditions. Second, the influences of various factors can be taken into account conveniently using the multifactor law, and the chloride diffusivity of each concrete element can be adjusted accordingly at each time step. Third, plentiful simulation results of each element in concrete structure — including free chloride, bound chloride, total chloride, binding capacity, binding rate, and any influencing factor — can be extracted easily at each time step and be postprocessed further. These obtained results help deepen the insight on the mechanism of chloride penetration. Finally, the methodology is flexible and can be expanded further to incorporate other deterioration processes as individual physics environments, thus facilitating the overall assessment of durability and the service life estimation of concrete structures under multiple coupled deterioration processes.

4.5. Numerical example

A concrete slab with a thickness of 150 mm, reinforced at the slab bottom in one direction only, is selected herein to illustrate the proposed finite element-based computational framework. The total time length is assumed to be 30 years, which is divided equally into 120 time steps with up to 30 substeps for each time step. An automatic time stepping (i.e. adaptive loading) scheme in ANSYS can ensure that the substep size is neither too aggressive nor too conservative, which greatly helps achieve convergence. The averaged duration of each substep (less than one month) has been confirmed to be small enough to guarantee a convergent solution. The assumed material properties of concrete in Table 2.1 are remained, and the concrete element allows nonlinear stress and smeared cracking analysis. The reinforced concrete slab is shown in Fig. 4.7.

While the entire concrete slab is assumed to be chloride-free initially, a constant free chloride content of 3.5 kg/m^3 of concrete is applied on the bottom surface. The surface chloride content is derived from Stewart and Rosowsky (1998), where the mean surface chloride content for each state in the United States is determined statistically as 3.5 kg/m^3 of concrete. Meanwhile, an annually varying ambient temperature $T_{ambient} = 15 + 10 \cdot \sin(2\pi \cdot t)$ is also applied on the bottom surface by following Saetta et al. (1995). A constant temperature of 15 ^{0}C is maintained on the top surface, and the initial

temperature of 15 ^{0}C is assumed for the entire concrete slab. The boundary conditions are shown in Fib. 4.8.

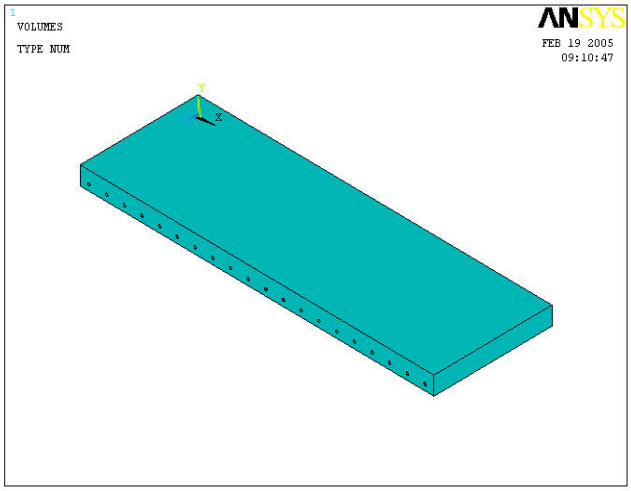

Figure 4.7. Reinforced concrete slab

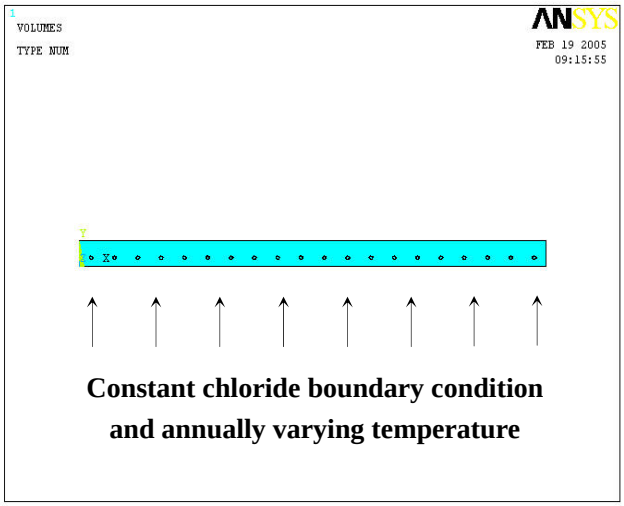

Figure 4.8. Boundary conditions

Considering the symmetric and repetitive characteristics of the geometry of the concrete slab and the initial/boundary conditions, only a representative part of the concrete slab is isolated as shown in Fig. 4.9 to carry out the chloride diffusion simulation process. The four side surfaces of the concrete slab are assumed to be isolated from heat and chloride flux, and restricted in *x* and *z* directions (note: the vertical direction *y* is set free).

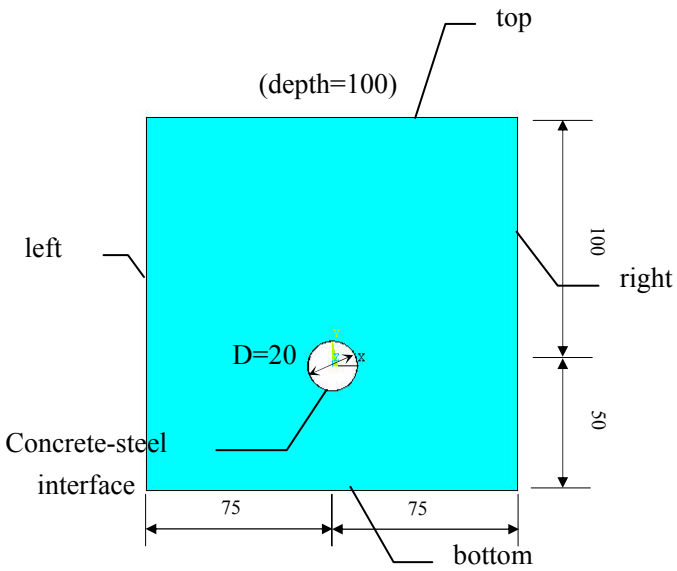

Figure 4.9. Cross-section of concrete slab

The diameter of the reinforcing steel is 20 mm, the center of the reinforcing steel is assumed 50 mm from the bottom surface of the concrete slab, and the depth of the concrete slab is assumed to be 100 mm. The finite element model is shown in Fig. 4.10. Various simulation results will be assessed at the target node, which is on the same level as the center of the reinforcing steel, and at four elements around the target node. The

simulation results are used later to determine the corrosion initiation time $t_{initiation}$.

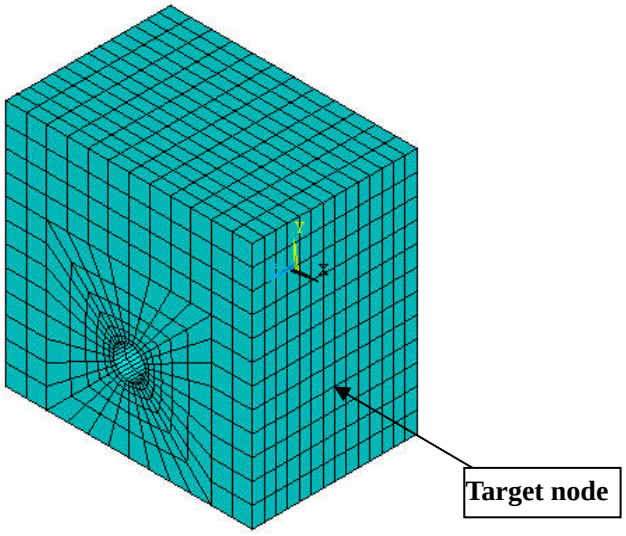

Figure 4.10. Finite element model

Based on three established binding isotherm models, three sets of simulation results are summarized in Figs. 4.11~4.23, respectively. The time-varying free, bound and total chloride contents, $C_{cl,f}$, $C_{cl,b}$ and $C_{cl,t}$ (units in kg/m^3 of concrete) at the target node are shown in Figs. 4.11(a)~(c), respectively. The time-varying chloride binding capacity of concrete $\frac{\partial C_{cl,b}}{\partial C_{cl,f}}$ (unit in m^3 of concrete /m^3 of concrete) at the target node is shown in Fig. 4.12. From Figs. 4.11 and 4.12, it is observed that the simulation results of the Langmuir and Freundlich isotherms are close to each other, and are highly different from the result of the linear isotherm.

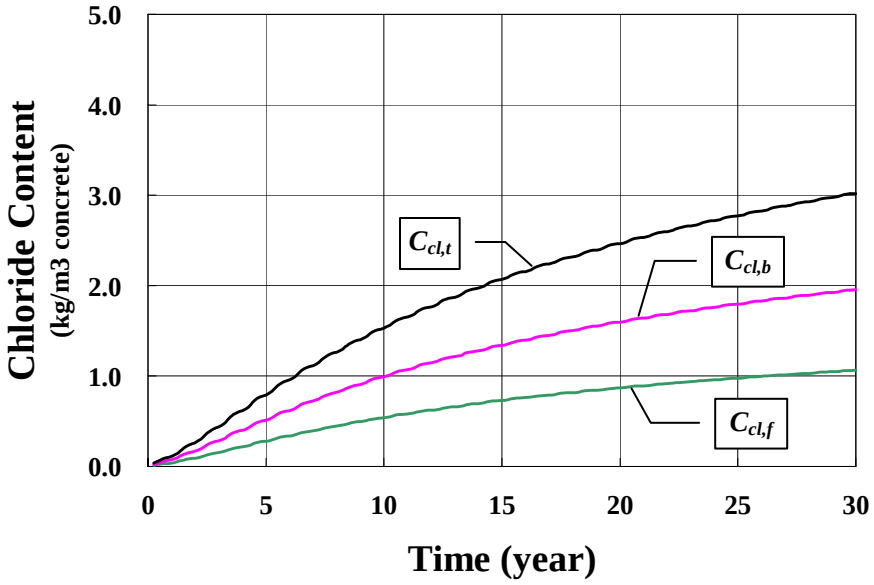

Figure 4.11(a). Chloride content for Linear isotherm

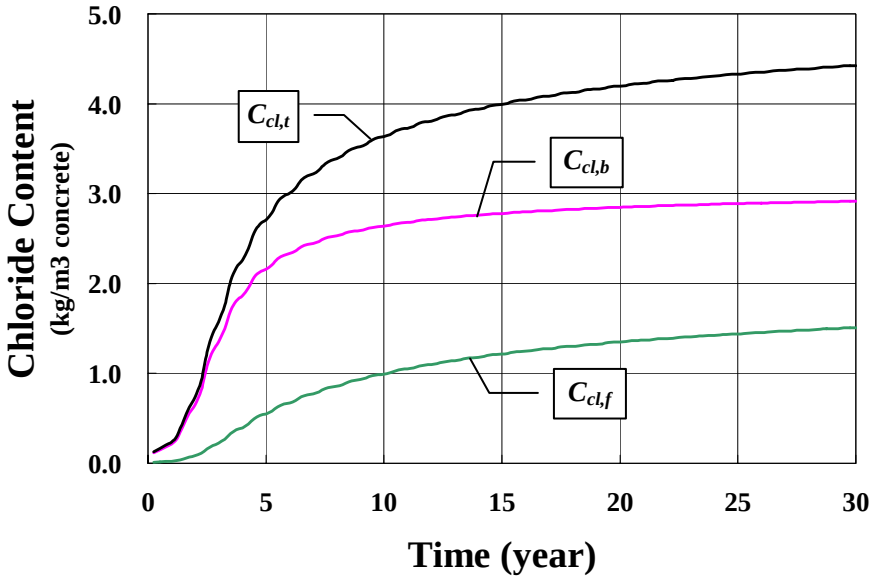

Figure 4.11(b). Chloride content for Langmuir isotherm

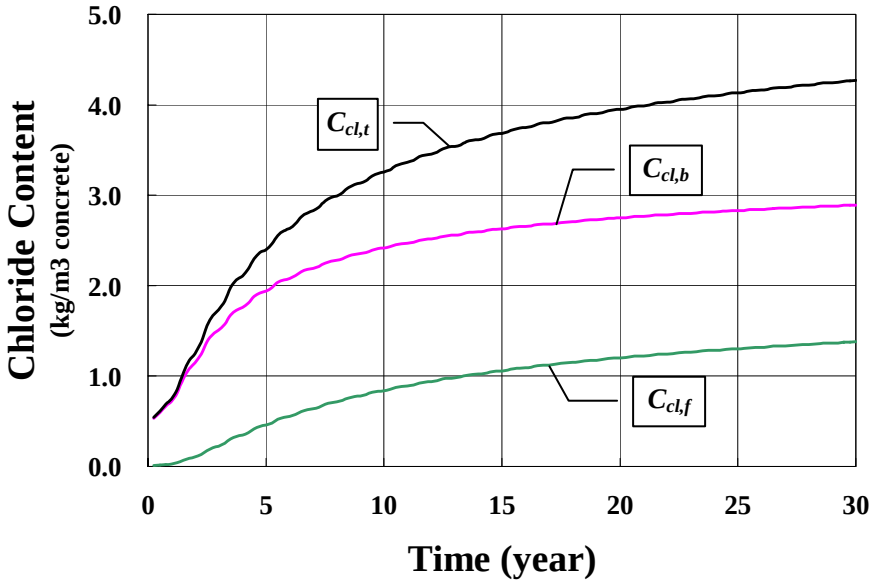

Figure 4.11(c). Chloride content for Freundlich isotherm

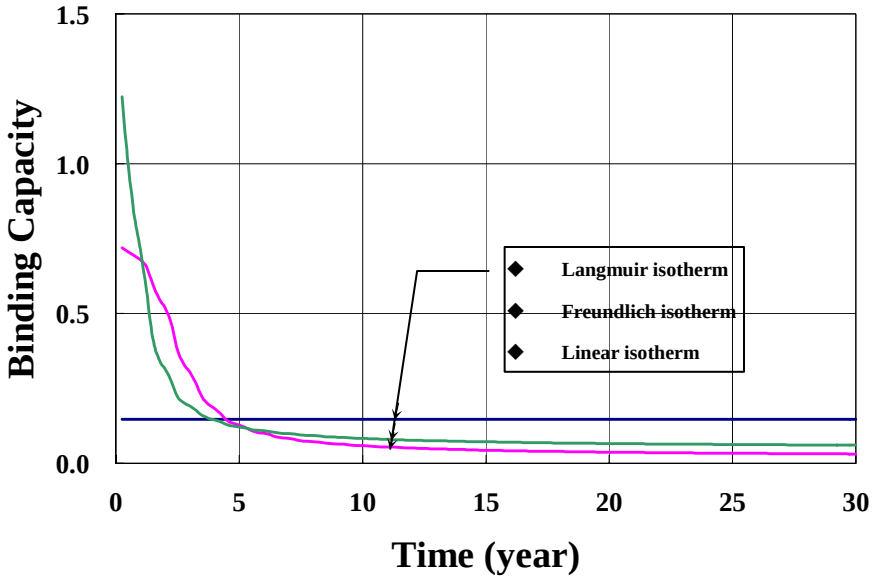

Figure 4.12. Binding capacity of concrete

The time-varying equivalent sink term, i.e. the binding rate of the free chloride $\frac{\partial C_{cl,b}}{\partial t}$ (unit in kg/m^3 of concrete · year) at the target node is shown in Fig. 4.13. It is observed that the fluctuation of the sink term is obviously caused by the seasonal variation of the ambient temperature.

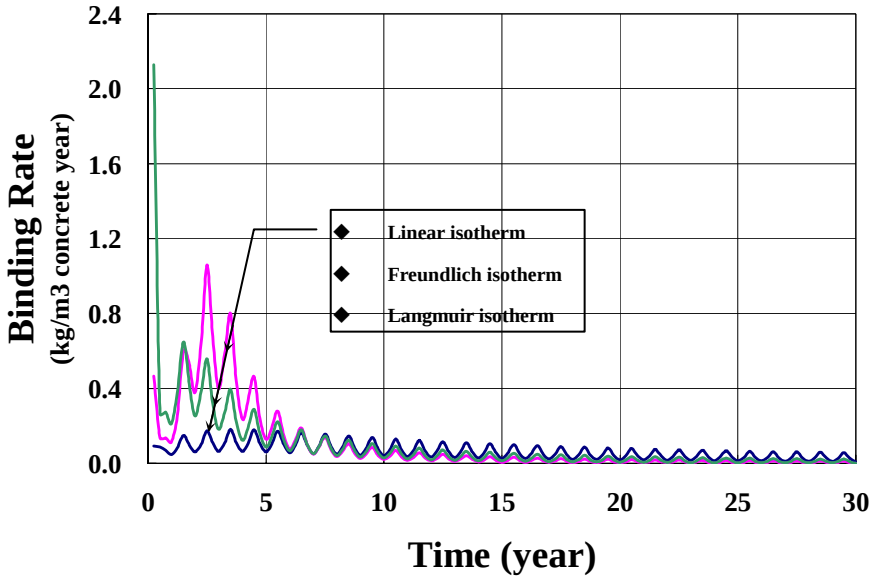

Figure 4.13. Binding rate of concrete

At the four concrete elements around the target node, the averaged time-varying $F_1(C_{cl,b})$ due to the chloride binding capacity, $F_2(t)$ due to the age of concrete, $F_3(C_{cl,f})$ due to the local chloride content, $F_4(T)$ due to the temperature, and $F_5(\rho_{local})$ due to the elemental LRCD are shown in Figs. 4.14~4.18, respectively.

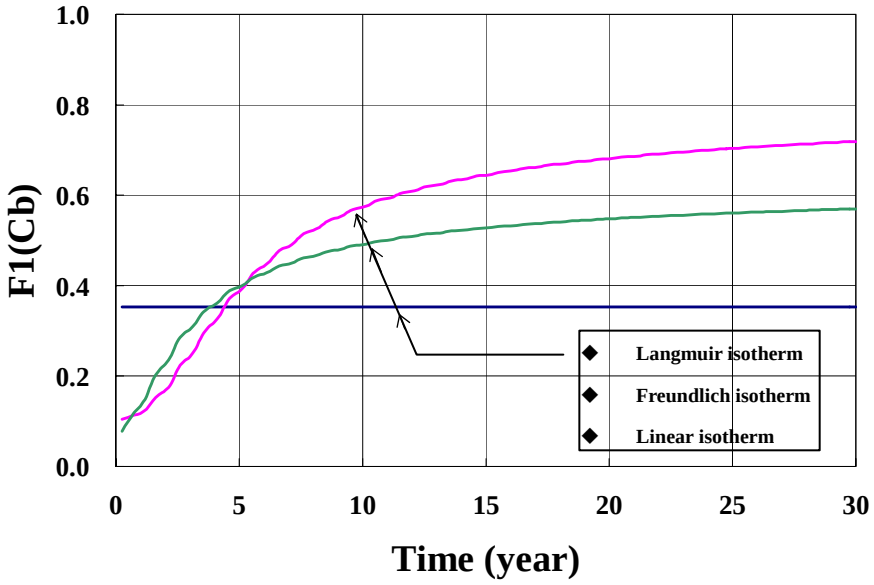

Figure 4.14. Influence of binding capacity on apparent chloride diffusivity

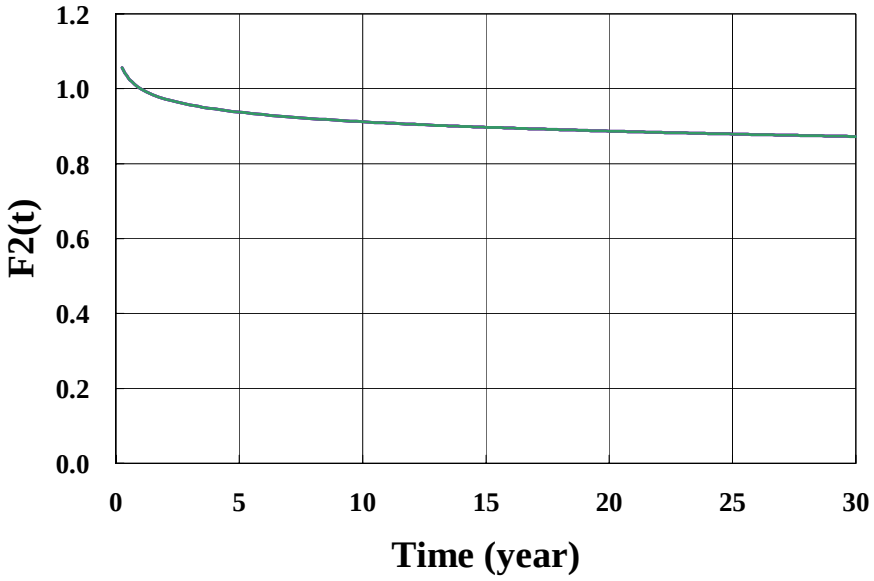

Figure 4.15. Influence factor of concrete age on chloride diffusivity

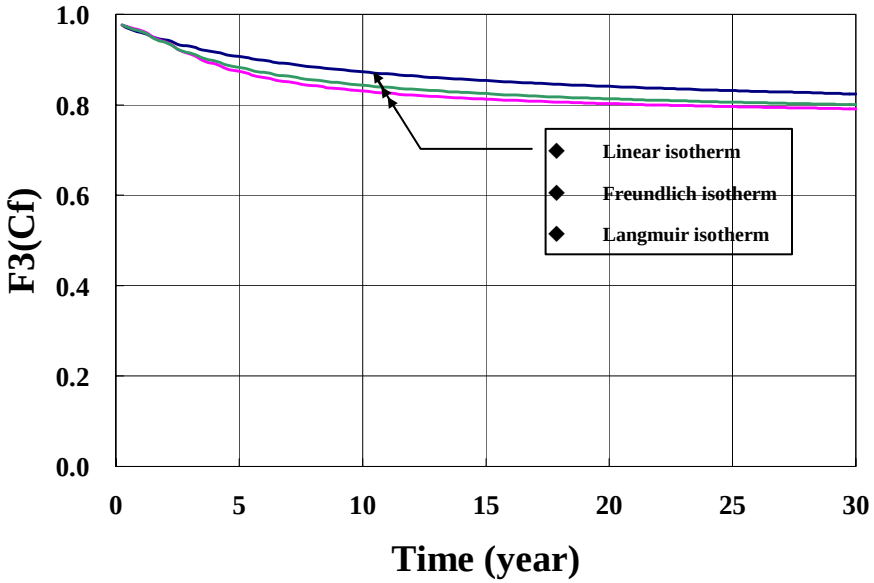

Figure 4.16. Influence of free chloride on chloride diffusivity

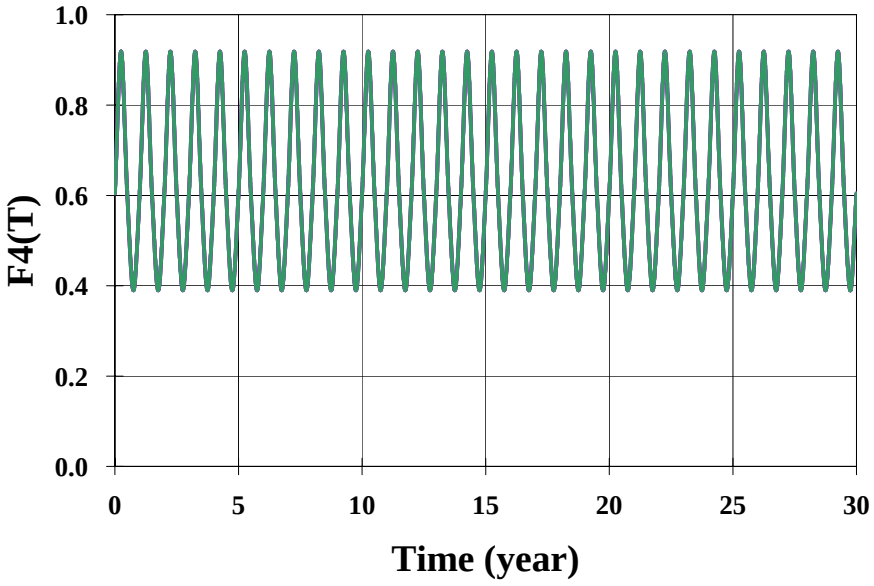

Figure 4.17. Influence of temperature on chloride diffusivity

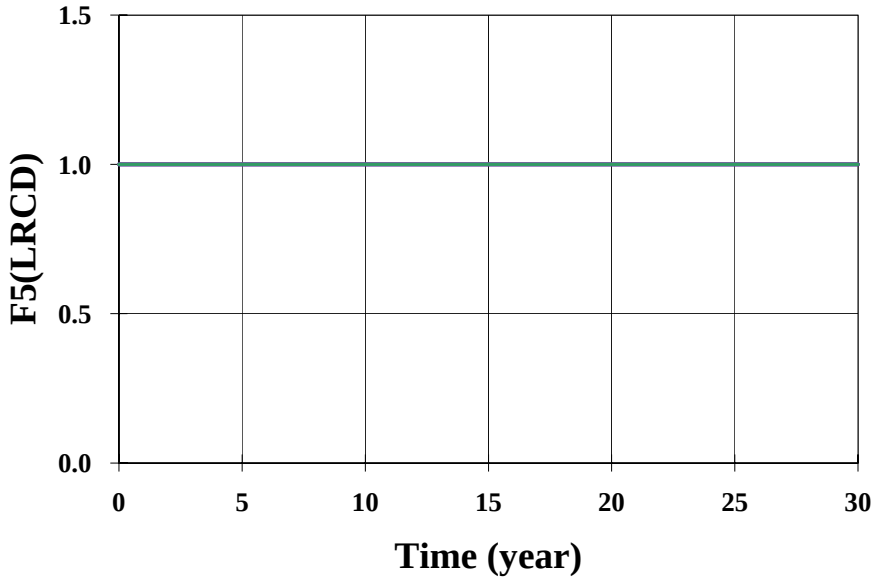

Figure 4.18. Influence of elemental LRCD on chloride diffusivity

$F_2(t)$ and $F_4(T)$ are similar for all three binding isotherm models due to the same time and temperature history. $F_5(\rho_{local})$ remains a constant of 1.0, which means thermal stress in concrete does not cause cracking at the four concrete elements during the chloride penetration process. $F_1(C_{cl,b})$ and $F_3(C_{cl,f})$ are different from each other for the three different binding isotherm models.

The averaged time-varying D_{cl}^{*} at the four elements around the target node, after considering the influences of the binding capacity, the age of concrete, the local chloride content, the temperature and elemental LRCD, is shown in Fig. 4.19. Considering the chloride diffusivity in concrete may vary over several orders of magnitude, the approximate mean value of the obtained apparent chloride diffusivity 1.0×10^{-4} m^2/year (or 3.17×10^{-12} m^2/s) is a little higher than an overall mean value of 2.0×10^{-12} m^2/s

observed in the U.S. (Stewart and Rosowsky 1998). The difference may be attributed to the inherent composition of concrete, the casting and curing conditions, or the assumed $D_{cl,0}$ etc. Considering the monotonically varying trends of $F_1(C_{cl,b})$, $F_2(t)$, and $F_3(C_{cl,f})$, the strong fluctuation of the apparent chloride diffusivity can only be caused by $F_4(T)$ due to the seasonal variation of the ambient temperature. In addition, the general varying trends of the apparent chloride diffusivity coincide only with those of $F_1(C_{cl,b})$ due to the chloride binding capacity, which reflects the tremendous influence of the chloride binding effect of concrete.

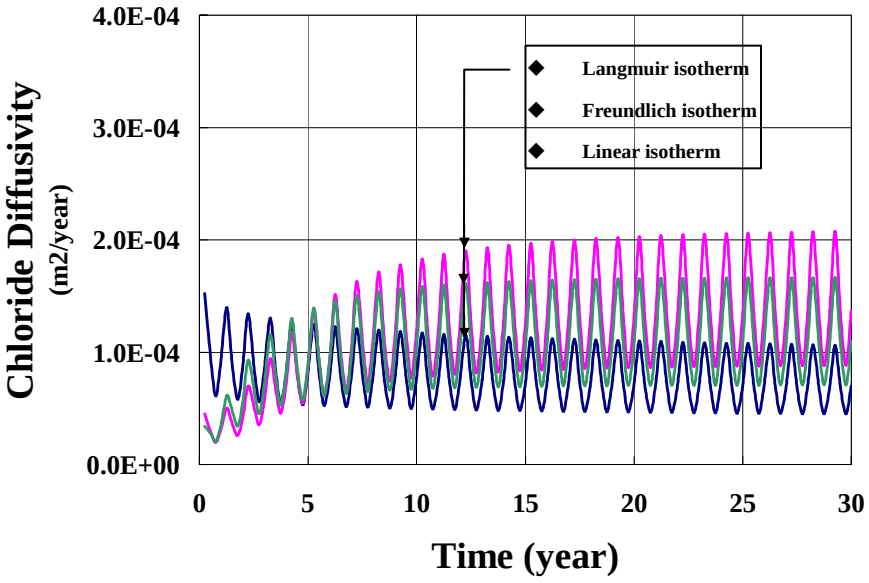

Figure 4.19. The average apparent chloride diffusivity

The free chloride content profiles at the 1st, 2nd, 5th, 10th, 20th and 30th year from the bottom to the top surface for the three binding isotherm models are shown in Figs.

4.20(a)~(c), respectively.

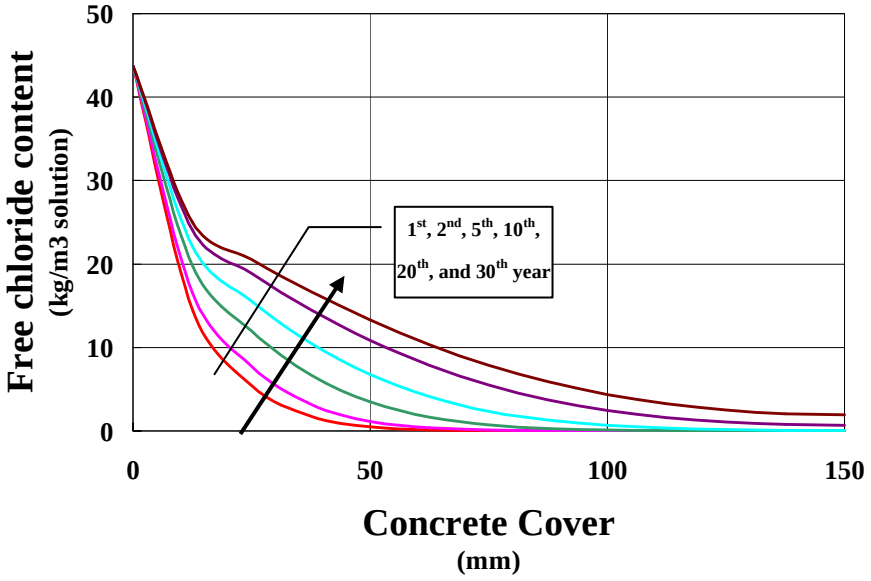

Figure 4.20(a). Free chloride content profiles for Linear isotherm

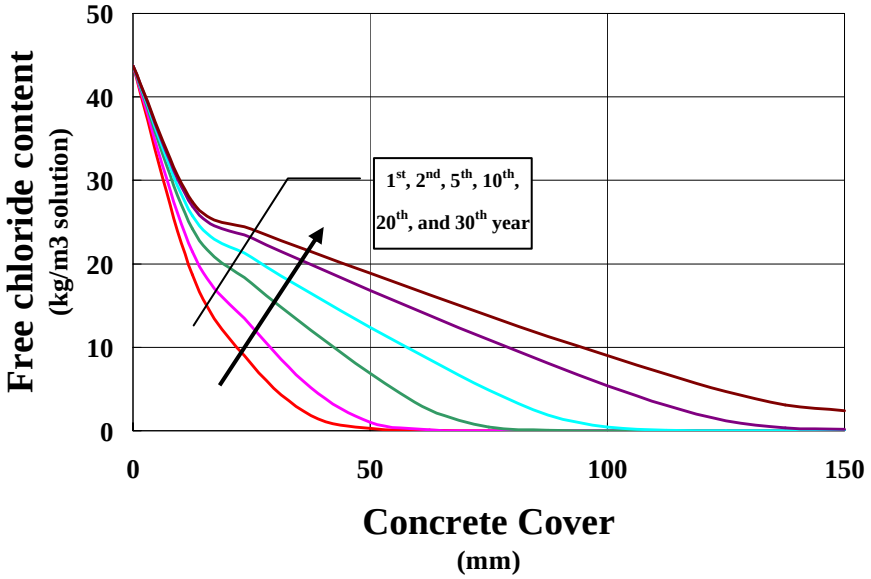

Figure 4.20(b). Free chloride content profiles for Langmuir isotherm

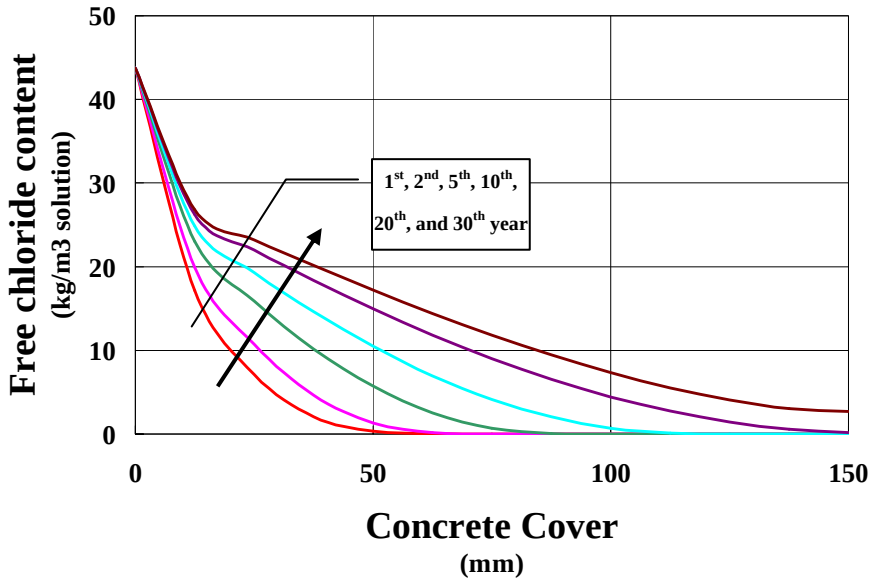

Figure 4.20(c). Free chloride content profiles for Freundlich isotherm

The bound chloride content profiles at the 1st, 2nd, 5th, 10th, 20th and 30th year from the bottom to the top surface for the three binding isotherm models are shown in Figs. 4.21(a)~(c), respectively. It is observed that the results of Langmuir and Freundlich isotherms agree with each other, and are different from the result of the linear isotherm.

The total chloride content profiles at the 1st, 2nd, 5th, 10th, 20th and 30th year from the bottom to the top surface for the three binding isotherm models are shown in Figs. 4.22(a)~(c), respectively. The agreements between the three isotherm models are similar to those in previous figures.

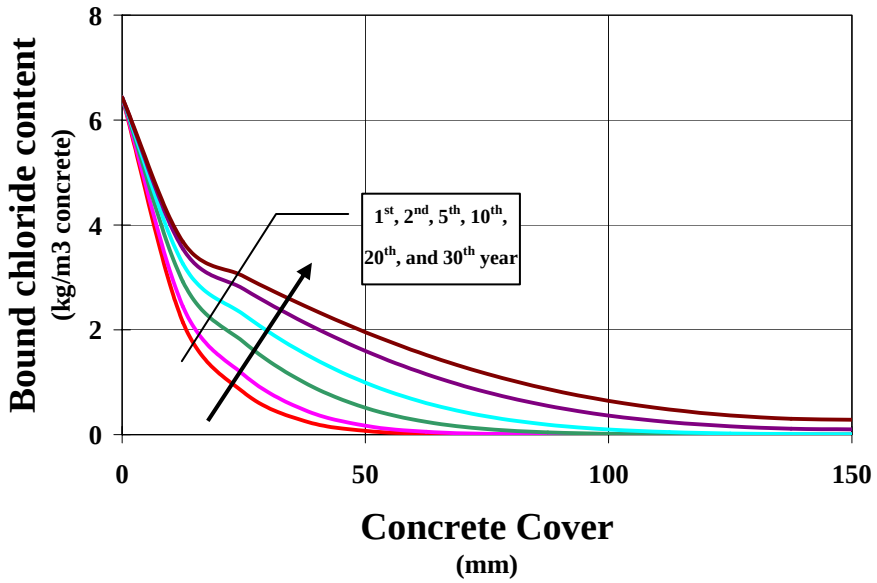

Figure 4.21(a). Bound chloride content profiles Linear isotherm

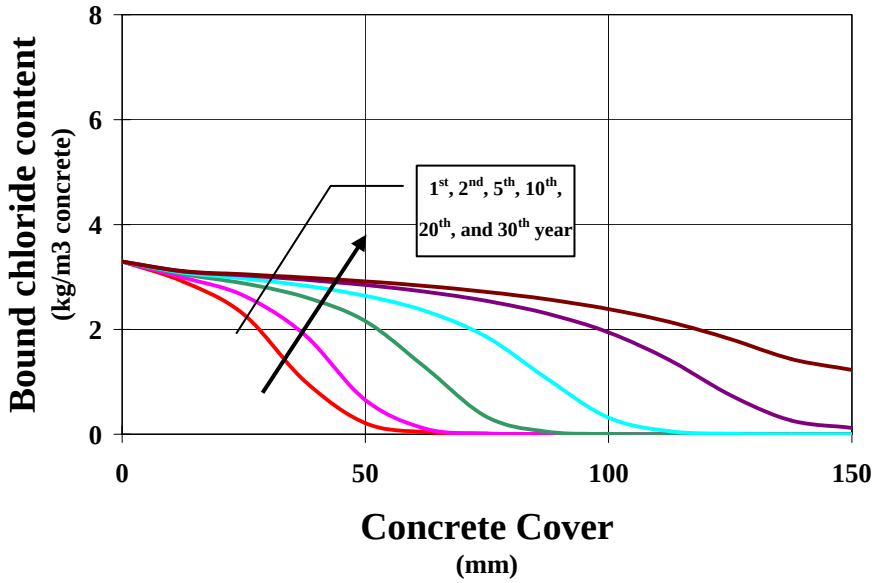

Figure 4.21(b). Bound chloride content profiles for Langmuir isotherm

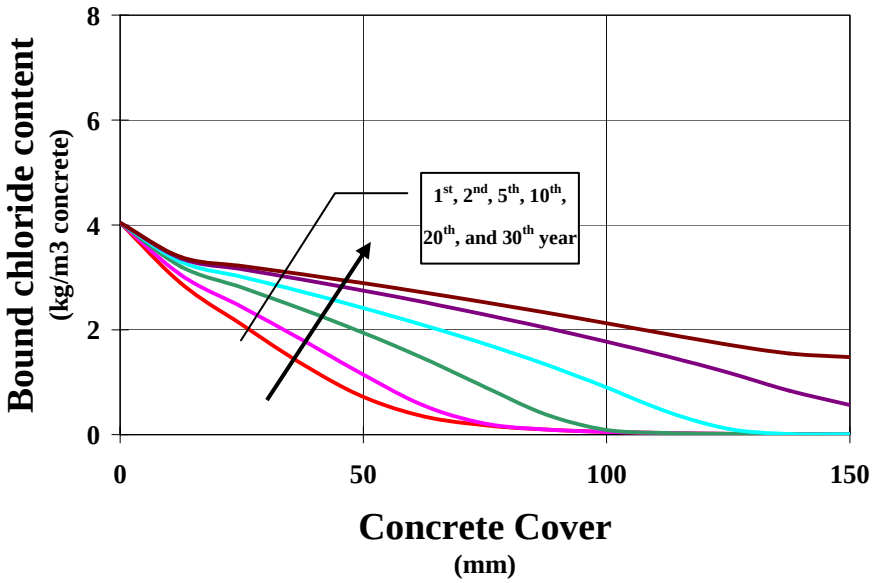

Figure 4.21(c). Bound chloride content profiles for Freundlich isotherm

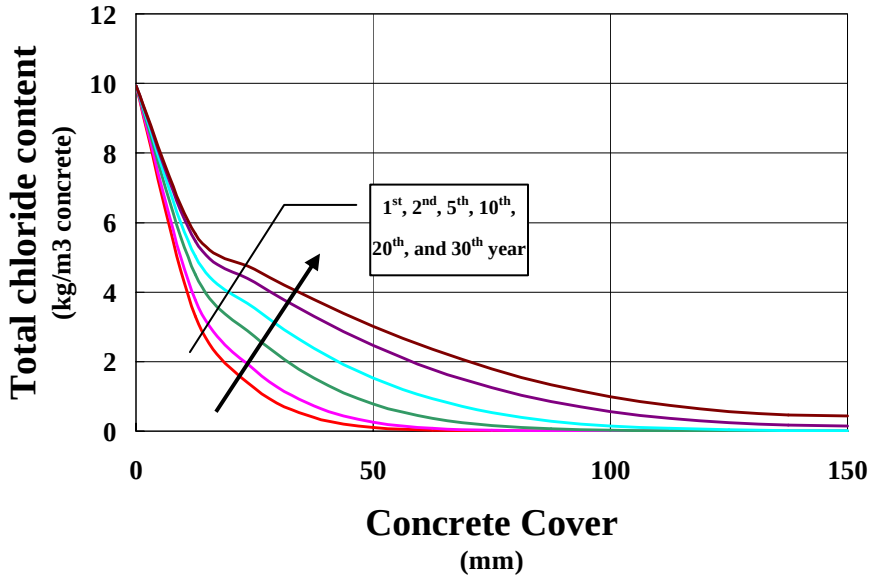

Figure 4.22(a). Total chloride content profiles for Linear isotherm

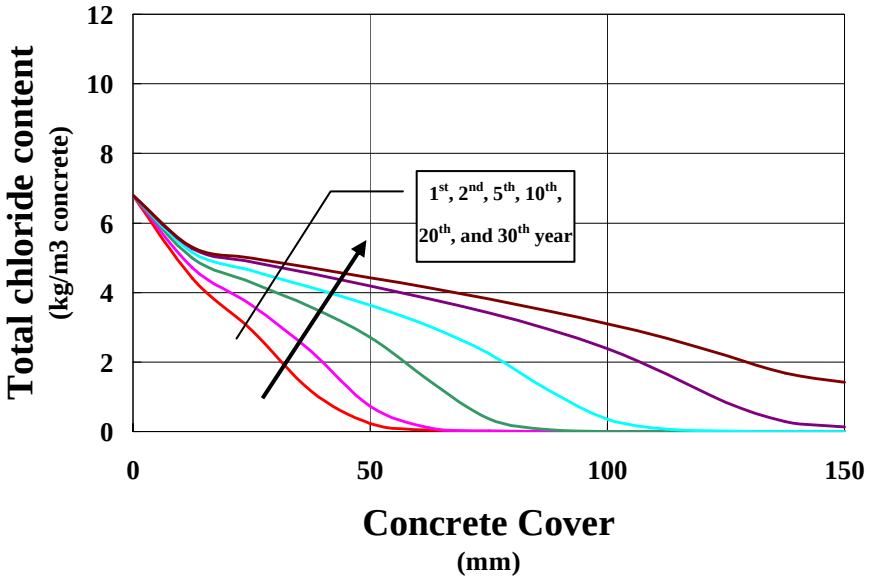

Figure 4.22(b). Total chloride content profiles for Langmuir isotherm

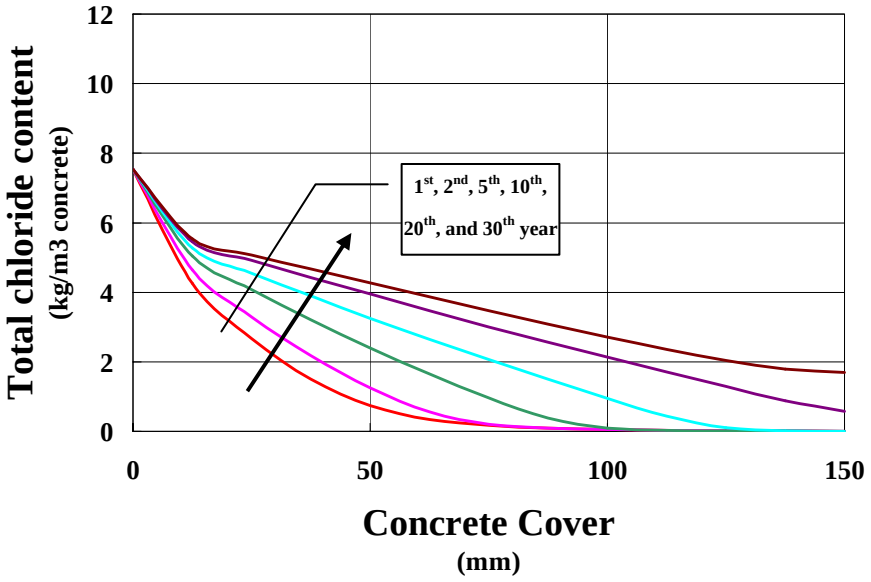

Figure 4.22(c). Total chloride content profiles for Freundlich isotherm

The binding rate profiles at the 1st, 2nd, 5th, 10th, 20th and 30th year from the bottom to the top surface for the three binding isotherm models are shown in Figs. 4.23(a)~(c),

respectively.

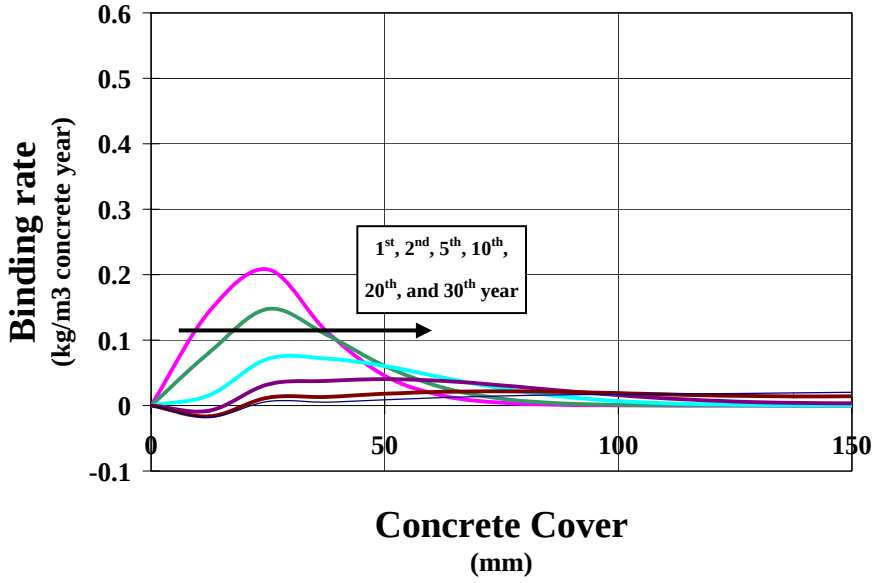

Figure 4.23(a). Binding rate profiles for Linear isotherm

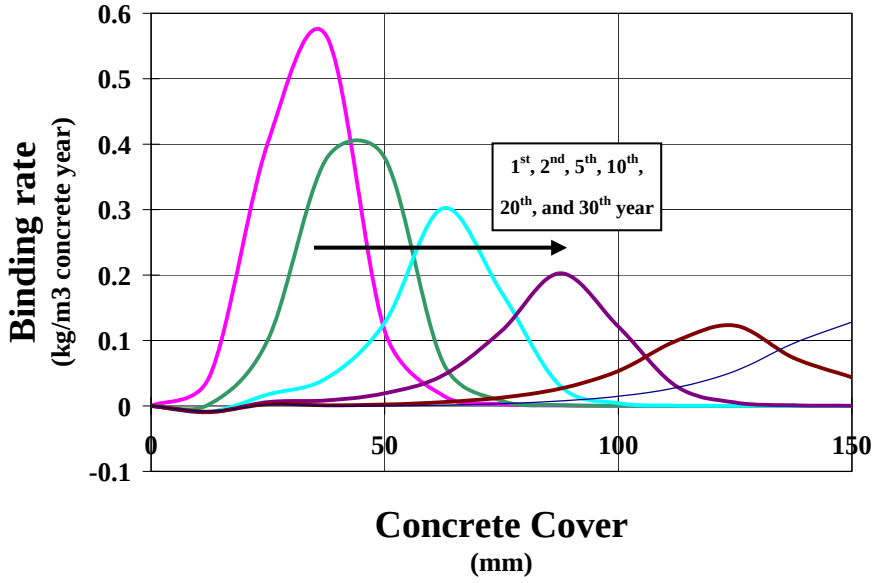

Figure 4.23(b). Binding rate profils for Langmuir isotherm

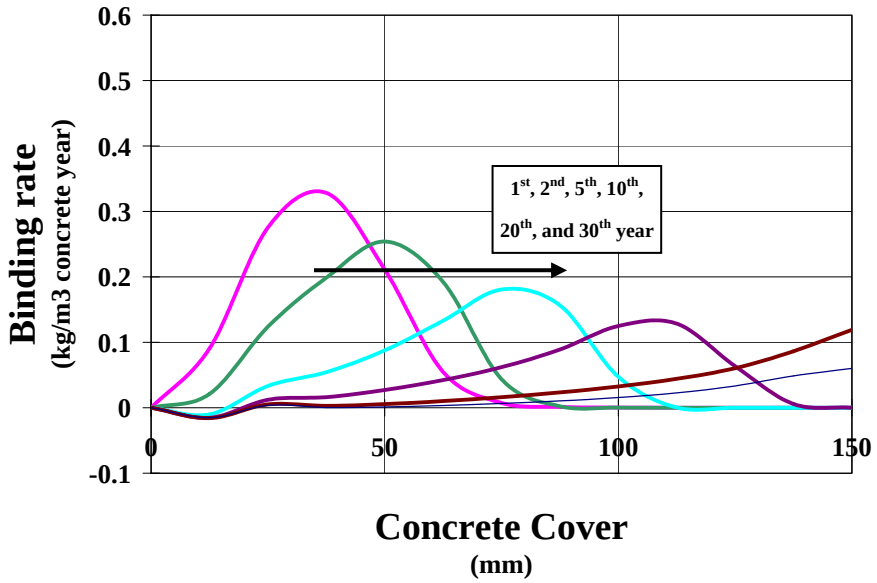

Figure 4.23(c). Binding rate profiles for Freundlich isotherm

Two interesting phenomena are observed: the peak value of the binding rate decreases with time, and the location of the peak binding rate moves away from the concrete surface. As the derivative of the bound chloride with respect to time, the binding rate follows the evolution of the bound chloride content profiles shown in Figs. 4.21(a)~(c). These observations deepen the insight of the binding effect of chloride in concrete.

The corrosion initiation time $t_{initiation}$ was defined earlier as the time till the free chloride content at the embedded reinforcement reaches a specified threshold value $C_{cl,cr}$. $t_{initiation}$ can be determined easily using the obtained free chloride content profiles, which is illustrated in Fig. 4.24. Due to the monotonic increase of the free chloride content at the embedded reinforcement, when the threshold value of the free chloride and the depth

of concrete cover are given, their intersection point must lie on the free chloride content profile curve of $t_{initiation}$.

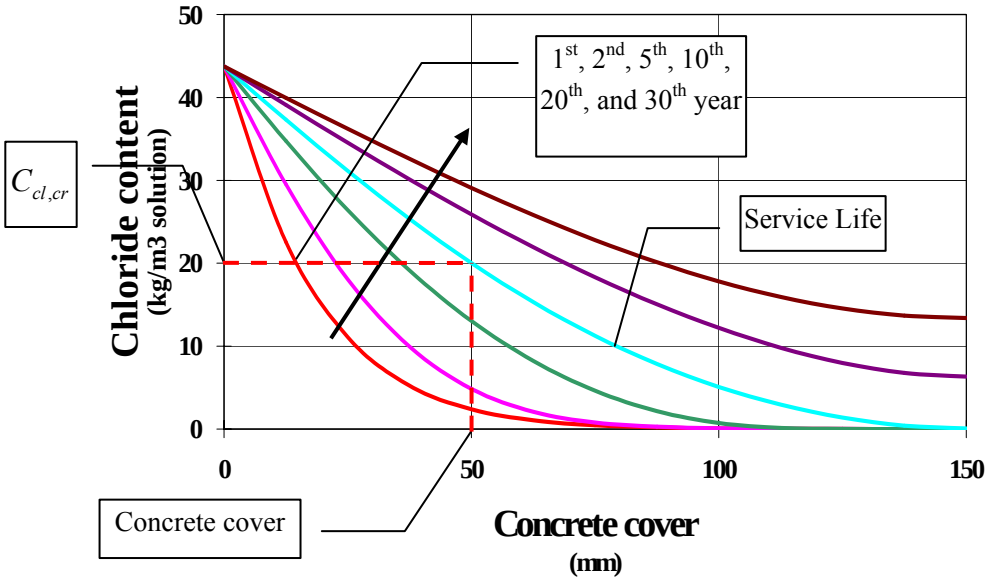

Figure 4.24. Schematic determination of $t_{initiation}$

In the numerical example, the distance from the center of the reinforcing steel to the bottom surface is assumed to be 50 mm. According to Stewart and Rosowsky (1998), the threshold chloride content $C_{cl,cr}$ shows variability, and is observed to be uniformly distributed within the range of 0.6~1.2 kg/m^3 of concrete. A value of 0.9 kg/m^3 of concrete (or 11.25 kg/m^3 of solution) is assumed tentatively to determine the values of $t_{initiation}$ to be 21.25 years, 8.5 years and 11.25 years for the linear, Langmuir and Feundlich isotherms respectively. These values of the corrosion initiation time are within

the usually observed range 7-20 years (Kong et al. 2002), which verifies the correctness of the proposed methodology to some extent. Meanwhile, different chloride binding isotherms result in obvious discrepancy in $t_{initiation}$, which demonstrates the importance of selecting an appropriate binding isotherm model.

In addition, some existing models in Section 4.2 can be utilized to verify the proposed methodology. Based on Clear's empirical model (1976) in Eq. (1), the corrosion initiation time $t_{initiation}$ can be obtained as 6.63 years, with t_c=1.97 in. (i.e., 5 cm), WCR=0.5, and $[Cl]$=43750 ppm (i.e., 3.5 kg/m^3 of concrete). This result is relatively close to the simulation result of 8.5 years from the Langmuir isotherm model.

According to Bazant's numerical model (1979a,1979b) in Eq. (6), t_c=5 cm, $C_{cl,cr}$=0.9 kg/m^3 of concrete, $C_{cl,0}$=3.5 kg/m^3 of concrete, the chloride diffusivity D_{cl} assumes an overall mean value of effective chloride diffusivity 2.0x10^{-12} m^2/s (i.e., 0.63 cm^2/year) observed in the U.S. (Stewart and Rosowsky 1998). As a result, the corrosion initiation time $t_{initiation}$ can be obtained as 8.33 years. This result agrees well with the simulation result of 8.5 years from the Langmuir isotherm model.

From the obtained simulation results, it is observed that different chloride binding isotherms may result in obvious discrepancy in $t_{initiation}$, which demonstrates the importance of selecting an appropriate binding isotherm model. As pointed out by Tang and Nilsson (1993), the conventional linear isotherm model is oversimplified and cannot be verified by experimental results. The Freundlich isotherm model is valid at high free chloride content, while the Langmuir isotherm applies at low free chloride content. Based

on this observation, both Xi and Bazant (1999) and Kong et al. (2002) chose the Freundlich isotherm model to characterize the chloride binding capacity. Considering a high surface chloride content of 3.5 kg/m^3 of concrete, the Freundlich isotherm model was initially thought to be a more appropriate model in this study. However, simulation results from the Langmuir isotherm model in this study agree better with two existing models (Clear 1976, Bazant 1979a, 1979b). A further investigation is needed to identify the most appropriate isotherm model.

4.6. Conclusion

Based on an existing FEA solver and an analogous transient thermal analysis, a finite element-based computational framework has been developed in this chapter to simulate the chloride penetration process and predict the evolution of chloride content profile in concrete. The influences of the chloride binding capacity of concrete, the age of concrete, the local chloride content, the temperature, and elemental LRCD on the chloride penetration are taken into account by adopting a multifactor law. Based on three established chloride binding isotherm models — linear, Langmuir, and Freundlich isotherms, three sets of simulation results are presented and compared for a reinforced concrete slab exposed to a constant chloride environment. The corrosion initiation times obtained are found to be within the observed range and agree well with existing models. The spatial and temporal distributions of free chloride, bound chloride, total chloride,

binding capacity, binding rate, and various influencing factors are easily computed with the proposed methodology, which helps to deepen the insight on the physical mechanism of chloride penetration. The proposed computational framework is general and can be expanded to include other deterioration processes, thus facilitating overall concrete durability and service life estimation under multiple deterioration processes. The methodology facilitates 3-D simulation, and the use of various boundary conditions in practical structures.

CHAPTER V

SIMULATION OF CORROSION-INDUCED REINFORCEMENT RUST EXPANSION AND CONCRETE CRACKING

5.1. Introduction

The durability of reinforced concrete structures is impacted by the chloride penetration and the susceptibility of reinforcement to chloride-induced corrosion, when exposed to marine environment, deicing salts or underground environment. Once the chloride content at the reinforcement reaches a threshold value and enough oxygen and moisture are present, the reinforcement corrosion will be initiated. Corrosion products then accumulate in the concrete-steel interface transition zone (ITZ), generate expansive pressure on the surrounding concrete, and cause crack initiation and propagation.

Quality concrete is able to prevent the embedded reinforcing steel from potential corrosion in three ways. First, hydration products of cement in concrete form a high alkaline pore solution environment, where the passivated film covering the steel surface remains chemically stable enough to protect reinforcing steel from corroding (Page and Treadaway 1982). Second, quality concrete usually possesses low porosity and permeability, which greatly minimizes the penetration of corrosion-induced agents (such as chloride, carbon dioxide, oxygen, and moisture etc.) through porous concrete. Third,

the high electrical resistivity of quality concrete restricts the corrosion by reducing the electrical current flow between the anodic and cathodic sites. However, quality concrete cannot always be attained in practice, especially when concrete with initial flaws (including micropores and microcracks) is exposed to adverse environments. Chloride penetration may result in the accumulation of chloride content at reinforcement to such a level that the high alkaline environment is destroyed and then the passivated film on the steel surface is disrupted (Townsend et al. 1981, Verbeck 1975). Once enough oxygen and moisture are present, the reinforcement corrosion will be initiated.

The corrosion products (including various iron oxides) with relatively lower density occupy much more volume than the original iron. As the corrosion progresses, the corrosion products accumulate in ITZ and generate expansive pressure on the surrounding concrete. The pressure builds up to such high level that cause crack initiation and propagation. In addition to the cracking in surrounding concrete, chloride-induced reinforcement corrosion results in loss of the concrete-steel interface bond, and reduction of the cross-sectional area of reinforcement, thus reduces the load carrying capacity of concrete structure (Mehta 1993).

The entire chloride-induced reinforcement corrosion process of reinforced concrete structures can be divided roughly into three phases as discussed in previous Section 4.1. Among the three phases, the first phase usually lasts for a relatively long period, depending on the corrosion resistance of reinforcement, the thickness and quality of concrete cover, and the ambient chloride content etc. The second phase is much shorter

than the first one, which is determined mainly by the porosity of ITZ and the corrosion rate. The third phase is the shortest one since the rust expansion-induced cracks propagate rapidly through the surrounding concrete. Considering the chloride-induced reinforcement corrosion only, the entire service life may be determined as the sum of all three phases. Under specified design requirements, the termination of service life may also be defined by an acceptable level of corrosion indicated on the vertical corrosion level axis of Fig. 4.1.

The chloride-induced reinforcement corrosion and cracking patterns corresponding to the three distinct phases defined in Fig. 4.1 are illustrated in following Fig. 5.1 (Liu and Weyers 1998).

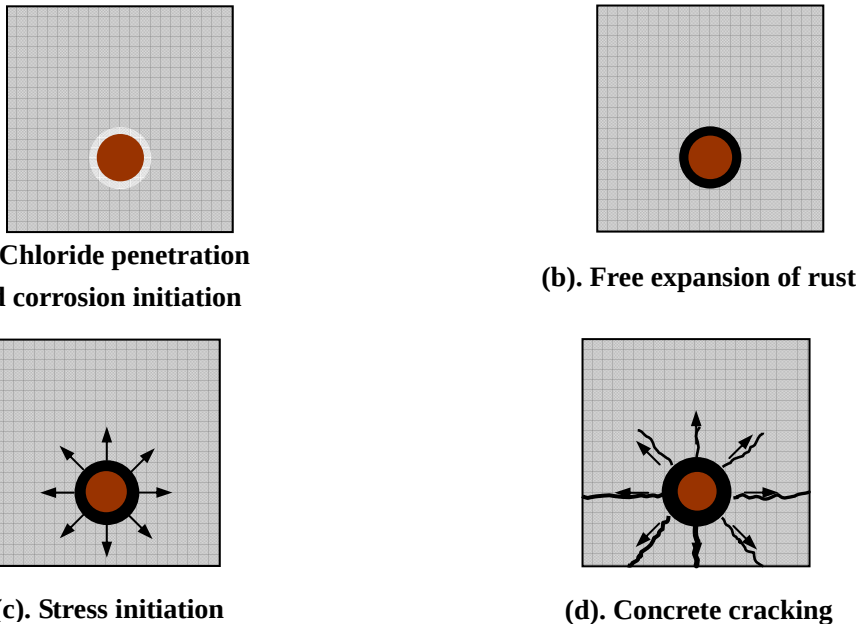

(a). Chloride penetration and corrosion initiation

(b). Free expansion of rust

(c). Stress initiation

(d). Concrete cracking

Figure 5.1. Chloride-induced reinforcement corrosion patterns

During the past decades, various empirical and numerical models have been proposed to estimate the deterioration caused by the chloride-induced reinforcement corrosion and to predict the service life of the reinforced concrete structure. Tuutti (1982) suggested a model to predict the service life, where the maximum acceptable corrosion level is related to the appearance of cracks. The deterioration process consists of two periods: initiation and propagation. The initiation period can be estimated as the time required for chloride to reach the reinforcement surface and trigger active corrosion, while the propagation period can be taken as the time elapsed until repair becomes mandatory. Cady and Weyers (1983) developed a deterioration model to estimate the remaining life of concrete bridge components in corrosive environment, assuming that chloride-induced reinforcement corrosion is the main cause of deterioration. The model predicts bridge deck deterioration level in terms of percentage area of the entire deck. Based on the physical mechanism for corrosion of reinforcing steel in concrete exposed to marine environment, Bazant (1979a, 1979b) proposed a mathematical model to determine the time to cracking of the concrete cover. In this model, the time to cracking is assumed to be a function of corrosion rate, cover depth, spacing of steel rebars, and mechanical properties of concrete. Based on field and laboratory observations, Morinaga (1990) developed an empirical model to predict the time to cracking. It is assumed that concrete cracking will first occur when there is a critical quantity of corrosion products forming on the reinforcement. Liu and Weyers (1998) suggested a similar corrosion-cracking model to compute the time to cracking using the critical amount of

rust, which consists of the amount of corrosion products needed to fill the ITZ voids plus the amount of corrosion products needed to generate sufficient tensile stresses to crack the cover concrete. In summary, a realistic numerical model for chloride-induced reinforcement corrosion process should be able to closely track each of the corrosion phases shown in Fig. 5.1.

The simulation of the first phase — the penetration of chloride has been implemented previously in Chapter 4, and this chapter concentrates mainly on the simulation of the subsequent two phases — the reinforcement rust expansion and the concrete cracking caused by chloride contamination. It should be emphasized that all three phases of the chloride-induced deterioration process are considered separately in this study.

5.2. Corrosion-induced reinforcement rust expansion model

Reinforcement corrosion is essentially an electrochemical process, where at the anode iron is oxidized to iron ions that pass into solution, and at the cathode oxygen is reduced to hydroxyl ions. The anode and the cathode form a short circuited corrosion cell, with the flow of electrons in the steel and of ions in the concrete pore solution (Tuutti 1982, Schiessl 1988, Elsener 2000).

Depending on various factors such as the pH value of the pore solution, the availability of oxygen and moisture, the content of aggressive agents etc., the corrosion products possess complex stochiometry and may expand by about four to six times the

original volume of iron corroded. When compared with the parent metal — iron, the characteristic physical properties of the typical corrosion products are summarized in Table 5.1:

Table 5.1. Characteristic physical properties of corrosion products

Corrosion product	Fe	FeO	Fe_3O_4	Fe_2O_3	$Fe(OH)_2$	$Fe(OH)_3$	$Fe(OH)_3 \cdot 3H_2O$
Relative volume ratio†	1.0	1.7	2.0	2.1	3.6	4.0	6.2
Molecular weight	56	72	232	160	90	107	161
Density ($\times 10^3$ kg/m^3)	7.85	5.93	16.24	10.67	3.50	3.75	3.64
Specific volume (g/cm^3)	0.127	0.169	0.062	0.094	0.286	0.267	0.275
Relative specific volume	1.0	1.32	0.48	0.74	2.24	2.09	2.16

† Courtesy of Pantazopoulou and Papoulia (2001)

Two corrosion products are generally thought to be dominant — ferrous hydroxide $Fe(OH)_2$ and hydrated red rust $Fe(OH)_3$ (Pantazopoulou and Papoulia 2001, Thoft-Christensen 2000). For simplicity, this study follows a general practice to represent the density of the corrosion product ρ_r as a fixed fraction of the density of iron ρ_s as:

$$\rho_r = \rho_s / r \tag{5.1}$$

where r assumes a constant value of 2.17, suppose that half the corrosion products is

$Fe(OH)_3$, and the other half is $Fe(OH)_2$ (Pantazopoulou and Papoulia 2001, Thoft-Christensen 2000).

The mass of iron consumed M_s (g) is related to the amount of current I_{corr} (A) that flows through the electrochemical corrosion cell. The corrosion process can be characterized using Faraday's law as:

$$\frac{dM_s}{dt} = \frac{I_{corr} A}{nF} \tag{5.2}$$

where A = 55.85 g/mol is the atomic weight of the ion corroded, and Faraday's constant F = 96500 Coulomb/mol. The valence of the reaction empirically assumes a weighted average value of n = 2.5 ($n = 2$ for $Fe(OH)_2$, and $n = 3$ for $Fe(OH)_3$) (Pantazopoulou and Papoulia 2001, Jung et al. 2003). Thus, Faraday's law can be reduced further as:

$$\frac{dM_s}{dt} = 2.315 \times 10^{-4} \cdot I_{corr} \quad (g/\sec) \tag{5.3}$$

M_s can thus be obtained by integrating $\frac{dM_s}{dt}$ over time since the initiation of corrosion. The corresponding mass of corrosion products generated M_r (g) is expressed as:

$$M_r = M_s / r_m \tag{5.4}$$

where r_m ranges between 0.523 for $Fe(OH)_3$ and 0.622 for $Fe(OH)_2$, and assumes a weighted average value of 0.5685 (Liu and Weyers 1998, Pantazopoulou and Papoulia 2001).

Faraday's law forms the foundation for all existing reinforcement corrosion models that assume a constant rate of iron consumption and rust generation. To simulate the mechanical effects of rust expansion, a corrosion-induced rust expansion model is proposed as illustrated in Fig. 5.2, where D_b is the original diameter of steel bar, D_{rb} is the reduced diameter of steel bar after corrosion, and D_{eb} is the corresponding diameter of rust expansion front.

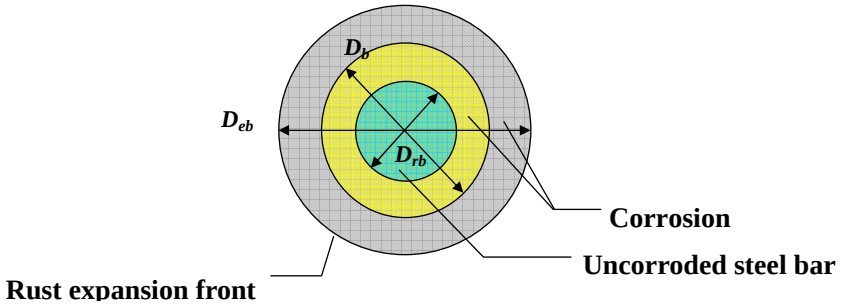

Figure 5.2. Corrosion-induced rust expansion model

The corrosion current density i_{corr} is defined as the corrosion current per unit steel surface. A relationship between I_{corr} (A) and i_{corr} (A/m^2) can be established as:

$$I_{corr} = \begin{cases} \pi \cdot D_b \cdot i_{corr} \cdot L & (t = 0) \\ \pi \cdot D_{rb} \cdot i_{corr} \cdot L & (t > 0) \end{cases} \tag{5.5}$$

where L is the length of the corroded steel bar.

The mass and volume of iron corroded per unit length (i.e., $L = 1.0\,\text{m}$) of the steel bar are obtained as:

$$\Delta M_s = 2.315\times10^{-4}\cdot I_{corr}\cdot\Delta t = \begin{cases} 2.315\times10^{-4}\cdot\pi\cdot D_b\cdot i_{corr}\cdot\Delta t & (t=0) \\ 2.315\times10^{-4}\cdot\pi\cdot D_{rb}\cdot i_{corr}\cdot\Delta t & (t>0) \end{cases} \quad (g/m) \tag{5.6}$$

$$\Delta V_s = \frac{\Delta M_s}{\rho_s} = \begin{cases} \frac{5.90}{2}\times10^{-11}\cdot\pi\cdot D_b\cdot i_{corr}\cdot\Delta t & (t=0) \\ \frac{5.90}{2}\times10^{-11}\cdot\pi\cdot D_{rb}\cdot i_{corr}\cdot\Delta t & (t>0) \end{cases} \quad (m^3/m) \tag{5.7}$$

Correspondingly, the outward volume expansion is obtained as the difference of the volume of rust generated and the volume of iron corroded as:

$$\Delta V = \Delta V_r - \Delta V_s = \frac{\Delta M_r}{\rho_r} - \frac{\Delta M_s}{\rho_s} = \Delta M_s\left[\frac{\Delta M_r}{\Delta M_s}\frac{1}{\rho_r} - \frac{1}{\rho_s}\right] \quad (m^3/m) \tag{5.8}$$

$$= \begin{cases} \frac{16.514}{2}\times10^{-11}\cdot\pi\cdot D_b\cdot i_{corr}\cdot\Delta t & (t=0) \\ \frac{16.514}{2}\times10^{-11}\cdot\pi\cdot D_{rb}\cdot i_{corr}\cdot\Delta t & (t>0) \end{cases}$$

Subsequently, D_{rb} and D_{eb} at the i^{th} time step can be derived as:

$$D_{rb,i} = D_b - \sum_{n=1}^{i} 5.90\times10^{-11} \cdot i_{corr,n} \cdot \Delta t_n \qquad (m) \tag{5.9}$$

$$D_{eb,i} = D_b + \sum_{n=1}^{i} 16.514\times10^{-11} \cdot \frac{D_{rb,n-1}}{D_{eb,n-1}} \cdot i_{corr,n} \cdot \Delta t_n \qquad (m) \tag{5.10}$$

Thus, the time-dependent radial displacement on the rust expansion front surface at the i^{th} time step can be expressed as:

$$u_{r,i} = \frac{D_{eb,i} - D_b}{2} = \sum_{n=1}^{i} 8.257\times10^{-11} \cdot \frac{D_{rb,n-1}}{D_{eb,n-1}} \cdot i_{corr,n} \cdot \Delta t_n \quad (m) \tag{5.11}$$

So far, a corrosion-induced reinforcement rust expansion model has been developed as shown in Eq. (5.11). It is convenient to impose the transient radial displacement boundary condition on all nodes along the concrete-steel interface of a finite element model. It should be emphasized that the proposed rust expansion model is only a simplification, where the radial displacement of the rust expansion front is assumed to be consistent with that of the surrounding concrete. As rust expansion-induced concrete cracking progresses, steel bar may debond gradually from the surrounding concrete. The displacement response of the concrete surrounding the steel bar thus becomes less and

less compatible with that of the rust expansion front such that the imposed radial displacement boundary condition might artificially affect the cracking pattern.

5.3. Corrosion rate model

It can be observed in Eq. (5.11) that i_{corr} is the only factor controlling the corrosion-induced reinforcement rust expansion process. In this case, i_{corr} is called the corrosion rate by several researchers. Cady and Weyers (1983) regarded the corrosion rate as the key to predicting the time to cracking. A sensitivity analysis performed on Bazant's model (1979a, 1979b) indicated that the corrosion rate is the most significant parameter in determining the time to cracking of the cover concrete.

Several corrosion rate models have been proposed in the literature. In this study, two established corrosion rate models — the constant model and the dynamic model — are selected to incorporate with the reinforcement rust expansion model proposed in Section 5.2. Two sets of simulation results based on the two corrosion rate models will be generated and compared with each other.

Andrade et al. (1993) classified the reinforcement corrosion risk according to the mean annual value of corrosion rate i_{corr}, where constant corrosion rates are assigned to the concrete structure under corresponding service conditions. Both Hansen and Saouma (1999) and Hong (2000) used similar constant corrosion rate models to calculate the decreasing diameter of corroded steel bar. The constant corrosion rate model adopted in

this study assumes a value of i_{corr} = 1 μA/cm^2 corresponding to a moderate corrosion risk (Andrade et al. 1993, Stewart and Rosowsky 1998).

However, the constant corrosion rate model may not always be applicable, especially in a highly varying aggressive environment. Jung et al. (2003) expressed the corrosion rate as an exponential function of the chloride content, relative humidity, and cover depth. Based on available chloride corrosion database (2927 measurements from seven series of chloride contaminated specimens, up to five years of outdoor exposure), Liu and Weyers (1998) proposed a nonlinear regression model, in which the corrosion rate varies with chloride content, temperature, ohmic resistance, and active corrosion time. This dynamic corrosion rate model takes the following form as:

$$i_{corr} = 0.926 \cdot \exp\left[7.98 + 0.7771 \ln\left(1.69 C_{cl,t}\right) - \frac{3006}{T} - 0.000116 R_c + 2.24 t^{-0.215} \right] \tag{5.12}$$

where i_{corr} is the corrosion current density (μA/cm^2); $C_{cl,t}$ is the total chloride content (kg/m^3 of concrete); T is temperature at the depth of reinforcement (Kelvin); R_c is the ohmic resistance of the cover concrete (ohms); and t is the corrosion time (year).

Following the computational methodology proposed in Chapter 4, the total chloride content $C_{cl,t}$ and temperature T at the depth of reinforcement can be determined. As to the ohmic resistance R_c, Liu (1996) established a regression relationship between the

ohmic resistance of concrete and total chloride content for outdoor specimens as:

$$R_c = \exp\left[8.03 - 0.549\ln\left(1 + 1.69C_{cl,t}\right)\right] \tag{5.13}$$

Therefore, the dynamic corrosion rate model in Eq. (5.12) can be combined with the proposed rust expansion model to simulate the corrosion-induced reinforcement rust expansion process.

According to Thoft-Christensen (1997, 2000, 2001a, 2001b), there is a porous zone around the steel/concrete interface caused by the transition from cement paste to steel, entrapped/entrained air voids, and corrosion products diffusing into the capillary voids in the cement paste. The volume of this porous zone is directly related to the surface area of reinforcement, water to cement ratio, degree of hydration, and degree of consolidation.

Very close to the steel bars the concrete porosity is close to unity, but the porosity decreases with the distance from the bars. The porosity is typically of the order of 0.5 at about 10~20 μm distance from the bar, which means the porous zone is very narrow (Thoft-Christense 1997, Thoft-Christense 2001). Let δ_{por} be the thickness of an equivalent zone with porosity unit one around a steel bar. Thoft-Christensen (Thoft-Christense 2000) assumes that δ_{por} has a log-normal distribution with the mean value of 12.5 μm.

As the corrosion is initiated on the surface of the steel bar, the porous zone will be gradually filled with rust. Once the total amount of rust exceeds the amount needed to

completely fill the porous zone at t_{stress}, expansive pressure and crack propagation are to be caused on the surrounding concrete as shown in Fig. 5.1. Based on the two established corrosion rate models, a recursive algorithm is required to apply the proposed reinforcement rust expansion model Eq. (5.11), and the time needed to completely fill the porous zone around the steel bar t_{stress} can be determined.

5.4. Cracking simulation

As discussed in Section 3.2, there usually exist two approaches to simulate the concrete cracking. Based mainly on fracture mechanics, the discrete cracking approach regards the crack propagation as the result of stress singularity or strain energy release at the tip of crack (Shah et al. 1995, Bazant and Planas 1998). Cracks are treated directly as geometric discontinuities, where the intact portion of concrete is generally assumed to behave elastically, while the crack propagation is modeled by changing the topology of the finite element model. The separation of two crack faces may be accomplished by introducing additional nodes and remeshing the local domain. Adaptive remeshing is required to implement the simulation.

Based on conventional solid mechanics, the smeared cracking approach describes the cracked concrete as a fictitious continuum. Cracks are assumed to be spatially distributed over the entire volume represented by finite element. The stiffness matrix of each concrete element is modified accordingly to accommodate the mechanical degradation

due to cracking. Without changing the topology of finite element model, this approach proves efficient when incorporated in finite element analysis (Darwin 1993). Mandke and Smalley (1994) and Kachlakev et al. (2001) used this approach to model concrete cracking under mechanical loads. Saoma and Chang (2003) followed the same approach to simulate the reinforced concrete deterioration due to reinforcement corrosion, where the forced displacement boundary conditions are applied on the crack surfaces.

In spite of some potential limitations (including the sensitivity to mesh size etc.), a smeared cracking approach combined with finite element analysis to model the crack propagation process is feasible due to its ease of implementation. Moreover, crack propagation paths can be tracked roughly. The finite element software ANSYS is adopted herein as illustration to simulate the mechanical response of concrete due to the corrosion-induced reinforcement rust expansion after t_{stress}.

For reinforced concrete structures, the steel rebar embedded in concrete can be modeled in two distinct ways. First, the reinforcing effect of the steel rebar is considered directly using the smeared reinforcement function of Solid65 concrete element, where the reinforcement has stiffness only in its axial direction and is assumed to be smeared spatially over the entire element. The stiffness of steel rebar in the uniaxial direction is weighted by its ratio of volume V_i^R, and the stiffness matrix of the concrete element is modified according to Eqs. (3.2)~(3.4). Second, concrete and steel rebar are modeled separately, where the steel rebar is modeled using its own element type (such as 3-D spar element Link8 in ANSYS). This second strategy can be implemented through two

approaches: introduce special interface elements (such as spring elements) between concrete and reinforcement to accommodate the slippage condition; or use coupled nodes on the interface to satisfy the displacement compatibility. The advantage of the second strategy is that realistic reinforced concrete structures can be simulated and the stress/strain state of concrete can be evaluated.

To model the corrosion-induced reinforcement rust expansion process in this study, the second strategy is adopted and the rust expansion process has been transformed into an equivalent time-varying radial displacement boundary condition. The displacement boundary condition is imposed on all nodes along the concrete-steel interface of a finite element model. The mechanical response of concrete (including stress and cracking states) to the corrosion-induced reinforcement rust expansion process after t_{stress} can be assessed.

So far, a comprehensive computational framework has been developed for simulating all three phases of the chloride-induced deterioration process — including the chloride penetration, the reinforcement corrosion and rust expansion, and the concrete cracking. The simulation procedure is summarized in Fig. 5.3. It should be mentioned that the adopted constant and dynamic corrosion rate models do not explicitly consider the presence of cracking. Since the corrosion rate usually increases with the more direct exposure of steel bar to aggressive environment through cracks, the obtained time to spalling $t_{spalling}$ might be not conservative.

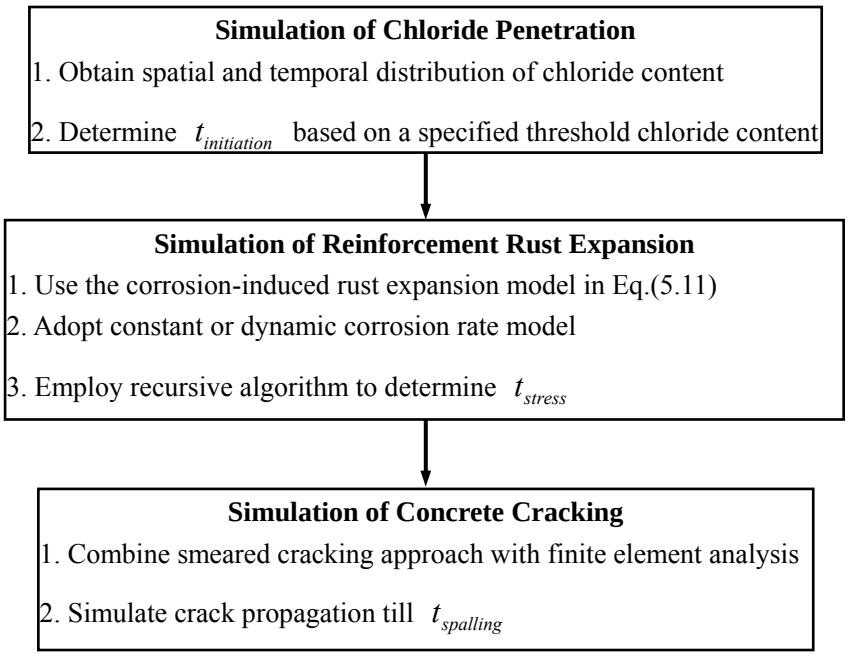

Figure 5.3. Simulation of chloride-induced deterioration

5.5. Numerical example

A numerical example, where an initially chloride-free reinforced concrete slab exposed to constant chloride environment, has been illustrated for simulating the chloride penetration process in Chapter 4. The numerical example is utilized continuously herein to illustrate the proposed computation framework and implement the remaining task — simulation of the chloride-induced reinforcement rust expansion process and concrete cracking process. The reinforcement concrete slab shown in Fig. 4.7 is preserved, where the chloride boundary conditions in Fig. 4.8 are applied on the same finite element model in Fig. 4.10.

The simulation results of the chloride penetration process based on the Freundlich

binding isotherm model, obtained in previous Section 4.5, are utilized herein. The corresponding chloride content history and temperature history at the depth of the reinforcement are obtained as shown in Figs. 5.4 (i.e. Fig. 4.11(c)) and 5.5, respectively.

The threshold chloride content to initiate the reinforcement corrosion is controversial, since it is affected by various factors, such as cement type, mixture proportions of the concrete, relative humidity, temperature, pH value of the pore solution, sulfate content etc. (Schiessl and Raupach 1990, Hansson and Sorensen 1990, Berman 1975, Clear 1983). According to Stewart and Rosowsky (1998), the values of the threshold chloride content are uniformly distributed within the range of 0.6~1.2 kg/m^3 of concrete. If the threshold chloride content assumes its mean value of 0.9 kg/m^3 of concrete, the corrosion initiation time $t_{initiation}$ is thus determined to be 11.25 years.

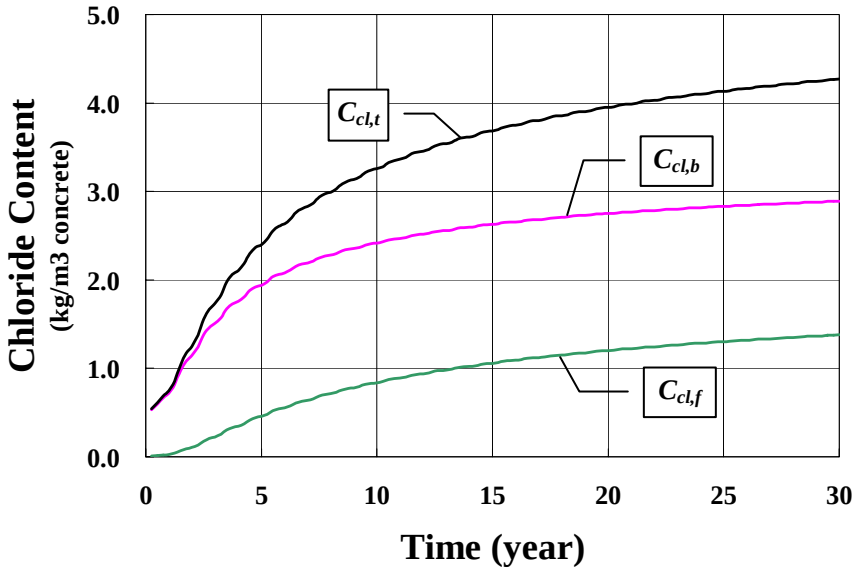

Figure 5.4. Chloride content for Freundlich isotherm

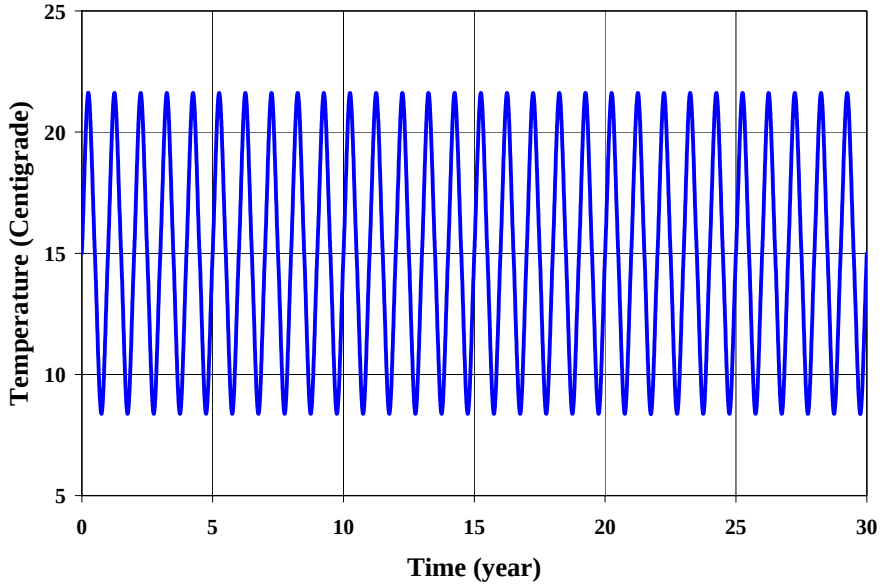

Figure 5.5. Temperature history

Thoft-Christensen (2000) assumes that δ_{por} has a mean value of 12.5 μ m. Employing proposed reinforcement rust expansion model Eq. (5-11) with the constant corrosion rate model, it takes 0.48 year after $t_{initiation}$ to completely fill the porous zone; and it takes 0.37 years with the dynamic corrosion rate model.

$$t_{stress} = t_{initiation} + \Delta t = \begin{cases} 11.25 + 0.48 = 11.73 \quad (years) & \text{(Constant model)} \\ 11.25 + 0.37 = 11.62 \quad (years) & \text{(Dynamic model)} \end{cases} \tag{5-14}$$

After the porous zone around the steel bar is completely filled with rust at t_{stress}, further corrosion progress will cause expansive stress and crack propagation in the surrounding concrete.

Both the representative part of the concrete slab in Fig. 4.7 and the finite element

model in Fig. 4.10 are preserved to simulate the subsequent reinforcement rust expansion and concrete cracking. The corresponding displacement boundary conditions are illustrated in Fig. 5.6, where only vertical displacement is allowed on the left, right, front and rear surfaces of the isolate representative part of the concrete slab, while all displacement constraints on the top and bottom surfaces are set free. The proposed corrosion-induced reinforcement rust expansion model is implemented by applying the proposed transient radial displacement in Eq. (5-11) on all nodes along the concrete-steel interface. In addition, the two corrosion rate models — the constant model and the dynamic model — are introduced to model the reinforcement rust expansion and concrete cracking. The assumed material properties of concrete are summarized in Table 2.1.

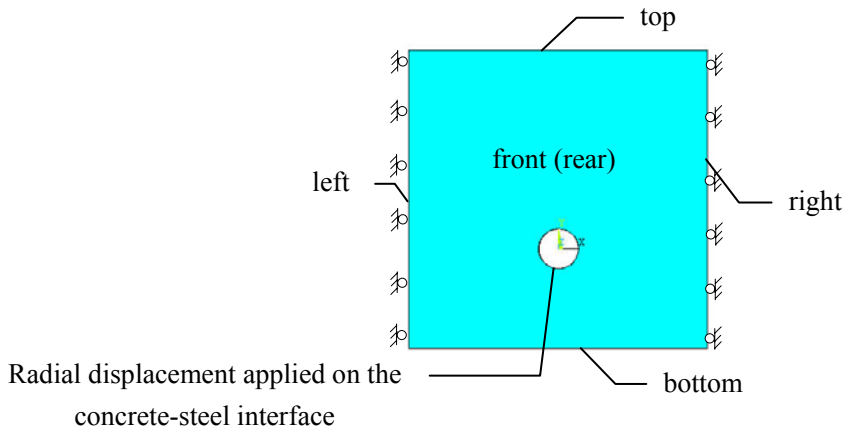

Figure 5.6. Displacement boundary conditions

The total chloride content $C_{cl,t}$, the temperature T and the ohmic resistance R_c at the depth of reinforcement after t_{stress} can still be excerpted from the previous

simulation results as shown in Figs. 5.7~5.9, respectively.

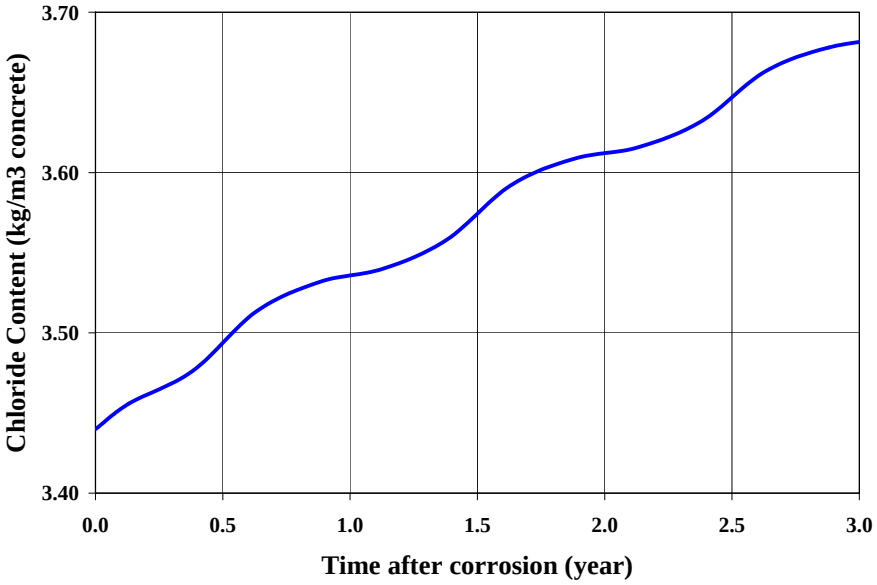

Figure 5.7. Total chloride content history

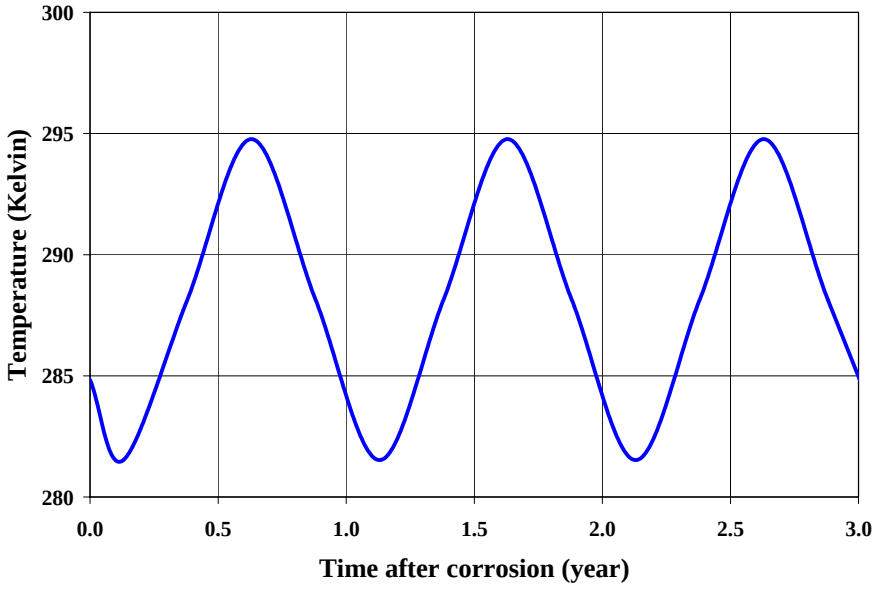

Figure 5.8. Temperature history

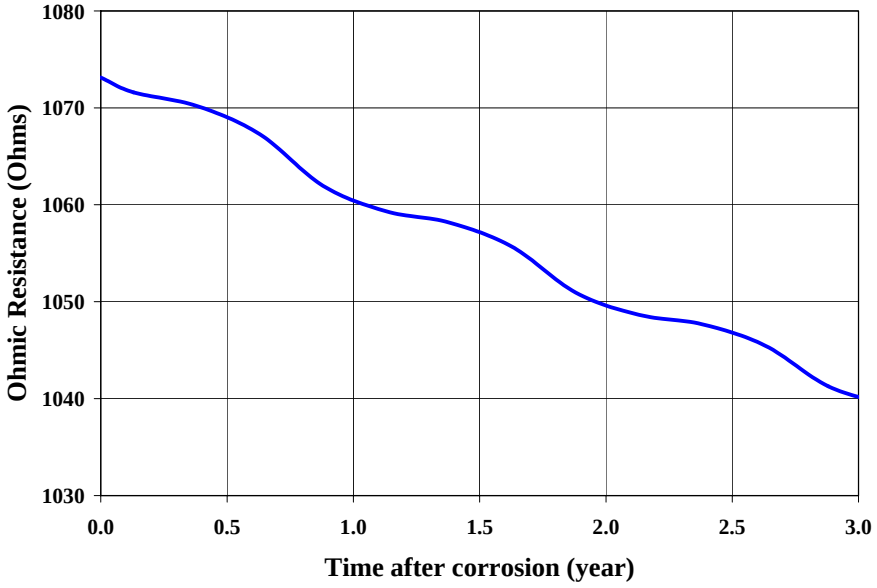

Figure 5.9. Ohmic resistance history

Based on the dynamic corrosion rate model in Eq. (5.12), the corresponding corrosion current density i_{corr} can be determined using above $C_{cl,t}$, T and R_c as shown in Fig. 5.10. It is observed that the fluctuation of i_{corr} is caused by the seasonal variation of temperature. Temperature has a significant effect on the corrosion rate, as with other chemical and electrochemical reactions. In addition, the mean value of the dynamic corrosion rate (0.012 A/m^2) is slightly higher than the constant corrosion rate (0.010 A/m^2), which implies that the assumed surface chloride boundary condition corresponds to the moderate corrosion risk and the dynamic corrosion rate model applies.

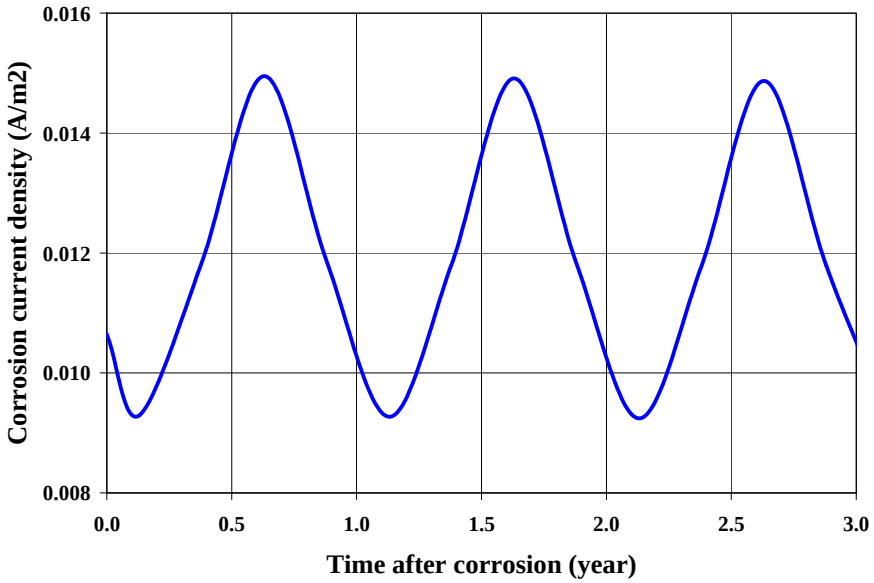

Figure 5.10. Dynamic corrosion rate i_{corr}

The two corrosion rate models produce two sets of simulation results. The diameter of the corroded steel bar D_{rb} and that of the rust expansion front D_{eb} are shown in Fig. 5.11. It can be observed that D_{rb} decreases monotonically with time, while D_{eb} increases monotonically with time. Meanwhile, the slopes of D_{rb} and D_{eb} for the dynamic corrosion rate model are always steeper than those for the constant corrosion rate model, since the mean value of the dynamic corrosion rate is slightly higher than the constant corrosion rate. The time-dependent radial displacement u_r is shown in Fig. 5.12, where the radial displacement increases monotonically with time, and the dynamic corrosion rate model predicts larger radial displacement than the constant corrosion rate model.

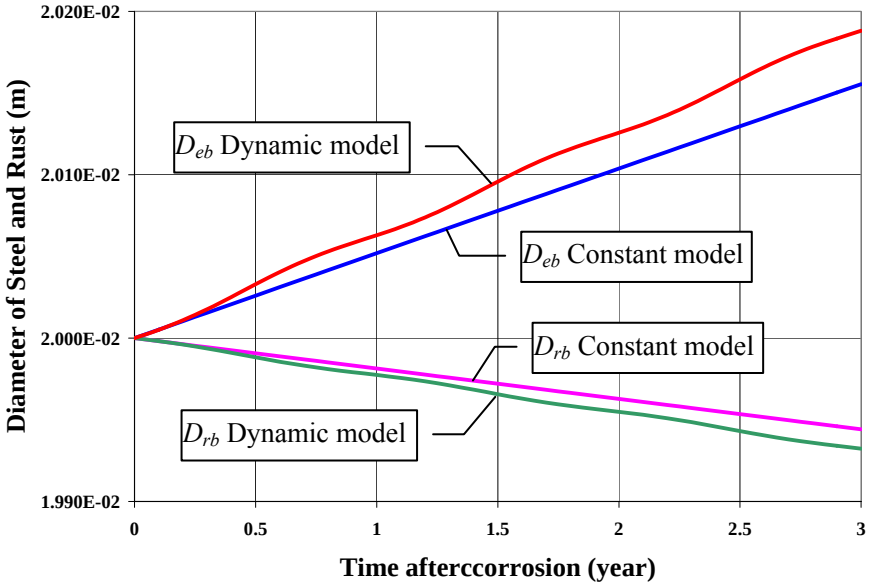

Figure 5.11. D_{rb} **and** D_{eb}

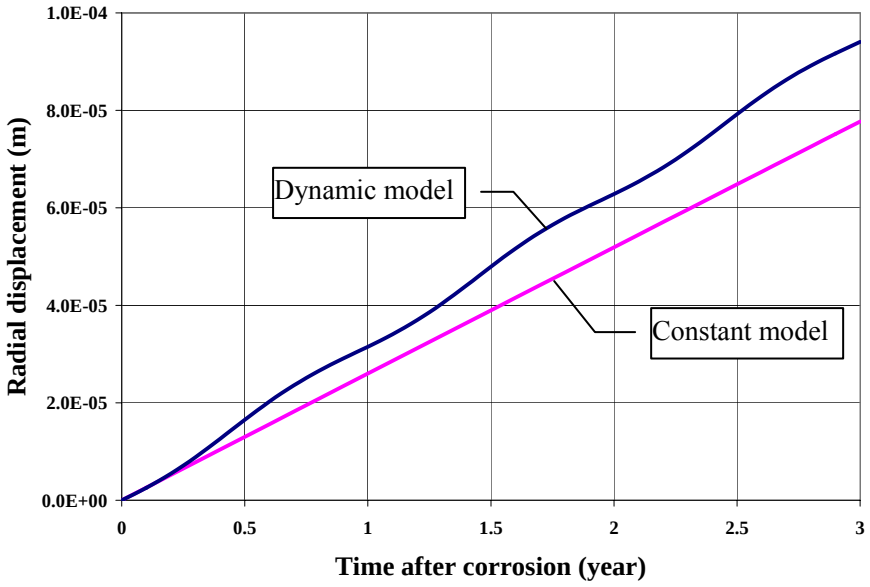

Figure 5.12. Radial displacement boundary condition

Since cracking patterns are very sensitive to the transient stress state, the time step must be kept small enough to obtain a stable solution in simulating the crack propagation. In this simulation the time step is set as 0.02 year, while the entire time length after t_{stress} is chosen to be 1.0 year, only for the sake of illustration. To reflect the general varying trend of the number of cracked concrete elements, the GRCD with the crack propagation process is demonstrated in Fig. 5.13. It can be observed that the two sets of crack propagation results are quite similar. Although the GRCD increases monotonically with time, the distribution of cracks in the entire concrete slab is not uniform, and most cracks are found closely around the steel bar. In addition, the GRCD gradually approaches a constant value, which helps to identify some critical modes of structural failure, such as delamination or spalling of the concrete cover. Thus, the time to spalling $t_{spalling}$ can be determined.

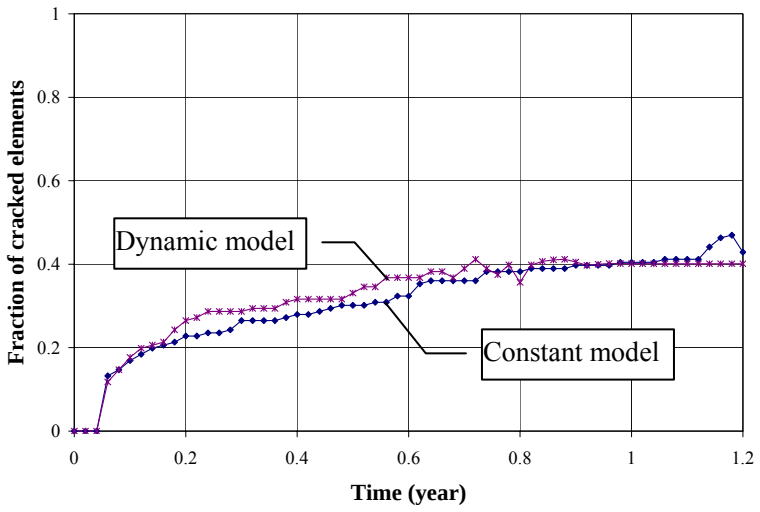

Figure 5.13. GRCD history

The crack propagation patterns caused by the reinforcement expansion can be observed in Fig. 5.14. For both corrosion rate models, cracks appear first at the same time t = 0.06 year after t_{stress} and the crack patterns looks similar to each other. Meanwhile, it is observed that the crack patterns agree well with the expectation in Fig. 5.1(d), which verifies the feasibility of the proposed simulation methodology.

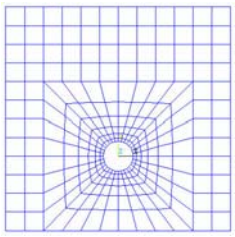

(a-1) time = 0 year

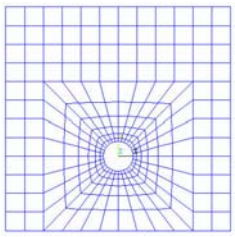

(b-1) time = 0 year

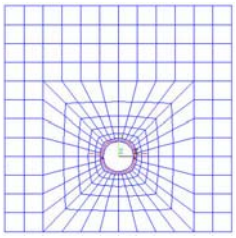

(a-2) time = 0.06 year

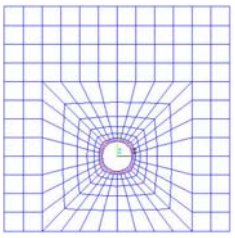

(b-2) time = 0.06 year

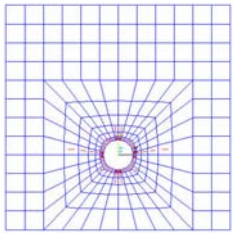

(a-3) time = 0.12 year

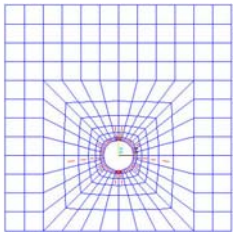

(b-3) time = 0.12 year

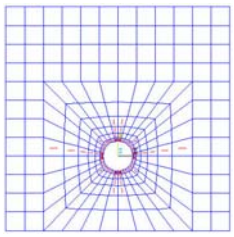

(a-4) time = 0.18 year

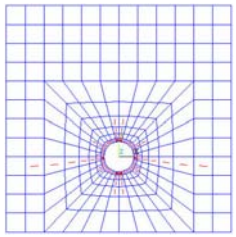

(b-4) time = 0.18 year

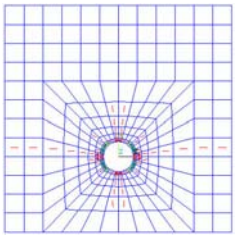

(a-5) time = 0.40 year

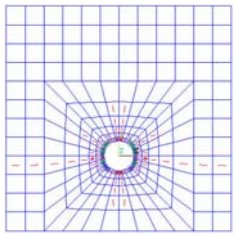

(b-5) time = 0.40 year

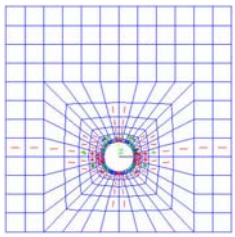

(a-6) time = 0.80 year

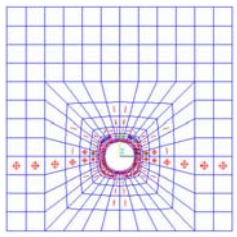

(b-6) time = 0.80 year

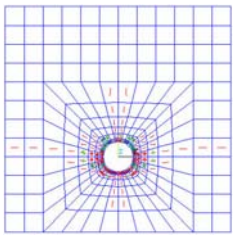

(a-7) time = 1.00 year

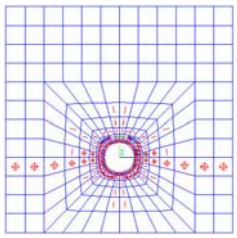

(b-7) time = 1.00 year

Figure 5.14. Crack propagation patterns

(Note: 1. Series-a on left column for constant corrosion rate model, Series-b on right column for dynamic corrosion rate model; 2. The symbols | and ○ indicate different orientations of the cracks, and symbol ⊕ indicates multiple cracks distinguished with different colors.)

5.6. Discussion of simulation results

Several obvious crack paths can be found in Fig. 5.14, which indicates the most possible crack propagation paths for the reinforced concrete slab under chloride-induced reinforcement corrosion. In addition, crushing due to compression is observed in those concrete elements closely around the steel bar, which is consistent with practical field observations.

One interesting phenomenon is noticed that two crack propagation paths along the horizontal direction proceed rapidly, while other crack paths advance relatively slowly. This observation confirms the experimental result by Dagher and Kulendran (1992) that, for a concrete slab with closely spaced bars and thick concrete cover, cracks may grow and connect between the steel bars and form a delamination plane inside a slab. Once such a delamination plane forms, the entire concrete slab becomes an unstable structure. On the one hand, the expansive stresses accumulated in concrete surrounding the steel bar will be released rapidly. On the other hand, geometric deformation and displacement will increase rapidly. For a quasi-brittle material like concrete, it is difficult, if not impossible, to ensure the accuracy of the simulation results beyond this stage. As a result, few numerical models proposed so far are able to simulate accurately the crack propagation till the occurrence of delamination or spalling. The substantial contributions made earlier only predicted the time to crack initiation (Liu and Weyers 1998, Bazant 1979a, Bazant 1979b, Morinaga 1990), much earlier than the occurrence of delamination and spalling.

The proposed simulation methodology provides valuable information to estimate the damage pattern and extent in concrete structures till the occurrence of delamination or spalling. Of course, the load carrying capacity of concrete structure at the time of delamination or spalling $t_{spalling}$ has been reduced so much that makes it hard to meet the design requirements.

The corrosion can be either pitting corrosion, where a very small anode is surrounded by a large area of cathode, or uniform corrosion with a homogeneous distribution of micro anodes and cathodes. Uniform corrosion may cause more overall loss in iron, but pitting corrosion causes more loss in cross-sectional area and hence is more dangerous. The proposed corrosion-induced reinforcement expansion model implies an assumption of uniform corrosion, without considering the pitting effect (i.e. localized corrosion). Uniform corrosion is usually encountered under carbonation or high chloride contamination, thus the applicability of the proposed model needs more verification. To overcome the difficulty of simulating the pitting effect, it is possible to apply a user-defined uneven radial displacement boundary condition around the steel-concrete interface as suggested by Dagher and Kulendran (1992) and Stewart and Rosowsky (1998). However, the improvement is rather limited, and the simulation process is quite time consuming. More efforts are needed to consider the pitting effect, balancing computational effort and accuracy.

5.7. Conclusion

An integrated finite element-based computational framework is illustrated in this chapter to simulate the chloride-induced deterioration process from chloride penetration to reinforcement rust expansion to concrete cracking. The reinforcement corrosion model is based on Faraday's law, and the rust expansion process is characterized in finite element analysis using an equivalent time-varying radial displacement boundary condition. Two established corrosion rate models — the constant model and the dynamic model — are combined with the proposed reinforcement rust expansion model. The cracking simulation is implemented using a smeared cracking approach. The simulation results and the predicted crack patterns for a reinforced concrete slab exposed to a constant chloride environment agree well with the expectation in Fig. 5.1. In spite of some limitations, the proposed computational framework can be used to a large extent to simulate the chloride-induced deterioration process, and predict the service life for reinforced concrete structures subjected to chloride contamination.

Many of the variables describing the structure, materials, environment, and the deterioration process are random in nature. These uncertainties need to be properly accounted for in service life prediction through systematic time-dependent probabilistic analysis. Sensitivity analysis to identify the dominant variables and quantify their influence is valuable, both to reduce the computational effort, and to guide design decisions.

CHAPTER VI

TIME-DEPENDENT RELIABILITY ANALYSIS

6.1. Introduction

The service life of a structure may be defined as the sustainable period during which the structure is able to satisfy specified design requirements without requiring mandatory repairs. Durability-based structural design requires the availability of prediction models for the service life of reinforced concrete structure under various deterioration processes. On the one hand, service life predictors can estimate the time to first mandatory repair for concrete structure exposed to given service environments. On the other hand, the effectiveness of various influencing factors and corresponding protective measures can be evaluated and compared quantitatively.

A combination of coupled physical, chemical and mechanical deterioration processes may decay the material properties of concrete, impair the load carrying of concrete structure, and thus govern the service life of the reinforced concrete structure. A deterministic computational framework has been developed in Chapters 2 to 5 to predict the service life of reinforced concrete structures under multiple coupled deterioration processes. There exists a large amount of variability and uncertainty in the computational

framework. To complete a structural reliability assessment with various uncertainties considered, an appropriate approach is to combine the deterministic computational framework with advanced stochastic modeling. Time-dependent reliability analysis can then be performed to predict the failure probability and evaluate the probabilistic service life. Sensitivity analysis is implemented to quantify the influence of important variables.

The deterministic computational framework is implemented using a series of finite element-based methodologies, which functions essentially like a "black box" and relates implicitly various inputs to corresponding outputs. To obtain higher computational efficiency, the deterministic computational framework can be replaced by a response surface expressed as a series of approximate regression functions, which are obtained through performing deterministic analysis at a set of predetermined experimental points. To include the effect of various random uncertainties in the concrete material properties and the externally applied environments, several important random variables existing in the deterministic computational framework are identified. With the acquired statistics information on these random variables, a nonlinear response surface is constructed through combining the full-factorial experimental design with multilevel regression. Time-dependent reliability analysis of the reinforced concrete structure is then performed by combining the nonlinear response surface with Monte Carlo simulation. Meanwhile, sensitivity analysis is carried out to identify the most influential variables and the most efficient preventive measure to lengthen the service life of reinforced concrete structures.

For reinforced concrete structures subjected to marine environment, deicing salts or

underground environment, the service life is impacted severely by the chloride-induced reinforcement corrosion in concrete. For the sake of illustration, this chapter focuses mainly on performing the time-dependent reliability analysis of reinforced concrete structures under the chloride-induced reinforcement corrosion process. As shown in Fig. 4.1, the chloride-induced reinforcement corrosion process can be divided roughly into three phases — the chloride penetration process, the reinforcement rust expansion process, and the concrete cracking process (Xi and Ababneh 2000). Among the three phases, the first phase usually lasts for a relatively long period, depending on many influencing factors including corrosion resistance of the reinforcement, thickness and quality of the concrete cover, and corrosion protection measures taken etc. The second phase is shorter than the first one, which is determined mainly by the porosity of the ITZ and the corrosion rate of reinforcement. The third phase is the shortest since the reinforcement rust expansion-induced cracks propagate rapidly through the surrounding concrete. Based on the obtained simulation results in Chapter 5, for a reinforced concrete slab exposed to a chloride environment of moderate level, it will take 11.25 years for chloride to penetrate through the concrete cover and reach the embedded reinforcement, initiate the reinforcement corrosion process. Then, it will take about 0.37~0.48 year to completely fill the porous zone around the steel bar with corrosion products. Finally, even within less than 0.2 year, several obvious cracking paths can be found in concrete cross-section. It can be observed that the relative lengths of all three phases have been confirmed.

Considering the difficulty of modeling the reinforcement rust expansion and the concrete cracking during the second and third phases, many studies simplify the analysis by ignoring the last two phases and approximate the service life of reinforced concrete structures as the duration of the first phase only. Since the first phase occupies most of the service life, this study will follow the same practice by taking the corrosion initiation time $t_{initiation}$ as the service life of the reinforced concrete structure exposed to chloride-induced deterioration. Although the assumption will result in conservative prediction, the practice will not cause an unacceptable level of error.

6.2. Implementation of time-dependent reliability analysis

The service life of reinforced concrete structure should not be a fixed value as calculated by the deterministic computational framework developed, but a range of values based on the concrete material characteristics, the structural dimensions and the severity of various service environments. The stochastic nature of service life for reinforced concrete structures has been discussed extensively (Sentler 1984, Siemes et al. 1985, Clifton 1993, Prezzi et al. 1996).

During the past years, substantial efforts have been made in applying various probabilistic methods to the service life prediction and durability assessment of reinforced concrete structures. Hoffman and Weyers (1994) developed a probabilistic model for bridge deck exposed to de-icing salts and assumed that structural failure occurs

when reinforcement corrosion is initiated. Thoft-Christensen et al. (1992, 1995, 1996) proposed a comprehensive probability-based expert system, where the corrosion initiation due to chloride or carbonation, the corrosion propagation and concrete cracking, as well as the inspection and repair plan are taken into account. Frangopol et al. (1997) established a probabilistic corrosion model on the basis of the minimization of expected lifetime costs.

On the basis of the deterministic computational framework, this chapter develops a probabilistic framework to assess the time-dependent reliability and predict the service life of reinforced concrete structures exposed to chloride contamination. The chloride penetration process in concrete is simulated using a previously developed finite element-based methodology in Chapter 4. To include the influences of various random uncertainties in concrete material properties, external environments and the proposed deterministic computational framework, several independent random variables are identified. Nonlinear response surface is constructed through combining full-factorial experimental design with multilevel regression models. Monte Carlo simulation is then performed to predict the service life and assess the time-dependent reliability of reinforced concrete structure. Sensitivity analysis is carried out to quantify the influence of each random variable. The proposed probabilistic framework is illustrated for a reinforced concrete slab exposed to a constant chloride environment.

6.2.1. Identification of random variables

According to Khatri and Sirivivatnanon (2004), there exist three possible sources of uncertainties in the service life predictor. The first source is the natural variability in the material properties of concrete, such as mechanical behavior, thermal properties, porosity, permeability, and diffusivity etc. In any given concrete structure, there must be variation in the concrete quality due to variations in chemical composition of cement, water-cement ratio, level of compaction, extent of curing and the hydration degree etc. The second source is the uncertainties in the computational framework with the associated model parameters, such as the structural dimensions like the depth of concrete cover. The third source is the natural variability in the time-varying deterioration processes, or various detrimental environmental loadings the reinforced concrete structures are exposed to. As a result, the service life is expressed as a function of four independent random variables, including the concrete cover depth, the apparent diffusion coefficient, the surface chloride concentration and the chloride threshold value. Kirkpatrick et al. (2002) identified the same four random variables to evaluate the corrosion initiation time, while the duration from corrosion initiation to structural damage is assumed to be the fifth random variable to overcome the difficulty of simulating reinforcement rust expansion and concrete cracking process.

This study follows the similar practice above to consider the four independent random variables, including the concrete cover depth, the reference chloride diffusivity,

the surface chloride content, and the chloride threshold value, when predicting the service life of chloride-contaminated reinforced concrete structures.

Since the concrete element dimensions and the location of reinforcing steel can be controlled through on-site inspection, the actual dimensions should be relatively close to the design values. Therefore, one would expect that the underlying distribution of the concrete cover depth should be normal with relatively little variance, which is confirmed by Kirkpatrick et al. (2002). Khatri and Sirivivatnanon (2004) suggested a standard deviation of 4 mm for the cover depth of concrete slabs, and this chapter assumes the same standard deviation.

As the most important parameter controlling the overall properties of the concrete, water to cement ratio can determine the permeability and diffusivity of concrete. According to ACI 117-90 (2000), the tolerance for total water content is 3% and the tolerance for cement ranges from 1% to 4%. Therefore, the coefficient of variance (COV) of the water to cement ratio should be in the range of 3% to 5%. At these tolerances, it would be plausible to characterize the water to cement ratio by normal distribution. In this chapter, a water to cement ratio of 0.5 with COV of 4% is adopted to decide the statistics of the reference chloride diffusivity.

The reference chloride diffusivity is expressed as a function of water to cement ratio by following Snyder (2001):

$$\log_{10}\left(D_{cl,0}\right) = 6.0 \cdot WCR - 13.84 \tag{6.1}$$

where $D_{cl,0}$ is the reference chloride diffusivity, WCR is the water to cement ratio. With the mean value of water to cement ratio WCR = 0.5, the reference chloride diffusivity $D_{cl,0}$ assumes a mean value of 14.45×10^{-12} m^2/s herein.

Based on Eq. (6.1), the reference chloride diffusivity satisfies lognormal distribution. Substantial experimental results have indicated that the chloride diffusivity in concrete can span over several orders of magnitude, lognormal distribution is thus appropriate for characterizing the expected range of reference chloride diffusivity used in reliability analysis. Stewart and Rosowsky (1998) also adopted this assumption.

According to Hoffman and Weyers (1994), the surface chloride content for each state in the United States ranges from 1.2 kg/m^3 of concrete to 8.2 kg/m^3 of concrete. The mean value and the coefficient of variance are 3.5 kg/m^3 of concrete and 0.5, respectively. Meanwhile, the surface chloride content is modeled as lognormal distribution.

The chloride content at the depth of embedded reinforcement must reach a threshold value to dissolve the protective passive file around the reinforcement and initiate the reinforcement corrosion process. Several studies (Cady and Weyers 1983, Mehta 1991) have shown that the chloride threshold value tends to lie within the range of 0.6-1.2 kg/m^3 of concrete. The chloride threshold value is controversial, since it is influenced by various factors, such as cement type, mixture proportions of concrete, relative humidity, temperature, pH value of pore solution, sulfate content etc. (Berman 1975, Clear 1983,

Schiessl and Raupach 1990, Hansson and Sorensen 1990). Hoffman and Weyers (1996) thus proposed that the chloride threshold value is uniformly distributed within the range of 0.6~1.2 kg/m^3 of concrete.

The statistical information of all random variables is summarized in Table 6.1, which will be used in the subsequent reliability analysis to generate random samples.

Table 6.1. Statistical information summary of random variables

Random variable	Mean value	Std. deviation	Distribution
Cover depth	50 mm	4 mm	Normal
Reference chloride diffusivity (water to cement ratio)	4.74E-4 m^2/year (0.5)	1.34E-4 m^2/year (0.02)	Lognormal (Normal)
Surface chloride content	3.50 kg/m^3 of concrete	1.75 kg/m^3 of concrete	Lognormal
Chloride threshold	0.90 kg/m^3 of concrete	0.17 kg/m^3 of concrete	Uniform

6.2.2. Framework of time-dependent reliability analysis

The probabilistic performance assurance of a structural system may be referred to as reliability of the structure. In this sense, the reliability of the reinforced concrete structure represents the probability at which the design criteria can be satisfied. Unlike the conventional structural reliability analysis, where the loading effect represents the demand and the structural strength is the resistance, the major concern of the current service life prediction is the corrosion initiation time. The corrosion initiation time can be determined as the time necessary to reach the chloride threshold value at a specified depth of reinforcement. As a result, the chloride content at the reinforcement depth

corresponds to the demand $S(t)$, while the chloride threshold value to initiate the corrosion process represents the resistance $R(t)$. By including uncertainties in the four identified influential random variables, the evolution of chloride content profile at the depth of reinforcement can be represented by a time-dependent probabilistic distribution.

The time-dependent limit state is defined as

$$g(X,t) = R(X,t) - S(X,t) = 0 \tag{6.2}$$

where X represents the set of all influential random variables, and t is time. As a result, $R(X,t) - S(X,t) > 0$ represents the safety domain, while $R(X,t) - S(X,t) < 0$ represents the failure domain.

Since the first passage of limit state is adopted herein as the failure criterion, both the service life and the failure probability can be determined by considering the crossing rate associated with a target level — the chloride threshold value. The schematic determination of the probabilistic service life for reinforced concrete structure under chloride-induced reinforcement corrosion process is illustrated in Fig. 6.1.

The corresponding structural reliability can be defined as the probability at which $R(X,t) - S(X,t) > 0$, i.e,

$$\text{Structural reliability} = P\{R(X,t) - S(X,t) > 0\} \tag{6.3}$$

The failure probability of structure is obtained as

$$P_f = P\{R(X,t) - S(X,t) \le 0\} = 1.0 - P\{R(X,t) - S(X,t) > 0\} \tag{6.4}$$

Under reliability-based structural design, the failure probability of structure is required to not less than a desired target value P_{target} as follows:

$$P_f \ge P_{target} \tag{6.5}$$

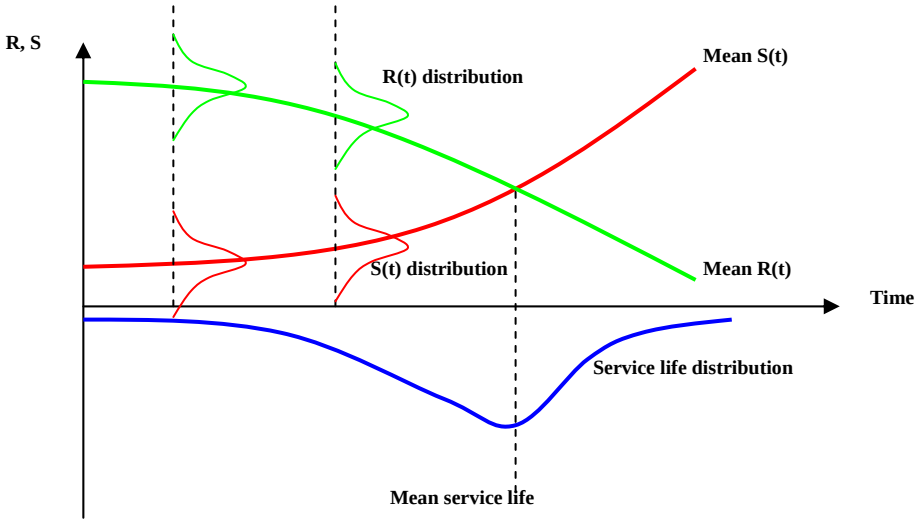

Figure 6.1. Schematic determination of probabilistic service life

Monte Carlo simulation is chosen herein to predict the service life and assess the

failure probability of the reinforced concrete structures. The whole analysis process can be summarized into three steps. First, *N* samples of the four influential random variables are generated respectively according to the acquired statistics information. Second, perform deterministic analysis *N* times using the proposed deterministic computational framework and calculate the corresponding service life of the chloride-contaminated reinforced concrete structure for each combination. Finally, the statistics information of the service life (including frequency histogram, PDF and CDF, as well as failure probability etc.) can be summarized from the obtained *N* service life samples.

Since the deterministic analysis with the proposed finite element-based deterministic computational framework is very time-consuming, evaluating large number of samples using Monte Carlo simulation becomes inefficient and impractical. To overcome the difficulty, the proposed deterministic computational framework can be replaced with a multi-dimensional response surface. The validity of the response surface approach is based on a fundamental assumption that the output variable can be approximated by a closed-form mathematical function of all influential random variables. The response surface is constructed by combining full-factorial experimental design with multilevel regression. The time-dependent reliability analysis can be performed directly on the basis of the response surface and Monte Carlo simulation. The complete time-dependent reliability analysis procedure is demonstrated in Fig. 6.2.

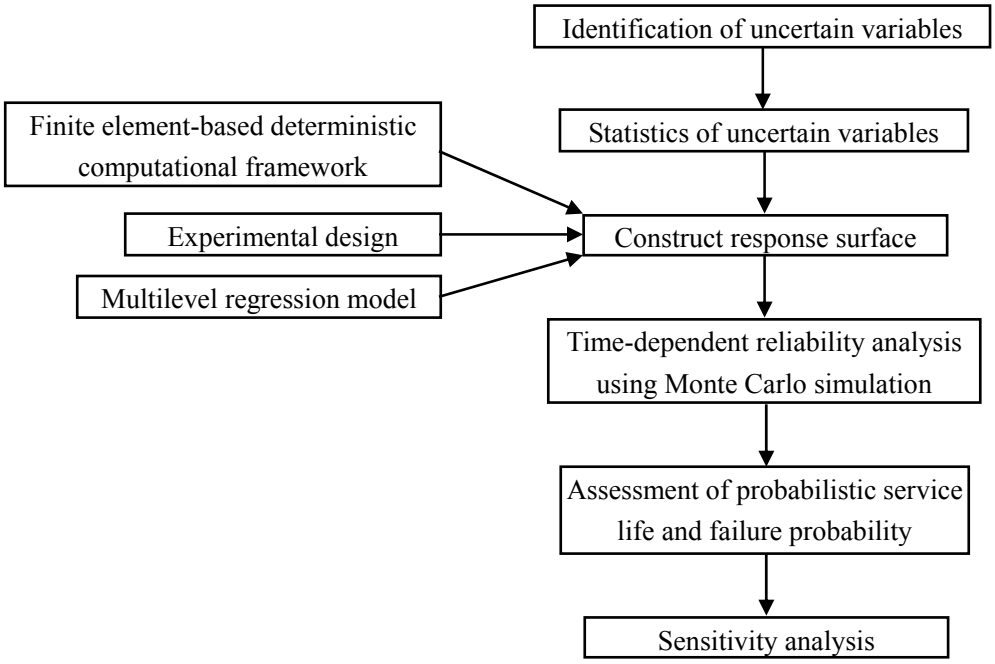

Figure 6.2. Time-dependent reliability analysis

6.3. Numerical example

The same numerical example used in Chapter 4 is used here. An initially chloride-free reinforced concrete slab shown in Fig. 6.3 is illustrated to implement a time-dependent reliability analysis. A constant free chloride content is applied on the bottom surface of the concrete slab, while an annually varying ambient temperature of $T_{ambient} = 15 + 10 \cdot \sin(2\pi \cdot t)$ is applied on the bottom surface (Note: t is time elapsed in years). A constant temperature of 15 ^{0}C is maintained on the top surface, and the initial temperature of 15 ^{0}C is assumed for the entire concrete slab.

As the output of deterministic analysis with the developed deterministic computational framework, the time-dependent evolution of chloride content at the depth

of reinforcement can be determined for any given concrete cover depth, reference chloride diffusivity and surface chloride content. The chloride threshold value, serving as the "resistance" of reliability analysis, is separated from the other three random variables and used especially to determine the service life.

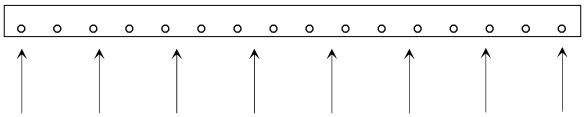

Figure 6.3. Reinforced concrete slab

In this study, a 3-level 3-factor full-factorial experimental design is performed with $3^3 = 27$ possible combinations, where three levels for each random variable are selected as shown in Table 6.2 to guarantee that most observations are within the range. Mean value of each random variable is adopted as the mid level value. For the concrete cover depth, the high level and low level values are assumed to be mean value ± double standard deviation. For the reference chloride diffusivity, the high level and low level values are derived from mean value ± double standard deviation of the water to cement ratio based on Eq. (6.1). For the surface chloride content and chloride threshold, the observed upper limit and bottom limit (Hoffman and Weyers 1994, 1996) are adopted as the high level and low level values, respectively.

Table 6.2. 3 levels of random variables

Random variable	Low level	Mid level	High level
Cover depth (mm)	42	50	58
Reference chloride diffusivity (m^2/year)	2.62 E-4	4.74 E-4	7.92 E-4
Surface chloride content (kg/m^3 of concrete)	1.20	3.50	8.20
Chloride threshold (kg/m^3 of concrete)	0.60	0.90	1.20

The deterministic analysis results for all 27 combinations are shown in Fig. 6.4, where the unit of the chloride content is in kg/m^3 of solution with a constant saturated free moisture content ω_e =0.08 m^3 of solution/m^3 of concrete.

In this study, a two-level regression approach is adopted to construct the response surface. The first level regression is to construct a general function that expresses the chloride content at the depth of reinforcement as a function of time. Based on the deterministic analysis results of the experimental design obtained in Fig. 6.4, a curve fitting software, CurveExpert (version 1.37), is used to implement the first level regression. According to the criterion of minimizing the sum of squared residuals, various possible mathematical models (including linear fit, polynomial fit, sinusoidal fit, logistic model, Gompertz model, exponential model, MMF model, Harris model etc.) are compared and Morgan-Mercer-Flodin (MMF) model has been identified to provide the optimal fit for each scenario with a consistently high coefficient of determination $R^2 \approx 1.0$. Therefore, MMF model is adopted to fit the chloride content versus time curve.

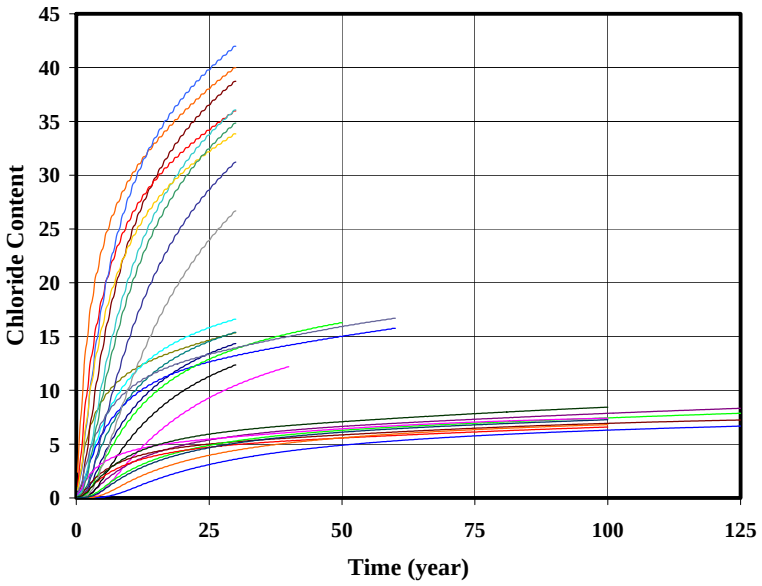

Figure 6.4. Deterministic analysis results

The MMF model takes the form as

$$Chloride\_Content(t) = \frac{a \cdot b + c \cdot t^{d}}{b + t^{d}} \tag{6.6}$$

where a, b, c and d are MMF model parameters, which can be determined automatically using CurveExpert as tabulated in Table 6.3.

Table 6.3. MMF model parameters

Test #	Cover depth (mm)	Reference diffusivity (m^2/year)	Surface chloride (kg/m^3 of concrete)	*a*	*b*	*c*	*d*
01	42	2.62E-4	1.20	-0.56068018	24.741086	8.7394247	1.0905068
02	42	2.62E-4	3.50	-0.33692382	39.517807	17.446899	1.5232465
03	42	2.62E-4	8.20	-0.8714139	26.359224	45.562091	1.3515539
04	42	4.74E-4	1.20	-0.56418458	8.4254594	7.7400629	0.82661531
05	42	4.74E-4	3.50	-0.93575297	7.8057642	18.623089	0.90141782
06	42	4.74E-4	8.20	-0.88714012	8.2073245	41.574271	1.0458888
07	42	7.92E-4	1.20	-0.64467815	4.5168902	10.29101	0.54672275
08	42	7.92E-4	3.50	-0.45836225	3.981567	18.581135	0.84552679
09	42	7.92E-4	8.20	-1.4250935	4.0300717	53.928922	0.71268632
10	50	2.62E-4	1.20	-0.30155484	86.002719	7.5804502	1.4247661
11	50	2.62E-4	3.50	-0.26013983	108.07277	15.452216	1.7733011
12	50	2.62E-4	8.20	-0.71003894	59.078386	40.650663	1.5465096
13	50	4.74E-4	1.20	-0.75623042	14.064257	9.5490634	0.92585511
14	50	4.74E-4	3.50	-0.35273643	24.590936	18.32413	1.4202696
15	50	4.74E-4	8.20	-0.91885623	17.658559	47.826476	1.2650445
16	50	7.92E-4	1.20	-0.83247183	5.7293617	9.560873	0.60999929
17	50	7.92E-4	3.50	-1.1477503	5.7474692	20.784391	0.76238848
18	50	7.92E-4	8.20	-1.0359166	6.0230785	44.718967	0.93333571
19	58	2.62E-4	1.20	-0.29403949	161.30948	7.4215035	1.4878178
20	58	2.62E-4	3.50	-0.27732166	223.78099	15.124232	1.8429531
21	58	2.62E-4	8.20	-0.5322851	137.81644	35.795926	1.7586076
22	58	4.74E-4	1.20	-0.37979292	41.794896	8.0181803	1.2783633
23	58	4.74E-4	3.50	-0.56418762	37.494296	18.843094	1.3871291
24	58	4.74E-4	8.20	-0.83047378	32.452845	43.994729	1.4117259
25	58	7.92E-4	1.20	-0.74119863	10.043785	9.83608	0.87442117
26	58	7.92E-4	3.50	-0.36929508	14.250115	19.414206	1.2912149
27	58	7.92E-4	8.20	-3.3600309	8.4389107	66.167452	0.82427807

The second level regression is to expresses MMF model parameters a, b, c and d as functions of the three random variables of concrete cover depth, reference chloride diffusivity and surface chloride content, respectively. Based on the first level regression

results in Table 6.3, commercial statistical software, MINITAB (Release 14), is used to implement the second level regression. A quadratic model is chosen to capture nonlinearility in the second level regression with some necessary modifications. On the one hand, all possible terms in a full quadratic model are rarely always needed in a practical application. Therefore, best subsets regression is performed to exclude unnecessary terms and find the most appropriate quadratic model. On the other hand, the regression can be improved further by applying some form of transformation (e.g. logarithmic transformation) to input or output variables. As a result, the second level regression results are summarized as follows.

$$a = -\exp(0.885 - 0.0523 \cdot C1 - 0.018 \cdot C3 + 83.0 \cdot C1 \cdot C2 - 2565401 \cdot C2^2 + 0.000221 \cdot C3^2)$$

$$\text{with} \quad R^2 = 72.3\% \qquad (6.7)$$

$$b = \exp(0.175 + 0.137 \cdot C1 - 8476 \cdot C2 + 0.0151 \cdot C3 - 97.5 \cdot C1 \cdot C2 + 8267104 \cdot C2^2 - 0.000139 \cdot C3^2)$$

$$\text{with} \quad R^2 = 98.6\% \qquad (6.8)$$

$$c = \exp(2.13 - 0.0152 \cdot C1 - 897 \cdot C2 + 0.04 \cdot C3 + 26.9 \cdot C1 \cdot C2 - 0.000177 \cdot C3^2)$$

$$\text{with} \quad R^2 = 98.8\% \qquad (6.9)$$

$$d = 0.633 + 0.023 \cdot C1 - 3129 \cdot C2 + 0.0214 \cdot C3 + 1695698 \cdot C2^2 - 0.000165 \cdot C3^2$$

with $R^2 = 93.0\%$ (6.10)

where $C1$ — the concrete cover depth (mm); $C2$ — the reference chloride diffusivity (m^2/year); $C3$ — the surface chloride content (kg/m^3 of solution).

In addition to applying the coefficient of determination R^2 to evaluate the approximation degree how the regression function approaches the true response surface, residual analysis is performed further using MINITAB to check whether or not the first level and the second level regressions have acceptable fit to the data. In summary, the residuals of a proper regression model ought to meet three basic criteria. First, residuals should have constant mean value of zero. Second, the variance of residuals should maintain constant with fitted values. Third, residuals should be random, not systematic. Two basic tools are used herein to check the three criteria. The standardized residuals versus fitted values plot is used to check the first two criteria, and the runs test on residuals sorted by ascending fitted values is used to check the randomness. In this study, the residual analysis is performed to verify the applicability of the multilevel regression for MMF model and its parameters *a*, *b*, *c* and *d* in Eqs. (6.7)~(6.10).

So far, a multilevel regression has been completed in developing the response surface, where the time-dependent chloride content at the depth of reinforcement is expressed as approximate mathematical function of three random variables of concrete cover depth, reference chloride diffusivity, and surface chloride content. Once the chloride threshold

value is specified, the service life of the chloride-contaminated reinforced concrete structure can be obtained by transforming Eq. (6.6) as

$$service\_life = \left(\frac{C4 - a}{c - C4} \cdot b \right)^{1/d} \tag{6.11}$$

where $C4$ — the chloride threshold value (kg/m^3 of solution).

The time-dependent reliability analysis is performed directly on the basis of the response surface and Monte Carlo simulation. Based on the statistical information in Table 6.1, totally 10,000 random samples are generated independently for each random variable. The histograms of the four random variables with their corresponding distribution fits are shown in Figs. 6.5~6.8, respectively.

As Monte Carlo simulation results, the histogram of service life and the associated time-dependent failure probability (the empirical CDF of service life) of the chloride-contaminated reinforced concrete structure are shown in Figs. 6.9 and 6.10, respectively.

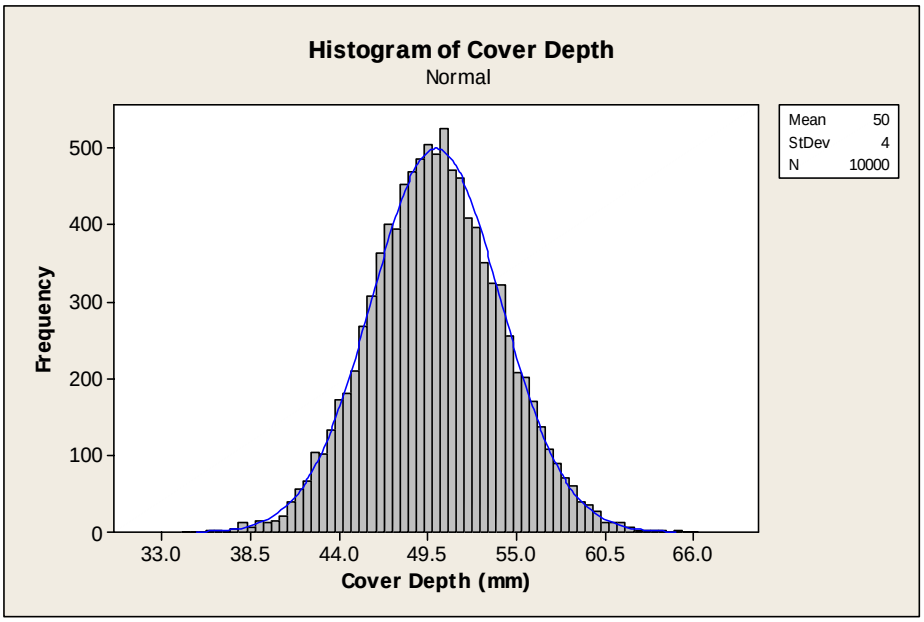

Figure 6.5. Histogram and distribution fit of concrete cover depth

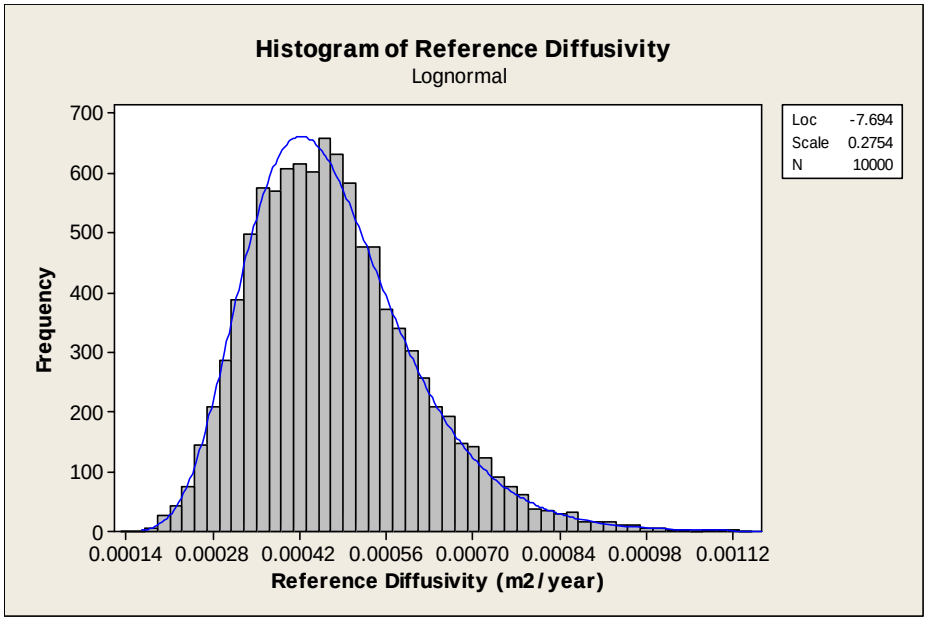

Figure 6.6. Histogram and distribution fit of reference diffusivity

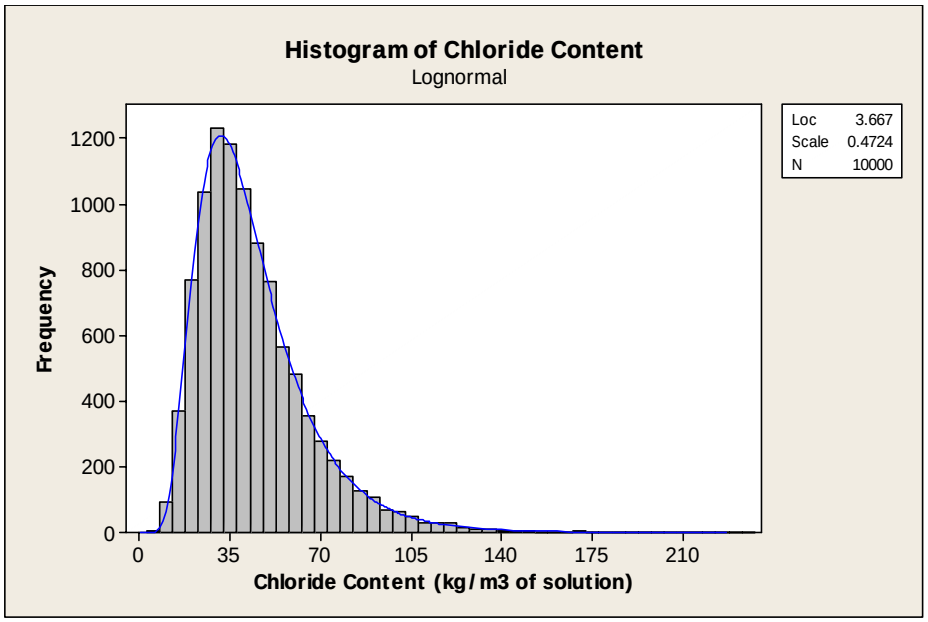

Figure 6.7. Histogram and distribution fit of surface chloride content

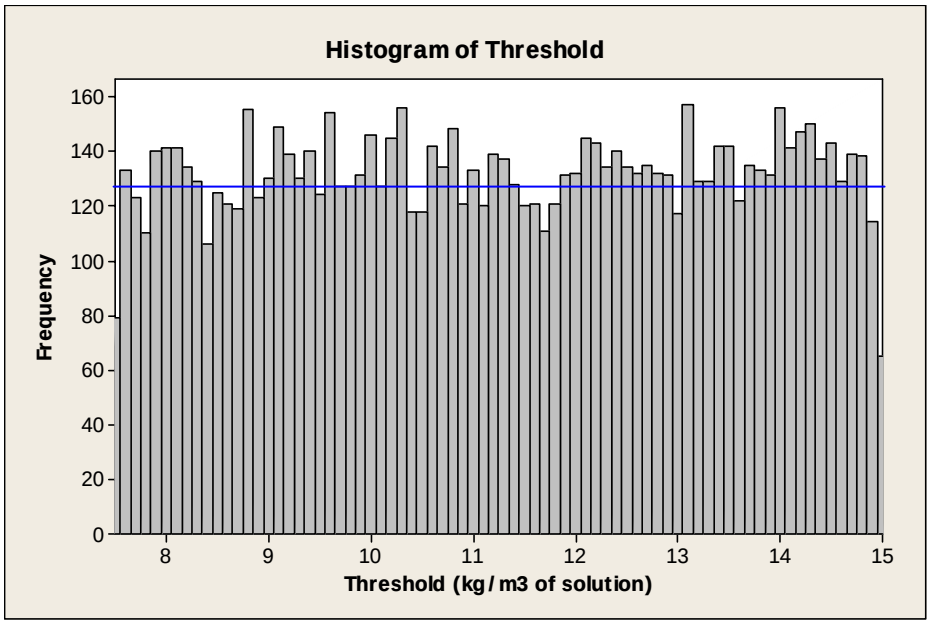

Figure 6.8. Histogram and distribution fit of chloride threshold value

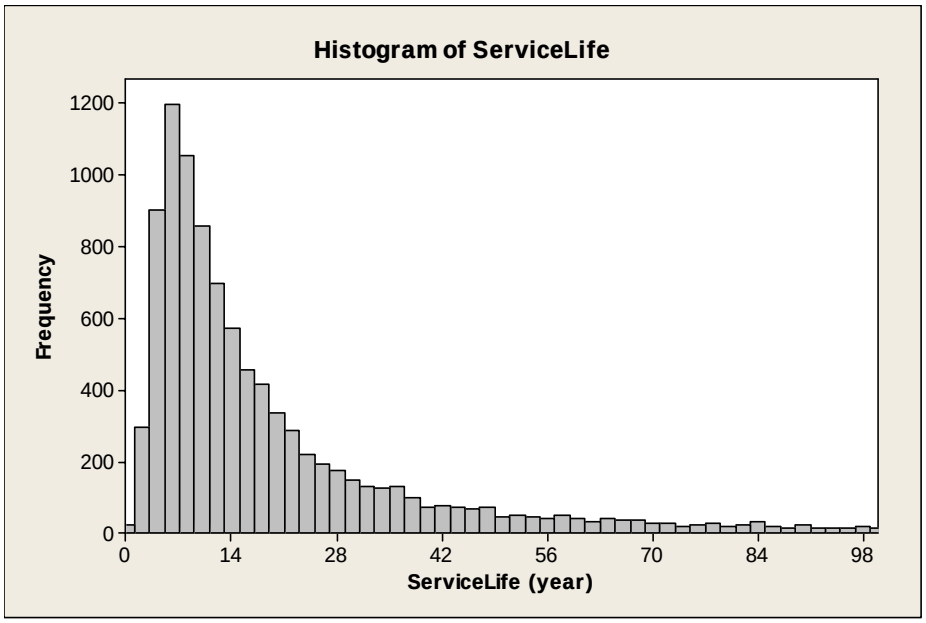

Figure 6.9. Histogram of service life

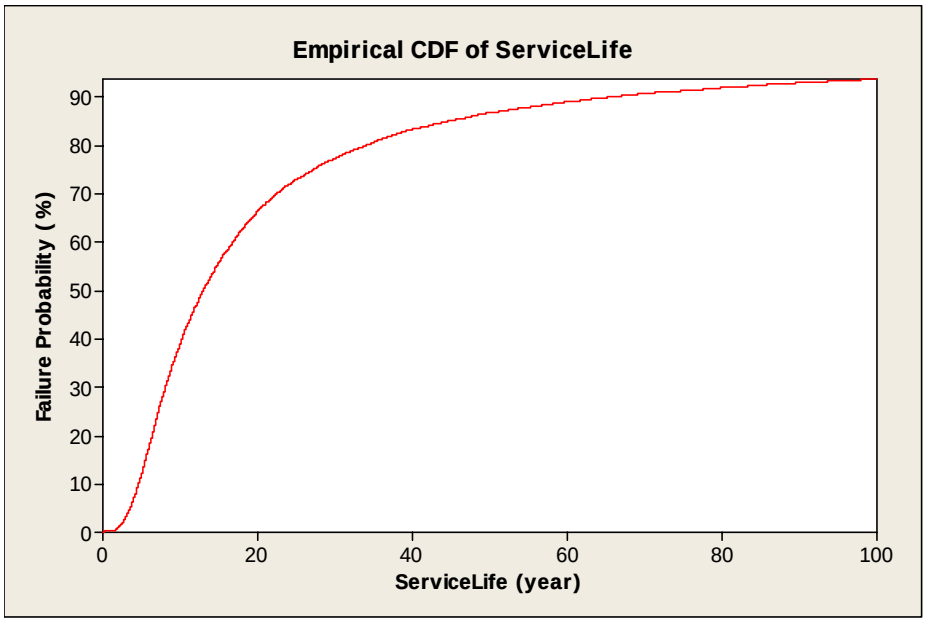

Figure 6.10. Time-dependent failure probability of service life

From Monte Carlo simulation results, the mean value, the median and the standard deviation of the service life for the chloride-contaminated reinforced concrete structure are 35.22 years, 12.97 years and 92.21 years, respectively. The median of the service life 12.97 years lies within the usually observed range 7-20 years (Kong et al. 2002) and is therefore especially important for durability-based structural design. Since the service life is directly based on Monte Carlo simulation of Eq. (6.11), some combination of randomly generated values of variables in Eq. (6.11) may lead to unreasonably large service life values for this study, about 1% of Monte Carlo runs with service life estimates greater than 1500 years were thus discarded.

Finally, the sensitivity analysis is implemented using Monte Carlo simulation. For each random variable of interest, 1000 random samples are generated with the other three random variables assuming the mean values. The influence of each random variable on the service life of the chloride-contaminated reinforced concrete structures is shown in Figs. 6.11~6.14, respectively.

It can be observed that the service life increases with the concrete cover depth and the chloride threshold value, and decreases with the reference diffusivity and the surface chloride content. Among the four influencing factors, the surface chloride content exerts the greatest influence on the service life. This conclusion is confirmed further in Fig. 6.4, where all 27 chloride content versus time curves are classified obviously into three groups according to the three levels of the surface chloride content. The concrete cover depth exerts the least influence on the service life.

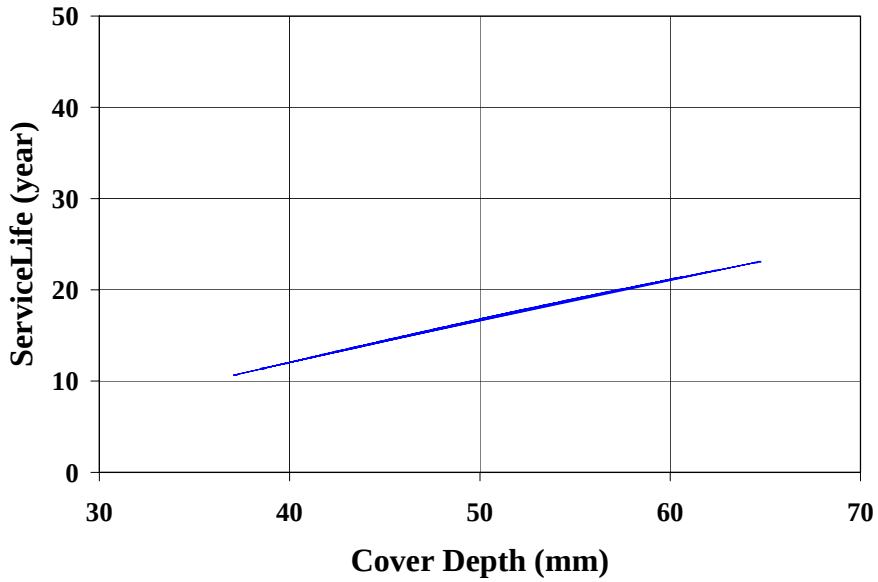

Figure 6.11. Relationship between service life and concrete cover depth

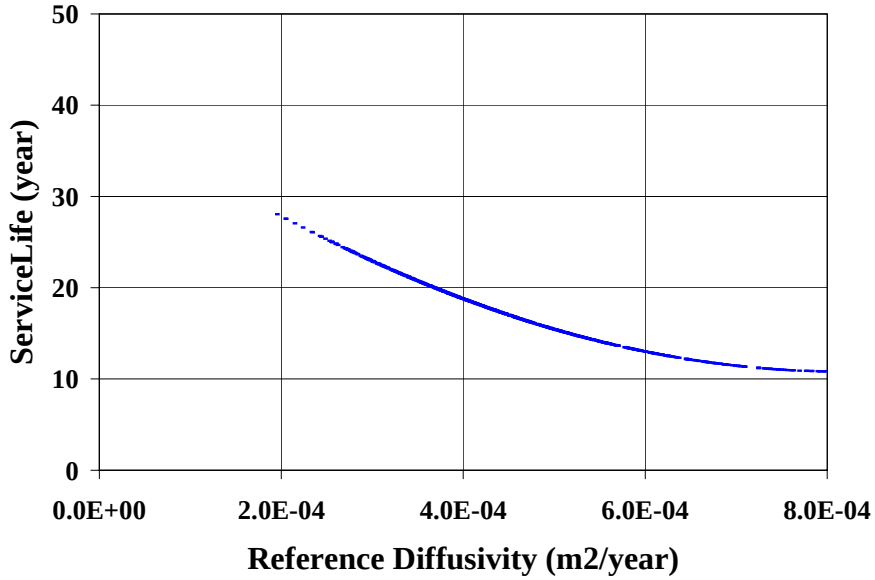

Figure 6.12. Relationship between service life and reference diffusivity

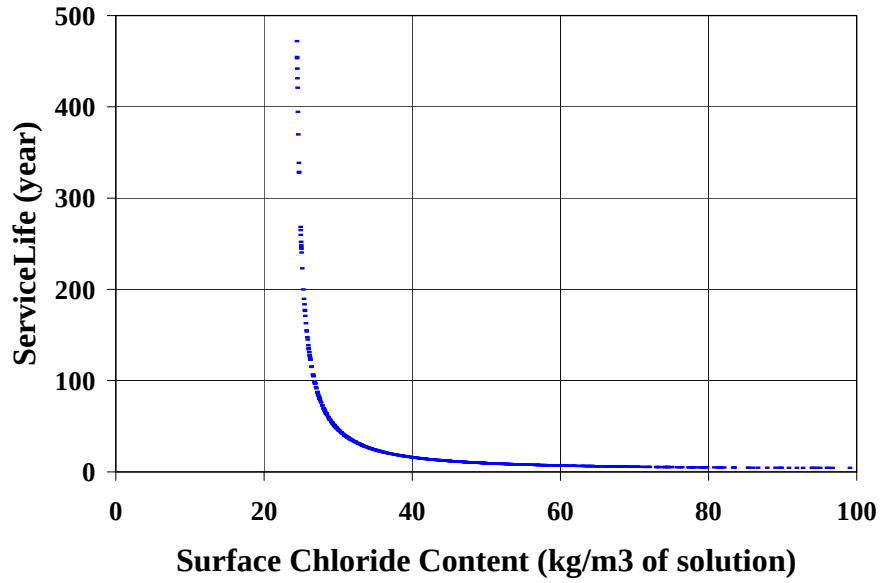

Figure 6.13. Relationship between service life and surface chloride content

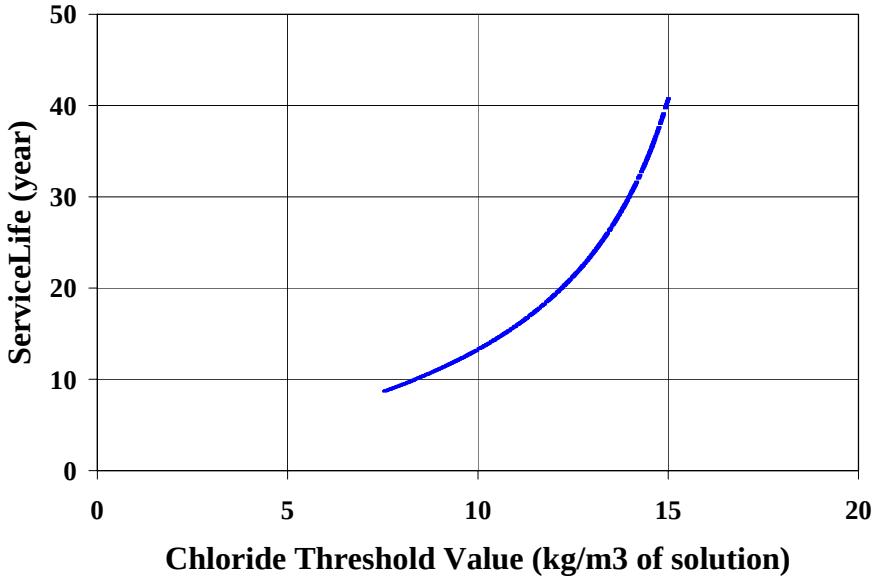

Figure 6.14. Relationship between service life and chloride threshold value

6.4. Conclusion

This chapter develops an integrated probabilistic framework to assess the time-dependent reliability and predict the service life of chloride-contaminated reinforced concrete structures exposed to chloride contamination. The chloride penetration process in concrete is simulated using a previously developed finite element-based deterministic methodology. To include various possible uncertainties in concrete material properties, environmental loadings and the proposed computational framework, four independent random variables in the deterministic model are identified. A nonlinear response surface is established by combining a 3-level full-factorial experimental design with multilevel regression. Monte Carlo simulation is then performed to predict the service life. The statistics of the service life and the associated time-dependent failure probability of the chloride-contaminated reinforced concrete structure are obtained. Sensitivity analysis is implemented to evaluate the influence of each random variable on the service life.

CHAPTER VII

CONCLUSIONS AND FUTURE WORK

7.1. Conclusions

A reinforced concrete structure may degrade through a combination of coupled physical, chemical and mechanical deterioration processes. Based on existing coupled multi-physics analysis solver in commercial software, this study developed an integrated finite element-based computational framework to quantitatively evaluate the resultant mechanical responses and assess the time-dependent durability of reinforced concrete structures under multiple coupled environmental loadings. Typical deterioration processes including heat transfer and associated thermal expansion/contraction process, moisture transport and associated wetting expansion/drying shrinkage process, carbon dioxide transport and associated carbonation process, chloride penetration process, reinforcement corrosion and rust expansion process due to chloride penetration, as well as the subsequent crack initiation and propagation were taken into account simultaneously. Various coupling effects among these deterioration processes were considered by adjusting the transport properties of concrete through a multifactor law. The concrete cracking analysis was implemented using a smeared cracking approach, and the crack-induced accelerated deterioration process was modeled using relative crack density

concepts. The developed computational framework is general and flexible, which makes it possible to include any additional deterioration process.

Due to a large amount of random variability and uncertainty existing in the material properties of concrete, various environmental loadings and the developed computational framework, an appropriate approach for assessing the structural durability is to combine the deterministic computational framework with advanced stochastic modeling. The finite element-based computational framework was thus expanded into a risk assessment framework. The most influential random variables in the computational framework were identified, and nonlinear response surface was established through combining experimental design with multilevel regression. Monte Carlo simulation was performed with the response surface to predict the statistics of service life and assess the associated time-dependent failure probability of reinforced concrete structures under multiple coupled deterioration processes. Sensitivity analysis was implemented to quantify the influence of each random variable on the estimation of service life.

The prominent advantages of the proposed computational framework can be summarized as follows. Making use of existing FEA solver in commercial software, the methodology is rather straightforward and efficient in simulating multiple coupled transport process of various aggressive agents. This facilitates 3-D simulation for practical concrete structures with arbitrary geometries exposed to randomly varying environmental loadings. Second, the various coupling effects can be taken into account

conveniently by adjusting the transport properties of concrete with a multifactor law. Third, plentiful simulation results — including the spatial distribution of temperature, relative humidity, moisture content, carbonate concentration, as well as various source/sink terms — can be extracted easily at each time step and be postprocessed further. The obtained information deepens the insight on the deterioration mechanism of concrete structures. Finally, the methodology is flexible and can be expanded to incorporate other deterioration processes as physics environments, thus facilitating the overall assessment of durability and service life of reinforced concrete structures under multiple coupled deterioration processes.

A first attempt has been made in this study to integrate various highly nonlinear deterioration processes into a finite element-based computational framework, evaluate the resultant mechanical responses and assess the time-dependent durability of reinforced concrete structures under multiple coupled environmental loadings. Before the practical application of the computational framework, various potential limitations existing in the computational framework should be reemphasizing herein.

1) Each deterioration mechanism is characterized using a transport process of a typical aggressive agent. The transport process is assumed to follow a governing differential equation, which satisfies the mass/energy balance and thermodynamic/chemical equilibrium. Finite element method is utilized to numerically solve the differential equation and obtain the temporal and spatial distribution of the aggressive agent.

As an approximate approach, the finite element method may lead to errors. To obtain stable simulation results, convergence analysis has been performed by specifying the length of time step, assigning time substeps within each time step, giving the number of equilibrium iterations for each time substep, and adopting self-defined convergence criterion. However, the convergent results are still difficult to obtain when modeling highly nonlinear and coupled phenomena.

2) It should be emphasized that only the mechanical responses due to chemical deterioration processes, instead of the micro-scale chemical deterioration phenomena, are modeled in this study.

In this study, two typical chemical deterioration processes, carbonation and chloride-induced reinforcement corrosion were considered. It can be observed that the chemical reactions were not directly simulated. In contrast, the mechanical responses caused by these chemical deteriorations were incorporated into the developed computational framework. For instance, the corrosion-induced rust expansion process was modeled as an equivalent time-dependent radial displacement boundary condition, which was applied directly on nodes along the concrete-steel interface.

3) Due to the limitation of commercial finite element software, the ability is currently lacking to model multiphase transport mechanisms that exist even in a single deterioration process. Therefore, only one dominant transport mechanism is identified under some assumptions to characterize that particular deterioration process, while

other transport mechanisms are ignored for the sake of simplicity.

As mentioned in Chapter 2, based on the microstructure characteristics of concrete and the saturation degree of pore solution, several different moisture transport mechanisms, such as convection, diffusion, desorption and adsorption etc., may work concurrently. To overcome the limitation of commercial finite element software, the diffusion mechanism was assumed to dominate the moisture transport in concrete under partially saturated situation. As a result, the relative humidity gradient of pore moisture in concrete serves as driving force, and the Fisk's second law based on mass conservation governs the moisture transport process.

So it is with the chloride penetration through concrete in Chapter 4. Although the transport mechanism of chloride may occur in several forms (including diffusion, permeation, capillary sorption, and dispersion etc.), chemical ionic diffusion was identified as the main transport mechanism for chloride penetration, where the chloride content gradient serves as the driving force.

4) Mechanical stress response of concrete is highly dependent on the assumed constitutive relationship model.

As discussed in Chapter 2, developing an appropriate constitutive relationship model for concrete is highly challenging, and substantive efforts have been made to propose various numerical models in the past. Since the constitutive relationship model characterizes the nonlinear stress-strain relation of concrete, different models can make

significant difference in the mechanical stress states. Moreover, the stress state-dependent cracking will be affected. Due to numerous uncertainties and influencing factors existing, no unanimous constitutive relationship model applies any given concrete, which makes it difficult to obtain accurate estimation on the mechanical stress responses.

5) Mechanical cracking response of concrete is highly dependent on the assumed failure criterion. A smeared cracking approach is used to model concrete cracking, which has some intrinsic limitations (e.g., the sensitivity to mesh size etc.).

As elaborated in Chapter 3, failure criterion under multi-axial stress state was adopted to assess the occurrence of failure and identify the corresponding failure modes. In this sense, a proper choice of failure criterion can determine the correctness and accuracy of the mechanical cracking response caused by multiple coupled deterioration processes. Just like the constitutive relationship model, no unanimous failure criterion applies any given concrete.

6) The effect of relative crack density on transport properties of the cracked concrete is only conceptually formulated here, and needs to be verified and quantified with experimental work in a future study.

An original relative crack density concept was proposed in this study. The numerical relationship between the relative crack density and the transport properties was assumed based on the conceptual models by Aldea et al. (1999a, 1999b). Therefore, experimental results are needed to verify and quantify the numerical relationship.

7) Various potential coupling effects were considered by adjusting the transport properties of concrete through a multifactor law. As a simplistic assumption, the multifactor law may become inapplicable to highly nonlinear and correlated couplings existing among multiple deterioration processes.

In this sense, the applicability of the multifactor law needs to be verified further using more experimental results, although this simplistic method has been adopted extensively in numerous literature references. In addition, all influencing factors in the multifactor law are expressed as empirical functions of corresponding variables. More experimental results are needed to verify the accuracy and validity range of all these empirical functions.

8) Multiple coupled deterioration processes, including heat transfer process, moisture transport process, carbonation process, chloride penetration process, reinforcement corrosion and rust expansion process, and the subsequent concrete cracking process, were considered in this study. In the process of developing and illustrating the proposed computational framework, different combinations of these coupled deterioration processes were taken into account. Different assumptions were adopted for the sake of illustration only, when modeling the same transport process for different types of deterioration in different chapters.

For instance, a finite element-based computational framework was developed to model multiple coupled deterioration processes in Chapter 2, where the diffusion

mechanism was assumed to dominate the moisture transport in concrete. This is valid under the assumption of partial saturation situation, where the relative humidity gradient of pore moisture in concrete serves as driving force, and the Fisk's second law governs the moisture transport process.

To illustrate the developed computational framework, the simulation of the chloride-induced reinforcement corrosion process was implemented in Chapters 4 and 5. Although it is known that moisture transport may influence chloride penetration to some extent, the lack of established numerical models quantifying the coupling relationship makes it difficult to adopt the partial saturation assumption that was used in Chapter 2. Following Xi and Bazant (1999) and Martin-Perez et al. (2000), complete saturation assumption was adopted, where the Darcy's law under hydraulic pressure dominates the moisture transport in concrete. Acting as vehicle, fluid flow may facilitate the transport of various aggressive agents through forced convection. To simplify the analysis further, the potential influence of hydraulic pressure on chloride penetration was ignored. As a result, it was assumed that no coupling relationship exists between moisture transport and chloride penetration. These assumptions may be reasonable under some environmental conditions, and may not impair the illustration of the developed computational framework. For realistic applications, all assumptions ought to maintain consistent and compatible with the exposed environmental loadings.

9) As a preliminary attempt to quantitatively assess the concrete durability, the proposed computational framework needs to be verified/validate further through either

experimental results or available literature.

However, exact physical understanding and appropriate micro-scale test methods for many deterioration processes are still relatively lacking. NIST, ACI and ASTM (Frohnsdorff 1999) are cooperating with each other to develop standard test methods. RILEM TC116-PCD (Kropp and Hilsdorf 1995) is making efforts in the same direction. The standardization of the test methods and of the preconditioning procedure of specimens is urgently required. The main contribution of this study, however, is to develop a computational framework to quantitatively assess the durability of concrete, by integrating multiple deterioration process models.

7.2. Future work

Future work is possible along several directions — computational methodology development, experimental studies, and practical application.

With respect to computational methodology development, additional deterioration processes, such as freeze-thaw cycles, sulfate attack, leaching of concrete constituents, alkali-aggregate reaction etc., can be included in the developed computational framework. The reinforcement corrosion process caused by carbonation reaction should also be considered. Coupling models among various deterioration processes, source/sink term models of some deterioration processes, and the numerical relationship between the

relative crack density and the transport properties of moisture/aggressive agents are supposed to be verified further.

With respect to experimental studies, a large amount of statistical data on the material properties of concrete and various deterioration mechanisms are desired. In addition, data of the deterioration effects on concrete durability are to be collected. Reliability analysis in this study assumed the statistics of many model parameters only for the sake of illustration. The data collected in the future can be used to verify/validate the proposed finite element-based computational framework, before actual application.

As discussed in Section 1.2, the ultimate goal of this study is to apply the computational framework to quantitatively assess the long-term durability of underground SDF concrete containment vault and predict its service life under multiple coupled deterioration processes. To fulfill the ultimate goal, some important issues must be taken into account as follows:

1) All deterioration processes significant to the subsurface reinforced concrete structures should be incorporated into the developed computational framework.

Walton et al. (1990) summarized various deterioration processes considerable to the subsurface concrete barriers in low-level radioactive waste disposal facilities, including sulfate attack, reinforcement corrosion, leaching of concrete constituents, carbonation, freeze thaw attack, alkali-aggregate reaction, and thermal-induced and shrinkage-induced cracking etc. It can be observed that some of the deterioration processes have not been considered in the dissertation. Without considering the dominant deterioration processes,

it is insignificant to perform the durability assessment.

2) A large amount of in-situ data on various model parameters in the computational framework are relatively lacking.

First, to implement the durability assessment, a large amount of in-situ data is required, which includes the mechanical properties of concrete, transport properties of intact/cracked concrete, geometric dimensions of concrete structure, the dimension, amount and location of embedded reinforcement, ambient weather records, and various environmental loadings etc.

Second, it should be emphasized that the underground environment is distinctive from the overground environment, which may facilitate some deterioration processes while restraining some others. For instance, saturation assumption applies to many underground concrete structures. In that case, Darcy's flow instead of Fick's diffusion dominates the moisture transport in concrete. In contrast, carbonation reaction will be inhibited completely, since moisture fills the porous microstructure of concrete and thus prevents gaseous carbon dioxide from penetrating through concrete.

Third, the curing process of saltstone involves exothermic reactions, results in a large amount of heat generated and transferred to the concrete containment vault. The heat generation process may exert significant influence on the durability of the underground SDF concrete containment vault. The heat generated by saltstone can be regarded as a typical heat source term in the heat transfer governing equation, and it is straightforward to consider the saltstone heat generation in the previous developed finite element-based

computational framework.

3) Based on its configuration, the underground SDF concrete containment vault can be broken up into several different structural components, including roof, walls, floor etc. Each component is usually exposed to a particular local environment, which makes these structural components degrade at different rates.

With respect to the long-term durability, a single structural component can be identified as the most critical component, or the weakest component with the shortest estimation in service life. The occurrence of structural failure on the most critical component will determine the service life of the entire underground SDF concrete containment vault. When analysis is focused only on the most critical component, the entire durability assessment process will be simplified significantly.

APPENDIX

Summary of input model parameters

Input model parameter	Value adopted	Reference
Compressive strength	$f_c^{'} = 30$ MPa	Mehta (1993)
Tensile strength	$f_t = 3$ MPa	Mehta (1993)
Strain at peak stress	$\varepsilon_0 = 0.002$	Mehta (1993)
Ultimate strain	$\varepsilon_{cu} = 0.003$	Mehta (1993)
Elastic modulus	$E_c = 30$ GPa	Mehta (1993)
Poisson's ratio	$\nu = 0.2$	Mehta (1993)
Density	$\rho = 2400$ kg/m^3	Mehta (1993)
Thermal conductivity	$k = 2.0$ W/m·K	Mehta (1993)
Specific heat capacity	$c = 1000$ J/kg·K	Mehta (1993)
Thermal expansion coefficient	$\alpha = 1.0 \times 10^{-5}$ /K	Mehta (1993)
Water to cement ratio by mass	$WCR = 0.5$	Mehta (1993)
Hydral contraction coefficient	$\beta = 9.96 \times 10^{-3}$ m^3 of concrete/m^3 of moisture	Torrenti et al. (1999)
Model parameter	$A = 7.0E-10$ m^2/s	Torrenti et al. (1999)
Model parameter	$\theta = 0.05$	Torrenti et al. (1999)
Model parameter	$\psi = 0.4$	Torrenti et al. (1999)
Model parameter	$\gamma = 4$	Torrenti et al. (1999)
Model parameter	$W_0 = 128.8 \times 10^{-3}$ m^3 of moisture/m^3 of concrete	Kumaran (1996)
Model parameter	$B = 0.57$	Kumaran (1996)
Model parameter	$C = 0.64$	Kumaran (1996)
Activation energy of moisture diffusion process	$E = 2700$ J/mol	Saetta et al. (1995)

Activation energy of chloride diffusion process	$E = 44.6$ kJ/mol	Martin-Perez et al. (2001)
Activation energy of carbonation reaction process	$E_0 = 91.52$ kJ/mol	Saetta et al. (1995)
Gas constant	$R = 8.314$ J/mol · K	Saetta et al. (1995)
Reference diffusivity of CO_2	$D_{c,0} = 3 \times 10^{-8}$ m^2/s	Saetta et al. (1995)
Model parameter	$\zeta = 0.5$	Isgor and Razaqpur (2004)
Ideal carbonation rate	$v_0 = 2.80 \times 10^{-7}$ /s	Saetta and Vitaliani (2004)
Model parameter	$\eta_c = 0.733$	Saetta and Vitaliani (2004)
Model parameter	$\eta_m = 0.002$	Saetta and Vitaliani (2004)
Multiplication factor of moisture diffusivity	$MF = 20$	Cerny et al. (2001)
Multiplication factor of chloride diffusivity	$MF = 8$	Gerard and Marchand (2000)
Constant saturated moisture content	$\omega_e = 0.08$ m^3 of moisture/m^3 of concrete	Martin-Perez et al. (2000)
Model parameter (linear binding isotherm model)	$\alpha_{cl} = 0.147$	Onyejekwe and Reddy (2000)
Model parameter (Freundlich binding isotherm model)	$\alpha_{cl} = 1.037 \quad \beta_{cl} = 0.36$	Onyejekwe and Reddy (2000)
Model parameter (Langmuir binding isotherm model)	$\alpha_{cl} = 0.767 \quad \beta_{cl} = 0.21$	Onyejekwe and Reddy (2000)
Equivalent thickness of ITZ	$\delta_{por} = 12.5 \mu m$	Thoft-Christensen (2000)
Model parameter	$m = 0.04$	Martin-Perez et al. (2001)
Surface chloride content	$C_{cl,0} = 3.5$ kg/m^3 of concrete	Stewart and Rosowsky (1998)
Chloride threshold content	$C_{cl,cr} = 0.9$ kg/m^3 of concrete	Stewart and Rosowsky (1998)
Model parameter	$\kappa = 8.333$	Kong et al. (2002)
Model parameter	$n = 0.5$	Kong et al. (2002)
The atomic weight of iron	$A = 55.85$ g/mol	Pantazopoulou and Papoulia (2001)
Faraday's constant	$F = 96500$ Coulomb/mol	Pantazopoulou and Papoulia (2001)

REFERENCES

ACI (2002) ACI Committee 201, *Guide to Durable Concrete, ACI 201.2R-92*, American Concrete Institute, Farmington Hills, Michigan.

ACI (2002) ACI Committee 308, *Building Code Requirements for Structural Concrete and Commentary*, ACI 308-99, American Concrete Institute, Farmington Hills, Michigan.

ACI (2000) *ACI Manual of Concrete Practice*. Technical report, American Concrete Institute, Farmington Hills, Michigan.

Ahmad, S. (2003) Reinforcement corrosion in concrete structures, its monitoring and service life prediction — a review, *Cement and Concrete Composites*, Vol. 25, No. 4-5, pp. 459-471.

Aldea, C-M., Shah, S.P. and Karr, A.F. (1999a) Effect of Cracking on Water and Chloride Permeability of Concrete, *Journal of Materials in Civil Engineering*, Vol. 11, No. 3, pp. 181-187.

Aldea, C.M., Shah, S.P. and Karr, A. (1999b) Permeability of Cracked Concrete, *Materials and Structures*, Vol. 32, No. 219, pp. 370-376.

Alfaiate, J., Pires, E.B. and Martins, J.A.C. (1997) A Finite Element Analysis of Non-Prescribed Crack propagation in Concrete, *Computers & Structures*, Vol. 63, No. 1, pp. 17-26.

Andrade, C., Alonso, C. and Molina, F. J. (1993) Cover Cracking as a Function of Rebar Corrosion: Part I — Experimental Test, *Materials and Structures*, Vol. 26, No. 162, pp. 453-464.

ANSYS (2002) *ANSYS 7.0 Help*, ANSYS Inc., Canonsburg, Pennsylvania.

Arya, C. and Ofori-darko, F.K. (1996) Influence of Crack Frequency on Reinforcement Corrosion in Concrete, *Cement and Concrete Research*, Vol. 26, No. 3, pp. 345-353.

Bangash, M.Y.H. (1989) *Concrete and Concrete Structures: Numerical Modeling and Applications*, Elsevier Science Published Ltd., London, England.

Bangert, F., Grasberger, S., Kuhl, D. and Meschke, G. (2003) Environmentally Induced Deterioration of Concrete: Physical Motivation and Numerical Modeling,

Engineering Fracture Mechanics, Vol. 70, No. 7-8, pp. 891-910.

Baroghel-Bouny, V. (1994) Caracterisations des pates de ciment et des betons – Methodes, analyse, interpretations, *Rapport LCPC* (in French).

Basheer, L., Kropp, J. and Cleland, D.J. (2001) Assessment of the durability of concrete from its permeation properties: a review, *Construction and Building Materials*, Vol. 15, No. 2, pp. 93-103.

Bazant, Z. P. (1979a) Physical model for steel corrosion in concrete sea structures – theory, *ASCE Structural Division Journal*, Vol. 105, No. 6, pp. 1137-1153.

Bazant, Z. P. (1979b) Physical model for steel corrosion in concrete sea structures – application, *ASCE Structural Division Journal*, Vol. 105, No. 6, pp. 1155-1166.

Bazant, Z.P. (1995) Creep and Shrinkage Prediction Model for Analysis and Design of Concrete Structures – Model B3, *Materials and Structures*, Vol. 28, No. 168, pp. 357-365.

Bazant, Z. P., and Najjar, L. J. (1972) Nonlinear water diffusion in nonsaturated concrete, *Materials and Structures*, Vol. 5, No. 25, pp. 3-20.

Bazant, Z.P. and Oh, B.H. (1987) Spacing of Cracks in Reinforced Concrete, *ASCE Journal of Structural Engineering*, Vol. 109, No. 9, pp. 2066-2085.

Bazant, Z.P. and Planas J. (1998) *Fracture and Size-Effect in Concrete and Quasi-Brittle Materials*, CRC press, Boca Raton, Fla.

Bazant, Z.P., Sener, S. and Kim, J.K. (1987) Effect of Cracking on Drying Permeability and Diffusion of Concrete, *ACI Materials Journal*, Vol. 84, pp. 351-357.

Beeby, A.W. (1978) *Concrete in the Oceans*, Technical Report No. 1, Cement and Concrete Association, Slough, U.K.

Bentz, D.P., Clifton, J.R., Ferraris, C.F. and Garboczi, E.K. (1999) Transport properties and durability of concrete: literature review and research plan, National Technical Information Service (NTIS), U.S. Department of Commerce, *Technical Report No. FHWA-RD-00-073*, NISTIR 6395.

Bentz, D.P. and Garboczi, E.J. (1997) Three-dimensional computer simulation of Portland cement hydration and microstructure development, *Journal of the American Ceramic Society*, Vol. 80, No. 1, pp. 3-21.

Berke, N. S., and Hicks, M. C. (1994) Predicting chloride profiles in concrete, *Corrosion*

Engineering, Vol. 50, No. 3, pp. 234-239.

Berman, H.A. (1975) Sodium chloride, corrosion of reinforcing steel, and the pH of calcium hydroxides solution, *ACI Journal*, Vol. 72, No. 4, pp. 150-157.

Berke, N.S. and Hicks, M.C. (1994) Predicting chloride profiles in concrete, *Corrosion Engineering*, Vol. 50, No. 3, pp. 234-239.

Bhal, N.S. and Mital, M.K. (1987) Effect of Relative Humidity on Creep and Shrinkage of Concrete, *Journal of the American Ceramic Society*, Vol. 70, pp. 329-332.

Bisschop, J. and van Mier J.G.M. (2002). "How to study drying shrinkage microcracking in cement-based materials using optical and scanning electron microscopy?" *Cement and Concrete Research*, Vol. 32, No. 2, pp. 279-287.

Breysse, D. and Gerard, B. (1997) Transport of Fluids in Cracked Media, in: Reinhardt HW, editor, *Penetration and Permeability of Concrete,* RILEM Report 16, E & FN Spon, London, pp. 123-153.

BS8110 (1985) *BS8110: Part 2*, British Standards Institution, London.

Cady, P.D. and Weyers, R.E. (1983) Chloride penetration and the deterioration of concrete bridge decks, *Cement, Concrete & Aggregate*, Vol. 5, No. 2, pp. 81-87.

CEB (1992) *Durable Concrete Structures*, CEB Design Guide, Thomas Telford, UK.

Cerny, R. et al. (2000) The effect of compressive stress on thermal and hygric properties of Portland cement mortar in wide temperature and moisture ranges, *Cement and Concrete Research*, Vol. 30, No. 8, pp. 1267-1276.

Cerny, R., Drchalova, J., and Rovnanikova, P. (2001) The Effect of Thermal Load and Frost Cycles on the Water transport in Two High Performance Concretes, *Cement and Concrete Research*, Vol. 31, No. 8, pp. 1129-1140.

Cerny, R., Totova, M., Podebradska, J., Toman, J., Drchalova, J. and Rovanikova, P. (2003) Thermal and hygric properties of Portland cement mortar after high-temperature exposure combined with compressive stress, *Cement and Concrete Research*, Vol. 33, No. 9, pp. 1347-1355.

Chatterji, S. (1995) On the applicability of Fick's second law to chloride ion migration through Portland cement concrete, *Cement and Concrete Research*, Vol. 25, No. 2, pp. 299-303.

Chen, D., Li, W., Ni, K. and Mahadevan, S. (2004) Concrete degradation under multiple

processes, *Proceedings of ASCE Structures Congress 2004*, Nashville, Tennessee.

Chowdhury, S.H. and Loo, Y.C. (2001) A New Formula for Prediction of Crack Widths in Reinforced and Partially prestressed Concrete Beam, *Advances in structural Engineering*, Vol. 4, No. 2, pp. 101-109.

Clear, K. C. (1976) Time to corrosion of reinforcing steel in concrete slabs, Vol. 3. *Performance Agter 830 Daily Salt Applications*, Federal Highway Administration Report No. FHWA-RD-76-70, NIST PB-258 446.

Clear, K.C. (1983) Chloride at the threshold, *Report of Kenneth C. Clear Inc.*, pp. 1011.

Clifton, J.R. (1993) Predicting the service life of concrete, *ACI Materials Journal*, Vol. 90, No. 6, pp. 611-617.

Dagher, H.J. and Kulendran, S. (1992) Finite element modeling of corrosion damage in concrete structures, *ACI Structural Journal*, Title no. 89-S67, pp. 699-708.

Darwin, D. (1993) Reinforced Concrete. In *Finite Element Analysis of Reinforced Concrete Structures* Vol. II: Proceedings of the International Workshop. New York, ASCE, pp. 203-232.

DeBorst, R. (1997) Some Recent Developments in Computational Modeling of Concrete Fracture, *International Journal of Fracture*, No. 86, No. 1-2, pp. 5-36.

Desayi, P. and Krishnan, S. (1964) Equation For Stress Strain Curve of Concrete, *Journal of the American Concrete Institute*, Vol. 61, No. 3, pp. 345-350.

El-Dieb, A.S. and Hooton, R.D. (1995) Water permeability measurement of high performance concrete suing a high pressure triaxial cell, *Cement and Concrete Research*, Vol. 25, No. 6, pp. 1199-1208.

Elsener, B. (2000) Corrosion of steel in concrete, in: *Corrosion and Environmental Degradation*, M. Schutze (ed.), Vol. II, pp. 389-436, Wiley-VCH Weinheim.

Emerson, M. (1973) The calculation of the distribution of temperature in bridges, *TRRL report LR561*, Department of the Environment, Crowtowne, England.

Eurocode (1992) *Eurocode 2: Part I, British Standards Institution*, London.

Frangopol, D.M., Lin, K.Y. and Estes, A.C. (1997) Reliability of reinforced concrete girders under corrosion attack, *ASCE Journal of Structural Engineering*, Vol. 123, No. 3, pp. 286-297.

Frohnsdorff G. (1999) Modelling Service Life and Life-Cycle Cost of Steel-Reinforced Concrete, *NISTIR* 6327.

Gerard, B. and Marchand, J. (2000) Influence of Cracking on the Diffusion Properties of Cement-Based Materials, Part I: Influence of Continuous Cracks on the Steady-State Regime, *Cement and Concrete Research*, Vol. 30, No. 1, pp. 37-43.

Gordner, N.J. and Lockman, M.J. (2001) Design Provisions for Drying Shrinkage and Creep of Normal-Strength Concrete, *ACI Materials Journal*, Vol. 98, No.2, pp.159-167.

Granger, L. (1994) Comportement differe du beton dans les enceintes de centrales nucleaires: analyse et modelisation, *ENPC thesis*, Paris (in French).

Granger, L., Torrenti, J. M. and Acker, P. (1997) Thoughts about Drying Shrinkage: Experimental Results and Quantification of Structural Drying Creep, *Materials and structures*, Vol. 30, No. 204, pp. 588-598.

Hansen, E.J. and Saouma, V.E. (1999) Numerical Simulation of Reinforced Concrete Deterioration: Part II — Steel Corrosion and Concrete Cracking, *ACI materials journal*, Title no. 96-M41, pp. 331-338.

Hansson, C.M. and Sorensen, B. (1990) Threshold concentration of chloride in concrete for the initiation of reinforcement corrosion, in: *Corrosion Rates of Steel in Concrete*, ASTM STP 1065, Berke, N.S., Chaker, V., and Whiting, D. Eds., American Society for Testing and Materials, Philadelphia, Pa., pp. 3-16.

Hoffman, P.C. and Weyers, R.E. (1994) Predicting critical chloride levels in concrete bridge decks, in: Schueller, G.I., Shinozuka, M., Yao, J.T.P., Balkema, A.A. (Ed.), *Structural safety and reliability: Proceedings of ICOSSAR'93*, Rotterdam, pp. 957-959.

Hoffman, P.C. and Weyers, R.E. (1996) Probabilistic durability analysis of reinforced concrete bridge decks, in: Frangopol, D.M. and Grigoriu, M.D. (Ed.), *Probabilistic mechanics and structural reliability: Proceedings of the seventh specialty conference*, New York, pp. 290-293.

Hognestad, E.A. (1951) A Study of Combined Bending and Axial Load in Reinforced Concrete Members. *Bulletin No. 399*, Engineering Experiment Station, University of Illinois, Urbana, Illinois, Vol. 49, No. 22.

Hong, H.P. (2000) Assessment of Reliability of Aging Reinforced Concrete Structures, *ASCE Journal of Structural Engineering*, Vol. 126, No. 12, pp. 1458-1465.

Isgor O.B. and Razaqpur, A.G. (2004) Finite element modeling of coupled heat transfer, moisture transport and carbonation processes in concrete structure, *Cement and Concrete Composites*, Vol. 26, No. 1, pp. 57-73.

Ishida, T. and Maekawa, K. (2000) Modeling of pH profile in pore water based on mass transport and chemical equilibrium theory, *Translation from Proceedings of JSCE*, No.648/V-47, pp. 125-140.

JSCE (1989) JSCE Subcommittee on Durability Design for Concrete Structures, Proposed Recommendation on Durability Design for Concrete Structures, *Concrete Library JSCE*, No. 14, pp. 35-71.

Jung, W.Y., Yoon, Y.S. and Sohn, Y.M. (2003) Predicting the Remaining Service Life of Land Concrete by Steel Corrosion, *Cement and Concrete Research*, Vol.33, No. 5, pp. 663-677.

Kachlakev, D., Miller, T. and Yim, S. (2001) Finite Element Modeling of Reinforced Concrete Structures Strengthened With FRP Laminates, *Final Report SPR 316*, Oregon Department of Transportation.

Khatri, R.P. and Sirivivatnanon, V. (2004) Characteristic service life of concrete exposed to marine environments, *Cement and Concrete Research*, Vol. 34, No. 5, pp. 745-752.

Kirkpatrick, T.J., Weyers, R.E., Anderson-Cook, C.M. and Sprinkel, M.M. (2002) Probabilistic Model for the Chloride-Induced Corrosion Service Life of Bridge Decks, *Cement and Concrete Research*, Vol. 32, No. 12, pp. 1943-1960.

Kong, J.S., Ababneh, A.N., Frangopol, D.M., and Xi, Y. (2002) Reliability analysis of chloride penetration in saturated concrete, *Probabilistic Engineering Mechanics*, Vol. 17, No. 3, pp. 305-315.

Kropp, J. and Hilsdorf, H.K. (1995) *Performance criteria for concrete durability*, RILEM Report 12, E & FN Spon, London.

Kumaran, M.K. (1996) IEA-Annex XXIV: Heat and Moisture Transfer in Insulated Envelope Parts, Volume 3, *Material Properties* (Leuven: International Energy Agency).

Lan, Z. and Ding, D. (1992) Crack Width in Reinforced Concrete members, *International Journal of Structures*, Vol. 12, No. 2, pp. 137-163.

Leung, C.K.Y. (2001) Modeling of Concrete Cracking Induced by Steel Expansion, *Journal of Materials in Civil Engineering*, Vol. 13, No. 3, pp. 169-175.

Liang, M.T., Wang, K.L., and Liang, C. H. (1999) Service life prediction of reinforced concrete structures, *Cement and Concrete Research*, Vol. 29, No. 9, pp. 1411-1418.

Liu, Y. (1996) Modeling the time-to-corrosion cracking of the cover concrete in chloride contaminated reinforced concrete structures, *Ph.D. dissertation*, Virginia Polytechnic Institute.

Liu, Y. and Weyers, R.E. (1998) Modeling the dynamic corrosion process in chloride contaminated concrete structures, *Cement and Concrete Research*, Vol. 28, No. 3, pp. 365-379.

Liu, Y. and Weyers, R.E. (1998) Modeling the Time-to-Corrosion Cracking in Chloride Contaminated Reinforced Concrete Structures, *ACI Materials Journal*, Vol. 95, No. 6, pp. 675-681.

Lobry De Bruyn, C.A. (1957) *Proceedings RILEM Symposium on Bond and Crack Formation in Reinforced Concrete*, Vol II, Stockholm.

Loo, Y.C. and Guan, H. (1997) Cracking and Punching Shear Failure Analysis of RC Flat Plates, *ASCE Journal of Structural Engineering*, Vol. 123, No. 10, pp. 1321-1330.

Mandke, J.S. and Smalley, A.J. (1994) Parameter studies for enhanced integrity of reciprocating compressor foundation blocks, Mechanical and fluids engineering division, southwest research institute, *Technical Report No. TA 94-1*.

Mangat, P.S., and Molloy B.T. (1994) Prediction of free chloride concentration in concrete using routine inspection data, *Magazine of Concrete Research*, Vol. 46, No. 169, pp. 279-287.

Martin Marietta Energy Systems, Inc., EG&G Idaho, Inc., Westinghouse Hanford Company and Westinghouse Savannah River Company (1992) Radiological Performance Assessment for the Z-Area Saltstone Disposal Facility, *WSRC-RP-92-1360*, Westinghouse Savannah River Company, Aiken, SC.

Martin-Perez, B. (1998) Service Life Modeling of RC Highway Structures Exposed to Chlorides, *PhD dissertation*, Deptartment of Civil Engineering, University of Toronto, Toronto.

Martin-Perez, B., Pantazopoulou, S. J., and Thomas, M. D. A. (2001) Numerical solution of mass transport equations in concrete structures, *Computers and Structures*, Vol. 79, No. 13, pp. 1251-1264.

Martin-Perez, B., Zibara, H., Hooton, R.D., and Thomas, M.D.A. (2000) A study of the effect of chloride binding on service life prediction, *Cement and Concrete Research*,

Vol. 30, No. 8, pp. 1215-1223.

Masi, M., Colella, D., Radaelli, G., and Bertolini, L. (1997) Simulation of chloride penetration in cement-based materials, *Cement and Concrete Research*, Vol. 27, No. 10, pp. 1591-1601.

McDonald, D.B. and Roper, H. (1993) Prediction of drying shrinkage of concrete from internal humidities and finite element techniques, in: *Creep and Shrinkage of Concrete*, Bazant, Z.P. and Carol, I. (eds.), E & FN Spon, London.

Meakawa, K., Chaube, R. and Kishi, T. (1999) *Modeling of concrete performance – hydration, microstructure formation and mass transport*, E&FN SPON, London.

Mehta, P.K. (1991) *Concrete in the marine environment*, Barking, U.K., Elsevier Applied Science.

Mehta, P.K. (1993) *Concrete structure, properties and materials*, Prentice-Hall, Englewood Cliffs, New Jersey.

Mehta, P.K. (1994) Concrete Technology at the Crossroads – Problems and Opportunities. Concrete Technology – Past, Present, and Future. In *Proc. V. Mohan, Malhotra Symposium*, ed. P. Kumar Mehta, ACI, SP 144, pp. 1-30.

Mehta, P.K. and Monteiro, P. (2001) *Concrete — Microstructure, Properties and Materials, Prentice-Hall*, Englewood Cliffs, New Jersey.

Mills, R.H. (1985) Mass transfer of water vapor through concrete, *Cement and concrete Research*, Vol. 15, No.1, pp. 74-82.

Morinaga, S. (1990) Prediction of service lives of reinforced concrete buildings based on rate of corrosion of reinforcing steel, *Proceedings of Building Materials and Components*, Brighton, UK, pp. 5-16.

NEA (2002) Finite Element Analysis of Ageing Reinforced and Prestressed Concrete Structures in Nuclear Plant, *NEA/CSNI/R(2002)13*.

Ngo, D. and Scordelis, A.C. (1967) Finite Element Analysis of Reinforced-Concrete Beams, *Journal of the American Concrete Institute*, Vol. 65, No. 9, pp.757-766.

Nilsson, L. O., Massat, M., and Tang, L. (1993) Chloride binding capacity and binding isotherms of OPC pastes and mortars, *Cement and Concrete Research*, Vol. 23, No. 2, pp. 247-253.

Ohtsu, M. and Yosimura, S. (1997) Analysis of Crack Propagation and Crack Initiation

Due to Corrosion of Reinforcement, *Construction and Building Materials*, Vol. 11, No. 7-8, pp. 437-442.

Onyejekwe, O.O., and Reddy, N. (2000) A numerical approach to the study of chloride ion penetration into concrete, *Magazine of Concrete research*, Vol. 52, No. 4, pp. 243-250.

Page, C.L. and Treadaway, K.W.J. (1982) Aspects of electrochemistry of steel in concrete, *Nature*, Vol. 297, pp. 109-115.

Pantazopoulou, S.J. and Papoulia, K.D. (2001) Modeling Cover-Cracking due to Reinforcement Corrosion in RC Structures, *Journal of Engineering Mechanisms*, Vol. 127, No. 4, pp. 342-351.

Papadakis, V., Vayenas C.G. and Fardis, M.N. (1991) Fundamental modeling and experimental investigation of concrete carbonation, *ACI Materials Journal*, Vol. 88, No. 4, pp. 363-73.

Perre, P. and Turner, I.W. (1999) A 3-D version of TransPore: a comprehensive heat and mass transfer computational model for simulating the drying of porous media, *International Journal of Heat and Mass Transfer*, Vol. 42, No. 24, pp. 4501-4521.

Phifer, M.A. and Nelson, E.A. (2003) Saltstone disposal facility closure cap configuration and degradation base case: institutional control to pine forest scenario (U), *WSRC-TR-2003-00436*, Westinghouse Savannah River Company, Aiken, SC.

Phifer, M. A. (2003) Saltstone Disposal Facility Mechanically Stabilized Earth Vault Closure Cap Configuration and Degradation Base Case: Institutional Control to Pine Forest Scenario (U), *WSRC-TR-2003-00523*, Westinghouse Savannah River Company, Aiken, South Carolina.

Pihlajavaara, S.E. (1982) Estimation of drying of concrete at different relative humidities and temperature of ambient air with special discussion about fundamental features of drying and shrinkage, in: Bazant, Z.P. and Wittmann, F.P. (Eds.), *Creep and shrinkage in concrete structures*, John Wiley & Sons.

Piltner, R. and Monteiro, J.M. (2000) Stress Analysis of Expansive Reactions in Concrete, *Cement and Concrete research*, vol. 30, No. 6, pp. 843-848.

Prezzi, M. Geyskens, P. and Monteiro, P.J.M. (1996) Reliability approach to service life prediction of concrete exposed to marine environment, *ACI Materials Journal*, Vol. 93, No. 6, pp. 544-552.

Rapoport, J., Aldea, C-M., Shah, S.P., Ankenman, B. and Karr, A.F. (2002) Permeability

of Cracked Steel Fiber-Reinforced Concrete, *Journal of Materials in Civil Engineering*, Vol. 14, Issue 4, pp. 355-358.

Saetta, A.V., Schrefler, B.A., and Vitaliani, R.V. (1995) 2-D model for carbonation and moisture/heat flow in porous materials, *Cement and Concrete Research*, Vol. 25, No.8, pp. 1703-1712.

Saetta A., Scotta R., and Vitaliani R. (1993) Analysis of Chloride Diffusion into Partially Saturated Concrete, *ACI Material Journal*, Vol. 90, No. 5, pp. 441-451.

Saetta, A.V., Schrefler, B.A. and Vitaliani, R.V. (1993) The carbonation of concrete and the mechanism of moisture, heat and carbon dioxide flow through porous materials, *Cement and Concrete Research*, Vol. 23, No. 4, pp. 761-772.

Saetta A., Scotta R., and Vitaliani R. (1998) Mechanical Behavior of Concrete under Physical-Chemical Attacks, *Journal of Engineering Mechanics*, Vol. 124, No. 10, pp.1100-1109.

Saetta, A.V. and Vitaliani, R.V. (2004) Experimental investigation and numerical modeling of carbonation process in reinforced concrete structures, *Cement and Concrete Research*, Vol. 34, No. 4, pp. 571-579.

Sakata, K. (993) Prediction of Concrete creep and Shrinkage, Creep and Shrinkage of Concrete, *Proceedings of the Fifth International RILEM Symposium*.

Saouma, V.E. and Chang, S.-Y. (2003) Numerical simulation of reinforced concrete deterioration due to steel corrosion, freezing-thawing and mechanical load effects, Frangopol, D.M., Bruhwiler, E., Faber, M.H. and Adey, B. (Eds), *Life-cycle Performance of Deteriorating Structures: Assessment, Design and Management*, ASCE.

Schiessl, P. (1975) *Inter-Association Colloquium on the Behavior of in Service of Concrete Structures*, Vol II, Leige.

Schiessl, P. (1988) *Corrosion of steel in concrete*, RILEM Technical Committee 60-CSC, Chapman and Hall, New York.

Schiessl, P. and Raupach, M. (1990) Influence of concrete composition and microclimate on the critical chloride content in concrete, in: *Corrosion of Reinforcement in Concrete*, Page, C.L., Threadaway, K.W.J. and Bamforth, P.B. Eds., SCI, Society of Chemical Industry, Elsevier Applied Science, London, pp. 49-58.

Schmidt-Dohl, F. and Rostasy, F.S. (1999) A model for the calculation of combined chemical reactions and transport processes and its application to the corrosion of

mineral building materials, part I: Simulation model, *Cement and Concrete Research*, Vol. 29, No.7, pp. 1039-1045.

Schmidt-Dohl, F. and Rostasy, F.S. (1999) A model for the calculation of combined chemical reactions and transport processes and its application to the corrosion of mineral building materials, part II: Experimental varification, *Cement and Concrete Research*, Vol. 29, No.7, pp. 1047-1053.

Sentler, L. (1984) Stochastic characterization of carbonation of concrete, *Proceedings of the 3rd international conference on durability of building materials and components*, technical research center of Finland, pp. 569-580.

Sergi, G., Yu, S. W., and Page, C.L. (1992) Diffusion of chloride and hydroxyl ions in cementitious materials exposed to a saline environment, *Magazine of Concrete Research*, Vol. 44, No. 158, pp. 63-69.

Shadday M.A. (1993) Heat Transfer Modeling of the saltstone pouring and curing process (U), *WSRC-TR-93-528*, Westinghouse Savannah River Company, Aiken, SC.

Shah, S.P., Swartz, S.E. and Ouyang C. (1995) *Fracture Mechanics of Concrete*, Wiley, New York.

Shin, C.B. and Kim, E.K. (2002) Modeling of chloride ion ingress in coastal concrete, *Cement and Concrete Research*, Vol. 32, No. 5, pp. 757-762.

Siemes, A, Vrouwenvelder, A. and Van Den Beukel, A. (1985) Stochastic modeling of building materials performance in durability, in: L.W. Masters (Ed.), *Problems in service life prediction of building and construction materials*, Martinus Nijhoff, pp. 253-263.

Snyder K.A. (2001) Validation and Modification of the 4SIGHT Computer Program, *NISTIR 6747*.

Snyder K.A. and Clifton J.R. (1995) 4SIGHT Manual: A Computer Program for Modeling Degradation of Underground Low Level Waste Concrete Vaults, *NISTIR 5612*.

Steffens, A., Dinkler, D., Ahrens, H., (2002) Modeling carbonation for corrosion risk prediction of concrete structures, *Cement and Concrete Research*, Vol. 32, No. 6, pp. 935-941.

Stewart, M.G., and Rosowsky, D.V. (1998) Time-dependent reliability of deteriorating reinforced concrete bridge decks, *Structural Safety*, Vol. 20, No. 1, pp. 91-109.

Suzuki, K. Ohono, Y., Prapartanatorn, S. and Tamura, H. (1990) *Proceedings of Third SCI International Symposium on Corrosion of Reinforcement in Concrete*, Elsevier Applied Science, Society of Chemical Industry, London.

Tang, L. (1996) Electrical accelerated methods for determining chloride diffusivity in concrete: current development, *Magazine of Concrete research*, Vol. 48, No. 176, pp. 173-179.

Thoft-Christensen, P. (1992) A reliability based expert system for bridge maintenance, in: *Tekno vision conference on bridge and road maintenance management systems*, Copenhagen, Denmark, pp. 25-26.

Thoft-Christensen, P. (1995) Advanced bridge management systems, *Structural Engineering Review*, Vol. 7, No. 3, pp. 151-163.

Thoft-Christensen, P. (1997) Estimation of the service life time of concrete bridges, *Proceedings of ASCE Structures Congress XV*, Portland Oregon, USA.

Thoft-Christensen, P. (2000) Stochastic modeling of the crack initiation time for reinforced concrete structures, *Proceedings of 2000 ASCE Structures Congress*, Philadelphia, USA.

Thoft-Christensen, P. (2001a) Corrosion crack based assessment of the life-cycle reliability of concrete structures, *Proceedings of ICOSSAR'01*, Newport Beach, California, USA.

Thoft-Christensen, P. (2001b) What happens with reinforced concrete structures when the reinforcement corrodes? *Proceedings of the 2nd International Workshop on "Life-Cycle Cost Analysis and Design of Civil Infrastructure Systems"*, Ube, Yamaguchi, Japan, pp.35-46.

Thoft-Christensen, P., Jensen, F.M., Middleton, C. and Blackmore, A. (1996) Revised rules for concrete bridges, in: *International symposium of the safety of bridges*, institution of civil engineers and highways agency, London, UK, pp. 1-12.

Torrenti, J. M., Granger, L., Diruy, M. and Genin, P. (1999) Modeling concrete shrinkage under variable ambient conditions, *ACI Materials Journal*, title No. 96-M5, pp. 35-39.

Thoft-Christensen, P. (2003) Corrosion and Cracking of Reinforced Concrete, in *Life-Cycle Performance of Deteriorating Structures: Assessment, Design and Management*, ASCE, pp. 26-36.

Townsend, H.E., Cleary, H.J. and Allegra, L. (1981) Breakdown of oxide films in steel

exposure to chloride solutions, *NACE Corrosion*, Vol. 37, No. 1, pp. 384-391.

Tuutti, K. (1982). *Corrosion of steel in concrete*, Swedish Cement and Concrete Research Institute, Stockholm, Sweden.

Van Breugel, K. (1995) Numerical simulation of hydration and microstructural development in hardening cement-based materials, *Cement and Concrete Research*, Vol. 25, No. 2, pp. 319-331.

Van Breugel, K. (1998) *Simulation of hydration and formation of structure in hardening cement-based materials*, 2nd edition, Delft University Press, Delft.

Verbeck, G.J. (1975) Mechanism of corrosion in concrete, Corrosion of metals in concrete, *ACI SP-49*, pp. 21-38.

Walton, J.C., Plansky, L.E. and Smith, R. W. (1990) Models for estimation of service life of concrete barriers in low-level radioactive waste disposal, Report prepared for U.S. Nuclear Regulatory Commission, *NUREG/CR-5542 EGG-2597*.

Wang, K., Jansen, D.C. and Shah, S.P. (1997) Permeability Study of Cracked Concrete, *Cement and Concrete Research*, Vol. 27, No. 3, pp. 381-393.

Wang, Y., Li, L., and Page, C. L. (2005) Modeling of chloride ingress into concrete from a saline environment, *Building and Environment*, Vol. 40, No.12, pp. 1573-1582.

Wee, T.H., Wong, S.F., Swaddiwudhipong, S., and Lee, S.L. (1997) A prediction method for long-term chloride concentration profiles in hardened cement matrix materials, *ACI Materials Journal*, Vol. 94, No.6, pp. 565-576.

William, K.J. and Warnke, E.P. (1975) Constitutive Model for the Triaxial Behavior of Concrete, *Proceedings of the International Association for Bridge and Structural Engineering*, Vol. 19, ISMES, Bergamo, Italy, pp. 174.

Winship, G. (2003) Closure business unit saltstone vault study (U), *G-ADS-Z-00001*, Westinghouse Savannah River Company, Aiken, SC.

Xi, Y. and Ababneh, A. (2000) Prediction of the onset of steel corrosion in concrete by multiscale chloride diffusion, high performance concrete – workability, strength and durability. In: Leugn, C., Li, Z., Ding, J.T. editors. *Proceedings of the international symposium*, Hong Kong, pp. 181-186.

Xi, Y., and Bazant, Z.P. (1999) Modeling chloride penetration in saturated concrete, *ASCE Journal of Materials in Civil Engineering*, Vol. 11, No. 1, pp. 58-65.

Xi, Y., Bazant, Z.P. and Jennings, H.M. (1994) Moisture Diffusion in Cementitious Materials — Adsorption Isotherms, *Advanced cement based materials*, Vol. 1, No. 6, pp. 248-257.

Xi, Y., Willam, K. and Frangopol, D.M. (2000) Multiscale modeling of interactive diffusion processes in concrete, *ASCE Journal of Engineering Mechanics*, Vol. 126, No. 258, pp. 258-265.

Yalcyn, H. and Ergun, M. (1996) The Prediction of Corrosion Rates of Reinforcing Steels in Concrete, *Cement and concrete research*, Vol. 26, No. 10, pp. 1593-1599.